



Public Service®

Public Service  
Company of Colorado  
P.O. Box 840  
Denver, CO 80201-0840

16805 WCR 19 1/2; Platteville, Colorado 80651

February 24, 1994  
Fort St. Vrain  
ISFSI  
P-94018

Mr. Cass R. Chappell, Section Leader  
Cask Certification Section  
Storage and Transport Systems Branch  
Division of Industrial and  
Medical Nuclear Safety, NMSS  
U.S. Nuclear Regulatory Commission  
Washington, D.C. 20555

Docket No. 71-9253

SUBJECT: Response to the NRC's Request For Additional  
Information Regarding the Model No. TN-FSV Packaging

- REFERENCES:
- 1) PSC Letter, Warembourg to MacDonald, dated  
March 31, 1993 (P-93033)
  - 2) NRC Letter, Chappell to Warembourg, dated  
September 15, 1993 (G-93149)

Dear Mr. Chappell:

Public Service Company of Colorado (PSC) submitted an application for Certification of a New Irradiated Fuel Transport Package for Fort St. Vrain, Model No. TN-FSV in Reference 1. In Reference 2, the Nuclear Regulatory Commission (NRC) forwarded a request for additional information (RAI) regarding this application. This letter addresses the questions raised by the NRC in Reference 2, and includes documentation of the results of the impact limiter testing that was recently completed.

Attachment 1 to this letter is PSC's response to the NRC's RAI. Attachment 2 contains revised pages for the Safety Analysis Report for the TN-FSV Packaging, previously provided in Reference 1. These revisions were necessary to reflect the results of the impact

9403040246 940224  
PDR ADOCK 07109253  
B PDR

*delete: LA*

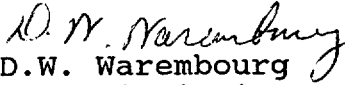
*NT01 1/3*

P-94018  
February 24, 1994  
Page 2

limiter testing and include information and changes identified while researching responses to the NRC's RAI. Included with this submittal package are enclosures that are referred to in Attachment 1.

Should you have any questions on the responses to the RAI or on the Safety Analysis Report revisions, please contact Mr. M. H. Holmes at (303) 620-1701.

Sincerely,

  
D.W. Warembourg  
Decommissioning Program Director  
and ISFSI Manager

DWW/JRJ

Attachments  
Enclosures

cc: Regional Administrator, Region IV

Mr. Robert M. Quillin, Director  
Radiation Control Division  
Colorado Department of Health

Attachment 1  
P-94018  
February 24, 1994

**PSC RESPONSES TO NRC QUESTIONS ON THE  
TN-FSV IRRADIATED FUEL SHIPPING PACKAGING**

## **DRAWINGS**

### **Question 1**

Revise Drawing No. 1090-SAR-3, Rev. 0, to include the weld callout, including inspection method, for the containment weld in Detail D.

### **Response 1**

TN Drawing No. 1090-SAR-3, Rev. 0 has been revised to include the full penetration symbol for the weld of the flange to the inner containment shell. Per the revised drawing, the welded joint will be examined radiographically for the full circumferential length followed by liquid penetrant examination.

## **STRUCTURAL**

### **Question 1**

Revise the application to show that the impact limiters remain attached after the 30-foot drop and puncture tests.

### **Response 1**

After submittal of the TN-FSV Safety Analysis Report, two half-scale static crush tests and two 30-foot drop tests on half scale models of the impact limiters were performed to evaluate the effectiveness of the impact limiters in dissipating the energy from the 30-foot drop and to ensure that the impact limiters remained intact on the cask after the drop.

Two static tests were performed:

- A side crush test.
- A corner crush test at an 80° angle from horizontal.

These orientations were selected because the impact limiter analysis presented in Appendix 2.10.1 indicated that they were the orientations where the highest g loadings were expected. The side orientation also puts large bending and shear loads on the attachment bolts. The side crush test is also a good approximation of the second hit in a shallow angle side drop (slapdown). The side crush test was continued to ensure that the amount of energy to be absorbed by the second impact limiter in a shallow angle side drop was met.

During the side crush test, five of the six attachment bolts broke. The bolts broke after 81% of the energy needed for the side drop was absorbed. This was well above the energy to be absorbed by a single impact limiter in either a side drop (50%) or a shallow angle drop (68%), thus providing evidence that the impact limiters would remain attached after a 30-foot drop.

Two dynamic tests were performed:

- A 30 foot drop at a 15° angle from horizontal. This is the most severe test for the attachment bolts. The impact limiter impacting second was cooled to -20°F for this drop.
- A 30 foot drop at an 80° angle from horizontal. This angle approximates the orientation of the cask when the center of gravity is directly above the corner of the cask.

Both drop tests were performed on the same impact limiters and test body. The drop testing was performed on a very cold day (Ambient temperature of 9°F). The bolts remained in place during both drops. The impact limiters also remained intact, with no major damage noted.

Puncture testing was not performed on the test impact limiters. However, as shown in the SAR, Section 2.7.2, the deceleration due to the 40 inch drop onto a puncture bar is small compared to that which will occur during a 30 foot drop. Damage to the impact limiters from the 30-foot drop tests did not create a geometry which would make the impact limiter attachments more vulnerable to a subsequent puncture test. If the puncture bar were to impact an attachment bolt directly, it might break. However, the remaining five impact limiter attachment bolts would keep the impact limiter on the cask.

The scale model testing is described in Appendix 2.10.3 of the revised SAR.

## **Question 2**

Revise the application to show that the inertia g values and forces used in ADOC computer code for the structural analyses are conservative, considering results of the impact limiter testing.

## **Response 2**

The g values and forces predicted by the ADOC computer code using maximum wood properties correlate well with the crush data from the static tests with a slight underprediction of forces by ADOC near the end of the force-deflection curves. However, the forces used in Appendix 2.10.1 of the SAR for the stress calculations are higher than those measured in the static crush tests for both orientations tested and are thus conservative. The highest stresses are predicted for the side crush and center of gravity over corner drop orientation which were tested; all other orientations analyzed in Appendix 2.10.1 have large margins of safety compared to allowable stresses. Therefore, the tests support the analytical conclusion that the impact limiter design is adequate and that stresses from the hypothetical 30-foot drop accident are below the allowable values.

The dynamic drop tests were not instrumented, and therefore it is impossible to derive information directly on the g-values and forces experienced in these drops. It is possible to extract some limited information from the deformations experienced by the impact limiters. Measurement of deformation is difficult and imprecise because crushing occurs on both the

inside and outside impact limiter surfaces and the impact limiters ovalize slightly. A comparison of the dynamic deformations to the recorded static deformations is further complicated because a significant amount of springback occurs when the impact is over.

With these limitations in mind, a rough comparison of static and dynamic deformation is discussed in Appendix 2.10.3. The correlation between dynamic and static deformation for the center of gravity over corner orientation was excellent. The correlation between dynamic and static deformation for the slapdown drop was not as good as for the center of gravity over corner orientation, although the correlation was good within the bounds of uncertainties described above. The absence of a perfect correlation is not surprising given that in addition to measurement uncertainties the static and dynamic tests in this case differed in two ways, namely:

1. The static crush test only approximates the slapdown event since the crush is actually a pure side crush; in a true dynamic slapdown, the impact orientation is not necessarily perpendicular to the axis of the cask because the cask and impact limiters go through a complex motion of primary impact followed by rotation followed by secondary impact.
2. Static crush tests were carried out at room temperature, whereas the dynamic tests were carried out at cold temperatures. In addition, the impact limiters were not at the same temperature; the primary impact limiter in the slapdown test was at ambient temperature of about 9°F, while the secondary impact limiter was closer to the chilled value of -20°F.

As discussed in Appendix 2.10.3, the dynamic tests results correlate reasonably well with the results from the static crush tests which confirm that the forces used in the stress analysis for the cask are conservative.

### **Question 3**

Provide results of the impact limiter tests (Appendix 2.10.3)

### **Response 3**

Appendix 2.10.3 is provided in the revised SAR.

# CONTAINMENT

## Question

The fuel particle failure rate used in the containment analysis (0.25%) was based on actual fuel particle failure experienced during reactor operation. Justify that the fuel particle failure rate would be the same during transportation, considering shock and vibration, temperature changes and other normal conditions of transport.

## Response

Section 4.2.1 of the Safety Analysis Report for the TN-FSV Packaging (SAR) states that a 0.25% fuel failure rate is assumed for normal conditions of transport. This is based on analysis that was performed to determine the maximum fuel failure fraction at final reactor shutdown. The analysis conservatively used a fuel element from segment 4, since these fuel elements have the highest predicted fuel failure fraction due to the presence of the highest manufacturing defects and their residence in the core for its entire life (889 EFPD). The analysis determined the maximum fuel failure fraction to be 0.25%, which is the weighted average of failed fissile and fertile fuel particle coatings calculated for a segment 4 fuel element (Reference 1).

PSC does not consider it credible that additional fuel failure could have occurred following reactor shutdown, or will occur during normal conditions of fuel storage or transport, due to the relatively mild conditions compared to those for which the fuel was designed. The carbide fuel particles used in FSV, known as TRISO coated particles, are extremely rugged. Fuel kernels consist of Uranium and Thorium Carbide (fissile) and Thorium Carbide (fertile). Each fuel kernel is encapsulated within four layers of coatings, designed to contain fission products under normal reactor operating conditions (approximately 1500 degrees F) and under extreme conditions representative of accidents (up to approximately 2900 degrees F).

The inner fuel particle coating layer consists of a low density pyrolytic carbon designed to adsorb fission recoils and provide a void volume for accumulation of fission product gases. This "buffer" coating is enveloped by an impermeable silicon carbide (SiC) layer, designed to prevent diffusion of metallic fission products at high temperatures, which is sandwiched between two high density isotropic pyrolytic carbon layers. These high density carbon layers also provide a barrier to prevent the escape of fission products, being impermeable to noble gases. The coatings act as miniature containment vessels, retaining gaseous and metallic fission products. TRISO fuel particles have survived extensive testing at high temperatures, long durations, at high neutron radiation fluxes and high burnup, representative of worst case in-core conditions, without releasing fission products (Reference 2, Appendix A.2). The fuel particles were tested at temperatures well over 1000 degrees F and operated at temperatures over 1500 degrees F for prolonged intervals without experiencing coating failures.

The coated carbide fuel particles were mixed with a coal tar pitch, molded and graphitized at high temperature to produce graphite fuel rods, 0.5 inch diameter, which were inserted into fuel holes bored in the graphite fuel elements.

In addition to being thermally rugged, the fuel particles are also mechanically very strong. Calculations identify a lowest compressive strength of 40,000 psi for fuel particles, which is substantially greater than the approximately 4,000 psi compressive strength of H-327 graphite and the approximately 7,000 psi compressive strength of H-451 graphite, the nuclear grades of graphite used in the FSV fuel elements. The design of the fuel particles, fuel rods and fuel elements assures that, mechanically, the graphite matrix of fuel rods or elements will fail before the fuel particle coatings. This has been demonstrated by crush tests.

Calculations show that while graphite fuel elements could crack or break under certain postulated conditions, fuel particle coatings would not be expected to fail, and there would be no release of fission products from fuel particles. Section 14.14.2 of the FSV Updated FSAR (Reference 2) discusses the possibility of fuel elements falling and breaking in the event of an earthquake during the final FSV defueling, concluding that fuel particle coatings would not fail. GA Technologies, Inc., the fuel fabricator, has evaluated more extreme conditions, assuming an explosion occurred adjacent to stored spent fuel elements. It concluded that the predicted blast overpressure of about 10,000 psi, in conjunction with fireball temperatures of about 5,000 K for a short duration, would not cause any intact TRISO fuel particle coatings to fail.

The thermal and mechanical ruggedness of the FSV fuel particle coatings is such that they are not anticipated to fail under accident conditions consisting of high impact forces and/or elevated temperatures. The conditions that the fuel elements are subjected to during storage and normal fuel shipping, such as ambient temperature variations and vibration, are mild compared to fuel particle coating design parameters. Coating failures under these conditions of storage and normal transport are not considered credible.

Based on the above discussion, PSC concludes that use of the 0.25% fuel particle coating failure fraction that was calculated following reactor shutdown will continue to represent a conservative value for predicting fission product release source terms. Additional fuel particle coating failures, as the result of temperature variations and vibration during normal fuel storage and shipping, are not considered credible since the TRISO coatings are designed (and demonstrated by operation and testing) to endure substantially more severe conditions.

## **SHIELDING**

### **Question 1**

Section 5.1 states that the maximum fuel element burnup is 70,000 MWD/MTU. Confirm that the burn-up specified is per metric ton uranium, rather than per metric ton uranium and thorium.

### **Response 1**

The 70,000 MWD/MTU maximum value after 4 out of 6 cycles of burnup was based on calculated 3-D fuel shipment data, and determined by scanning individual fuel block data for the maximum burnup. The "MWD/MTU" units are MegaWatt-Days/initial Metric tons of Thorium and Uranium as defined in Table 3.5-1 of the FSV Updated FSAR, where the initial metric tons includes: U-234, U-235, U-236, U-238 and Th-232. This burnup is consistent with enriched uranium used in water reactors, where U-238 replaces the fertile thorium. The reason such high burnup is possible for the HTGR is due to the integrity of the fuel particle coatings. The 70,000 MWD/MTU value was provided in the SAR for information on the maximum burnup. The value was not explicitly used in the generation of the gamma or neutron source terms or in the shielding calculation. (Input data for the source term generation is discussed in the Response to Shielding Question 2). Section 5.1 of the SAR has been updated to clarify the burnup units.

## SHIELDING

### Question 2

Specify the fuel parameters (e.g., isotopic composition, isotope masses, etc.) and fuel burn-up history (e.g. reactor power, number of cycles, up-time and down-time per cycle, etc.) that were used to determine the shielding source terms. Show that these parameters and burn-up history adequately represent the FSV fuel and provide the bounding source terms.

### Response 2

The FSV core was divided into six fuel segments, identified as Segments 4 - 9 (segments 1 - 3 were previously shipped to INEL). Each segment consisted of approximately 1/6 of the 1482 fuel elements in the core. Each segment had slightly different initial fuel loadings. Segments 4 - 6 were part of the original core and had the highest burnup. Segment 7 was added at the first fuel reload (replacing Segment 1) and Segments 8 and 9 on the subsequent two reloads.

Each fuel segment was analyzed with an individual ORIGEN-S computer run. The average fresh fuel densities, which were obtained from input from General Atomics Fuel Cycle code (GARGOYLE), are shown in Table 1.

The operating history of the FSV plant was quite sporadic throughout its life. Therefore, modelling the actual power history was extremely difficult. Figure 1 summarizes the Fort St. Vrain operating history.

Instead of attempting to model the actual history, each fuel segment was analyzed using a one pulse burn (at 80% power) equivalent to the actual number of effective full power days (EFPD) seen by that segment, and decayed to the 1600 day point. The effective full power days and burn times used in the ORIGEN-S runs are listed in Table 2.

The use of a single pulse, rather than modelling the up and down time of the reactor provides conservative gamma and neutron source terms at the specified 1600 day decay time. As an example, Segment 4 was modelled using several pulses and down times. The pulsed history was modelled with ORIGEN-S using six 80% pulses and four down times, conserving actual EFPD. The results shown in Table 3 indicate modelling the power history with a single pulse provides conservative neutron and gamma source terms for the specified 1600 day decay.

The single thermal neutron flux used for each pulse was a normalized core average flux based on 80% power in Cycle 4 (final fuel cycle before shutdown). Data from the FSV computational fuel accountability records were used to determine the flux. The thermal neutron flux used was:

Normalized Thermal Neutron Flux:  $5.815E+13$  n/cm<sup>2</sup>s

Gamma and neutron source terms were generated for a representative fuel block from each fuel segment. The maximum calculated source term corresponded to a Segment 4 or Segment 6 fuel block (Segments 4 and 6 had about the same initial fuel loadings). The Segment 4 (or Segment 6) fuel block source terms were selected to conservatively represent all fuel blocks, providing bounding neutron and gamma source terms for the fuel. The calculated source terms for a fuel block (listed by fuel segment), are shown in Table 4 at 1600 days decayed.

SAR Section 5.2 has been revised to include initial fuel parameters.

Table 1

FRESH FUEL NUMBER DENSITIES PER FUEL BLOCK (GRAM-ATOMS)

	Segment 4	Segment 5	Segment 6	Segment 7	Segment 8	Segment 9
Th -232	4.351E+1	4.447E+1	4.347E+1	4.110E+1	4.110E+1	4.113E+1
U-234	1.940E-2	1.832E-2	1.940E-2	2.373E-2	2.492E-2	2.668E-2
U-235	2.465E+0	2.328E+0	2.465E+0	3.015E+0	3.166E+0	3.390E+0
U-236	7.377E-3	6.967E-3	7.379E-3	9.023E-3	9.477E-3	1.015E-2
U-238	1.526E-1	1.441E-1	1.525E-1	1.866E-1	1.960E-1	2.099E-1
Silicon	1.127E+2	1.109E+2	1.127E+2	1.002E+2	1.002E+2	1.013E+2
Carbon	9.043E+3	9.044E+3	9.258E+3	9.258E+3	9.285E+3	9.179E+3

Table 2

BURNUP DATA

Segment	Actual EFPD	ORIGEN-S Burntime (Days)
4	889.3	1111.6
5	889.3	1111.6
6	889.3	1111.6
7	715.3	894.1
8	526.5	657.5
9	232.0	290.0

Table 3

SINGLE/PULSED HISTORY

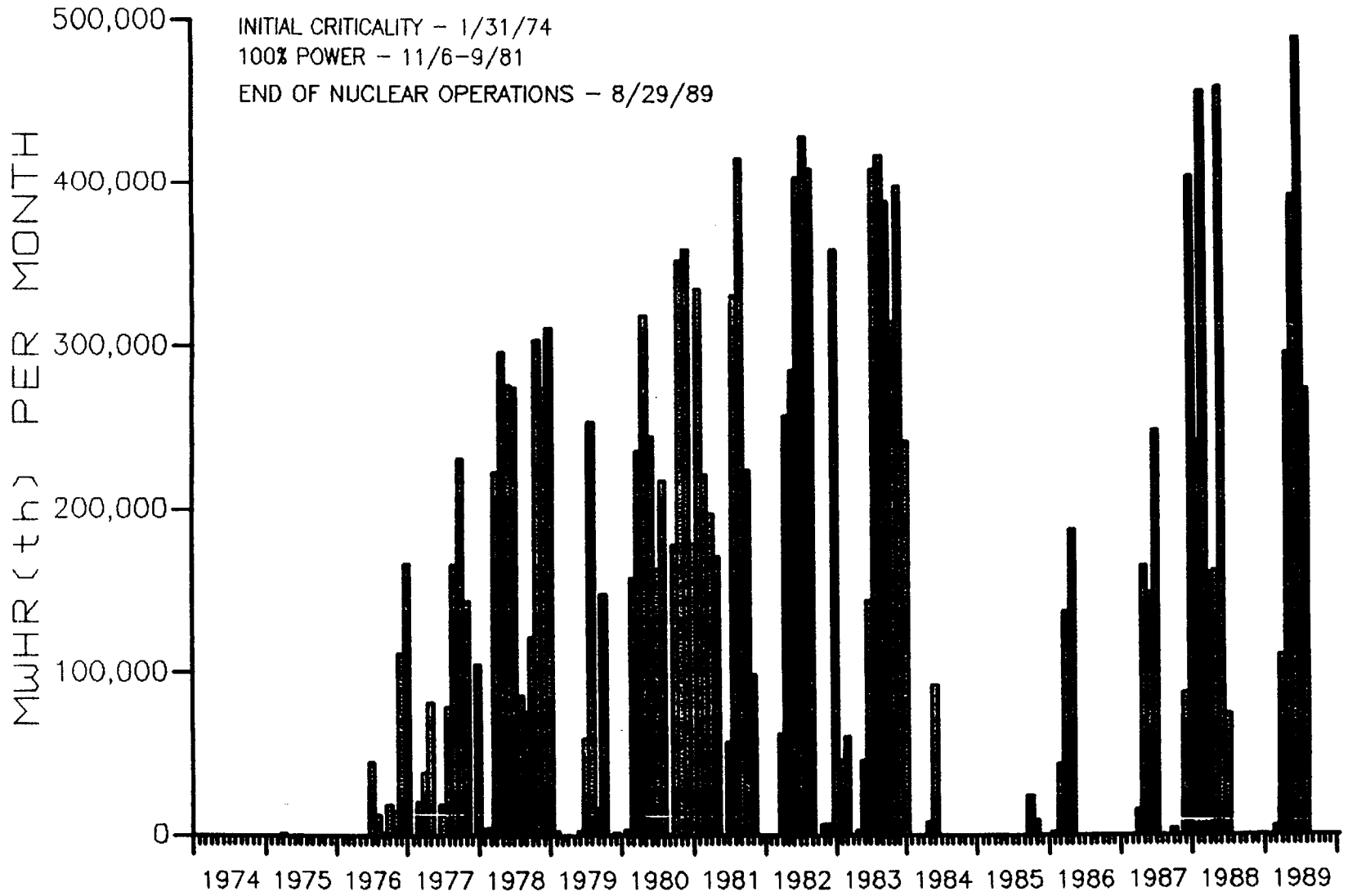
	Single Pulse	Pulsed History
Total Photon Spectrum after 1600 day decay (photons/sec)	1.21E14	1.14E14
Total Neutron Spectrum after 1600 day decay (neutrons/sec)	2.03E5	2.01E5

Table 4

SOURCE TERMS BY FUEL SEGMENT AT 1600 DAYS DECAYED

Fuel Segment	Total Gamma Source ( $\gamma$ /sec)	Total Neutron Source (n/sec)
4	1.21E14	2.03E5
5	1.17E14	1.92E5
6	1.21E14	2.03E5
7	1.12E14	1.19E5
8	8.49E13	4.41E4
9	3.66E13	4.37E3

Figure 1  
FSV Operating History



## SHIELDING

### Question 3

A 1.8 peaking factor was applied to neutron source term. This assumes that the neutron source term increases linearly with burn-up. Show that this assumption is valid. Note that for LWR fuels, the peaking factor is typically raised to the fourth power before it is applied to the neutron source term.

### Response 3

The neutron source does not increase linearly with burnup, as does the gamma source, and we didn't assume this in our calculations. The peaking factor applied to the neutron source spectrum represents a time weighted peak to average thermal flux calculated on a per block basis. The peaking factor per block was defined as the ratio of the thermal flux in each block divided by the core average thermal flux. Fuel data were used to search for the maximum peaking factor at various times during Cycle 4. The entire core (1482 blocks) was searched for the maximum peaking factor at various points in time. The 1.8 peaking factor was then calculated for the maximum block by time weighting the maximum peaking factor found at specific times over the operating cycle. This peaking factor did not occur in the same block throughout the operating cycle since the maximum peaking factor decreased for older fuel.

The "maximum" neutron source term calculated for the SAR was the result of applying a 1.8 peaking factor to the average neutron source calculated by ORIGEN-S code (using the average neutron flux discussed in the response to Shielding Question 2). A second method to calculate the "maximum" neutron source is to apply the 1.8 peaking factor to the input thermal flux. Table 5 compares three cases:

- Case 1: Average neutron source (using the average normalized flux of  $5.815E13$  n/cm<sup>2</sup>s as input to ORIGEN-S)
- Case 2: "Maximum" neutron source calculated by applying a 1.8 peaking factor to the average neutron source (SAR calculation)
- Case 3: "Maximum" neutron source calculated using the 1.8 peaking factor applied to the average normalized flux and then input into ORIGEN-S.

The comparison shows that Case 3 results in a higher neutron source than the SAR calculation (Case 2). Case 3 results in a total source 5.8 times the average source (Case 1), which is equivalent to the peaking factor of 1.8 raised to the power of three. The contribution of the neutron source is small in comparison to that of the gamma source and does not make a significant contribution to the overall dose. If the 5.8 peaking factor is applied to each block in the cask, the contribution to the dose at 2 m (most limiting case) would also increase by 5.8 (rather than 1.8), resulting in a total dose of 9.73 mrem/hr, which is still below the 10 mrem/hr limit. SAR Section 5.2 has been revised to reflect the

use of the 5.8 peaking factor. The use of the 5.8 peaking factor is conservative since the peaking factor did not occur in the same block over the operating history.

Table 5

PEAKING FACTOR COMPARISON

	Case 1 Source Calculated Using the Average Flux	Case 2 (SAR Calculation) Source Calculated by 1.8 x Resulting Average Source	Case 3 Source Calculated by 1.8 x Thermal Flux Input to ORIGEN
Total Neutron Source (n/sec)	2.9E5	5.2E5	1.7E6

## CRITICALITY

### Question 1

Describe the method for modeling the fuel including any homogenization of the fuel or cell weighting techniques and any techniques used to adjust the neutron cross sections. Describe the method used for determining atomic number densities with sufficient detail that the calculations can be repeated. Note that the application for the TN-FSV should be a stand-alone document, and should not be dependent on information in the FSV-1 application.

### Question 4

Describe the method for benchmarking the criticality codes and identify the critical experiments used. Identify which reported values of  $k_{eff}$  have been adjusted for bias.

### Responses 1 and 4

Questions 1 and 4 address the generation of neutron cross sections used in the FSV-1 analysis and critical experiments used to validate analytical methods. Fuel homogenization and atomic number density calculations are discussed in the Response to Question 3.

The HTGR critical experiment program provided both validation of cross section data and analytical methods used in FSV physics calculations.

Phase 1 of the program was a series of critical experiments designed strictly to check cross section data. Phase 2 of the program provided checks of analytical methods used to analyze special problems in HTGR design. The final phase of the program compared experimental results and analytical methods to investigate reactivity worths of control rods.

The first phase of the experiment evaluated 200 group cross-section sets used as input to the GGC code, which calculates neutron spectrum from material number densities and prepares group averaged effective macroscopic cross sections for use in either multigroup diffusion theory or transport codes. Reactivity measurements of several isotopes were conducted in a homogeneous carbon/uranium core mixture; C + U-235, depleted U-238, U-236, B(1/v), Th, Np-237 and Au, within five different spectrum cores (with carbon to uranium (C/U) ratios of 432, 859, 1718, 2500 and 5000). The measurements were performed strictly to check available HTGR cross-section sets (at that time) and select the sets which compared most favorably with experimental results. Of most concern were the cross sections of U-233 and Th-232 because of their importance in HTGR physics and the lack of available cross section information, especially for the Th-232 resonance.

In the HTGR critical assembly program, the experimental data was used to evaluate pertinent cross section data through well defined one-dimensional diffusion theory and/or transport theory calculational models. The basis for the analysis of the reactivity coefficient measurements were the nuclear data files, developed at General Atomic over a period of several years, for use with flux spectrum codes.

Five relatively homogeneous cores were used in this part of the critical assembly program, differing primarily in the neutron spectra (see Table 6). Cores 1 and 2 were soft spectrum cores, typical of HTGR lattices; the mean fission energy was about 0.1 eV, and the most probable energy was about 0.05 eV. The Maxwellian spectrum at a temperature of 300°K has a most probable energy of 0.0258 eV. The spectra of very lightly loaded graphite assemblies always appear hard relative to a Maxwellian spectrum because of the strong 1/E flux component in the higher thermal energies. The other cores had harder spectra; Core 5, with C/U = 432, had an epithermal spectrum. These hard spectrum cores were designed to yield data on the epithermal cross sections of HTGR type materials.

Data on the delayed neutron fraction, the prompt neutron lifetime, and on assembly criticality were also obtained during these measurements, and useful comparisons with theory were possible.

The five cores were constructed each with three distinct regions: 1) the center or exact region made up of fuel elements containing the desired C/U ratio; 2) the heterogeneous (called the driver) region containing a combination of fuel elements and graphite elements to give approximately the same C/U ratio as the exact region and 3) the reflector region. Figure 2 provides an example of the C/U=2500 core configuration. Exact material loadings for each core are provided in Table 10 of Reference 3. A version of DTF code was used to calculate self-shielding in the heterogeneous region.

Details of the comparison of calculated and experimental reactivity worths of elements of interest in each core along with delayed neutron fraction and prompt neutron lifetime data are included in Reference 3. Reference 3 is enclosed with this submittal to provide details of Phase 1 of the Critical Experiment Program. The comparison of the calculated and measured core multiplication constants for each core are summarized in Table 7. No bias was applied to the data. This completed the benchmark testing for the cross section data sets to be used in FSV analyses.

The strong negative Temperature Coefficient for the FSV HTGR is due primarily to the Doppler broadening of the Thorium resonances. Since the thorium fertile material is located within the Fissile and Fertile fuel particles (150 to 650 microns), and these are homogeneously distributed within the 0.5" fuel rod, the self shielding for these resonances needed to be addressed in the analytical model. Therefore, Phase 2 of the HTGR critical assembly program involved reactivity measurements for the HTGR lattice fuel element as a function of temperature. The HTGR lattice fuel element was loaded with fissile and fertile particles loaded into a 0.5" fuel rod which was loaded into a graphite element consisting of fuel rod coolant holes, which was an identical mockup for a FSV fuel element except for the size of the graphite element. This served as a benchmark for the analytical codes used to determine the Doppler effect on the Thorium resonances.

Phase 2 of the HTGR critical assemble program was designed to yield data on the multiplication constant for typical HTGR lattices, to provide benchmark data for the temperature coefficient, and to separate out the Doppler Broadening aspect of the temperature coefficients from the thermal temperature effects. The details of Phase 2 were documented through various GA quarterly reports (Reference 4).

The lattice region mocking up an HTGR geometry in the HTGR critical assembly was 22.7 inches in diameter. A surrounding fuel zone ( $C/U = 2500$ ) and the outer reflector region were adjusted as necessary to maintain criticality. The central fuel element in the lattice was used as a test region in which temperature coefficients were measured.

The core multiplication constant was calculated to be 1.024, 1% higher than the measured value of 1.013. The discrepancy was due to an underestimate of the lattice impurities, and therefore an overestimate of lattice infinite multiplication constant.

Thorium Doppler coefficients were measured by heating (external to the core) the central test element in an oven and then inserting the hot element into the core and measuring the change in reactivity from an identical test element at room temperature. Results are shown in Table 8.

The thorium capture rate and Doppler coefficient were shown to be quite accurate when the worth of the thorium in the central element, relative to a no-thorium case, was also measured and calculated at room temperature (see Table 9). Measurements were also made to determine the sensitivity of the Doppler coefficient to the Th-232 particle size. It was found that for particles between 100 and 600 microns, the Doppler coefficient is affected by about 10% (See Table 10).

The standard flux spectrum calculation design analyses is based on the GGC Code. Particle effects are usually neglected in this zero dimensional resonance calculation in which a  $1/E$  spectrum in the moderator is assumed and space-energy self shielding is ignored. However, this analytical approach gives an accurate estimate of the resonance absorption rate in HTGR lattices composed of intermediated sized ThC2 particles ( $\approx 450$  microns). The neglect of the particle heterogeneity leads to an estimate for the resonance absorption which is too high, while the use of a  $1/E$  spectrum to obtain average fine group cross sections in the resonance region (prior to the spectrum calculation which yields few group constants) leads to too low a resonance integral. This compensation is nearly complete for typical HTGR lattices as shown in Table 10. A more accurate analysis which takes particle heterogeneity and space-energy effects into account is also shown on the same Table. This shows correctly the dependence of the resonance integral on particle size.

Phase 3 of the program (Reference 5) conducted a series of measurements and calculations to investigate the reactivity worth of typical large HTGR type control rods containing either boron or hafnium. The measured results were compared with the results obtained from calculational methods used in the design and operation of High Temperature Gas Cooled Reactors.

Table 6

CHARACTERIZATION OF CRITICAL ASSEMBLIES USED IN  
REACTIVITY COEFFICIENT PROGRAM

	Assembly Number				
	1	2	3	4	5
C/U ratio in core	5000	2500	1718	859	432
Mean fission energy (ev)	0.074	0.12	0.20	0.40	12.7
Most probable thermal energy (ev)	0.050	0.059	0.061	0.085	0.140
Average of a unit $1/v$ cross section ( $0 \leq E \leq 2.38$ ev)	0.55	0.44	0.39	0.31	0.24
Core radius (cm)	71.5	64.0	59.0	56.5	54.7
Core length (cm)	183	183	183	183	183
Graphite reflector thickness (cm)					
Radial	15.1	7.5	8.4	7.5	6.8
Axial	0	0	0	0	0
Fast/thermal flux ratio ( $E_c = 2.38$ ev)	2.15	3.40	4.62	12.07	15.33

Table 7

CORE MULTIPLICATION CONSTANT FOR  
HOMOGENEOUS CRITICAL ASSEMBLIES

	Calculated Multiplication Constant	Measured Multiplication Constant
C/U = 5000	1.023 ± 0.005	1.013 ± 0.003
C/U = 2500	1.017 ± 0.005	1.014 ± 0.003
C/U = 1718	1.013 ± 0.005	1.013 ± 0.003
C/U = 859	1.012 ± 0.005	1.013 ± 0.003
C/U = 432	1.019 ± 0.005	1.016 ± 0.003

Note: The uncertainty in the calculated value is due to the uncertainty in the impurity content of core materials; the uncertainty in the measured value is due to core perturbations from control elements, etc.

Table 8

DOPPLER COEFFICIENT MEASUREMENTS  
IN THE HTGR CRITICAL ASSEMBLY LATTICE

Composition of Central Test Element	Reactivity Change (Dollars): 300°K to 600°K	
	Measured	Calculated
C/U = 2500, C/Th = ∞	-0.029	-0.028
C/U = 2500, C/Th = 300	-0.055	-0.053
C/U = 2500, C/Th = 200	-0.063	-0.062
C/U = 2500, C/Th = 100	-0.074	-0.074
C/U = 2500, Th-232 in C/Th = 100 lattice replaced by boron equivalent to the 1/v cross section of thorium	-0.0124	-0.0116

Table 9

CENTRAL REACTIVITY WORTH OF THORIUM  
IN THE HTGR CRITICAL ASSEMBLY LATTICE

Composition of Central Test Element	Reactivity Change (Dollars):	
	Measured	Calculated
C/U = 2500, C/Th = ∞	0	0
C/U = 2500, C/Th = 300	-0.45	-0.45
C/U = 2500, C/Th = 200	-0.61	-0.62
C/U = 2500, C/Th = 100	-0.99	-0.95
C/U = 2500, Th-232 in C/Th = 100 lattice replaced by boron	-0.45	-0.44

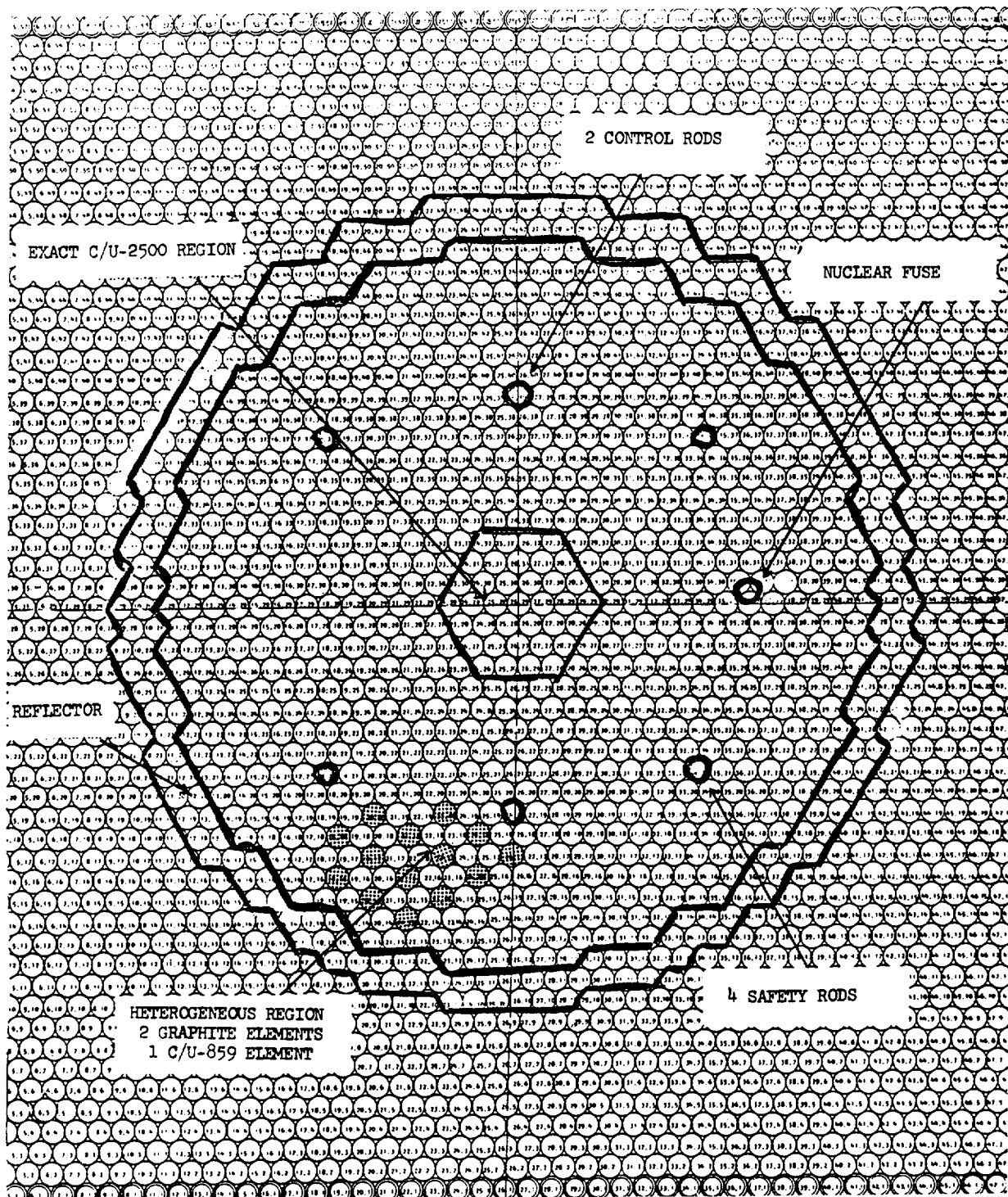
Table 10

SENSITIVITY OF DOPPLER COEFFICIENT TO Th-232 PARTICLE SIZE  
(C/Th = 320 In Test Element)

Particle Size, μ	Reactivity Defect, 300°K to 600°K Δρ (\$) Calculated		
	Measured	Standard GGC Calculation; Particle Effects Neglected	Improved Calculation: Particle Effects Plus Space Dimensional Spectrum Calculation
125	0.054	0.052	0.054
450	0.052	0.052	0.053
600	0.050	0.052	0.052

Figure 2

C/U-2500 Core Configuration



## CRITICALITY

### Question 2

Provide and justify the conversion ratio of U-233 production versus loss of U-235. Show that the net reactivity change in the fuel during burnup is negative.

### Response 2

The use of fresh fuel rather than burned material is always conservative for FSV fuel since the burned material is less reactive. The conversion ratio is on the order of 0.7 (given in FSV Updated FSAR Table 3.5-1, Reference 2), which yields a negative reactivity change during burnup.

To show this negative reactivity change, the MICROX two region lattice code was used to calculate the difference in reactivity between fresh, unburned FSV fuel versus fuel which is discharged after a typical operating cycle of depletion. The number densities for fresh fuel and "burned" fuel were taken from the data discussed in shielding question 2, using Segment 4 fuel. All fission products and burnable poisons were neglected in the analyses. The full buildup of U-233 (which occurs at about 200 days after shutdown) was used.

The results, shown below, indicate that the discharged fuel is considerably less reactive than fresh fuel, supporting the assumption that using the isotopics of unburned fuel provides the most conservative results when assessing FSV shipping criticality.

Temperature (K)	Fresh Reactivity minus Burned Reactivity (delta $\rho$ )
300	0.0666
600	0.0662
900	0.0643
1200	0.0619

$$\text{where } \Delta \rho = \frac{(K_{\infty} \text{ fresh}) - (K_{\infty} \text{ burned})}{(K_{\infty} \text{ fresh}) (K_{\infty} \text{ burned})}$$

The SAR (Section 6.1.2) has been updated to reflect the negative reactivity change of burned fuel.

## **CRITICALITY**

### **Question 3**

Provide the data that were used in the criticality computer programs in sufficient detail that the calculations can be repeated with an alternative computer code.

### **Response 3**

#### Fuel Element Description:

The individual fuel elements are hexagonal in cross section with dimensions of 14.17 in . across flats by 31.22 in high. Internal coolant channels within each element are aligned with coolant channels in the elements above and below. The active fuel is contained in an array of small diameter holes, which are parallel with the coolant channels, and occupy alternating positions in a triangular array within the graphite structure. There were two types of fuel elements in the FSV core: a standard fuel element and a control rod element (in the center of each fuel region), see Figures 3 and 4. Drawings R1803-110 and R1801-101 of a standard fuel element and drawings R1803-210 and R1801-201 of a control rod element have been included as an enclosure to this submittal for additional detail.

In the standard fuel element, the fuel holes are drilled from the top face of the element to within about 0.3 in of the bottom face. The fuel holes in all the elements are 0.5 inches in diameter. The bonded rods of coated fuel particles are stacked within the holes. The fuel holes and coolant channels are distributed on a triangular array of about 0.74 inch pitch spacing with an ideal ratio of two fuel holes for each coolant channel. Edge effects change the ratio slightly, therefore each fuel element contains 210 fuel holes and 108 coolant channels.

The center control rod fuel element in each region is similar to the surrounding fuel elements, but contains enlarged channels which were used for the two control rods and the reserve shutdown absorber material. The control rod channels have a 9.72 inch centerline spacing and a diameter of 4.0 inches. The reserve shutdown channel has a diameter of 3.75 inches. Each control rod fuel element contains 120 fuel holes and 57 coolant channels.

An engagement hole, for fuel handling purposes, is located at the center of each fuel element. The lifting ledge at the lower end of the engagement hole was used to make contact with the fuel element handling pickup head.

#### Fuel Particle Description:

The fuel is in the form of carbide particles, coated with a highly retentive coating, and bonded with a carbonaceous matrix into fuel rods within the fuel holes. This matrix contains a coal tar pitch or a petroleum derived pitch binder.

The fuel rods contain homogenous mixtures of fissile and fertile particles. The fissile particles contain 93.15% enriched U-235 and thorium. Fertile particles contain only

thorium, as discussed in the response to the containment question. The fuel particles are coated with a four-layer TRISO coating. The inner layer is a porous pyrolytic carbon, referred to as buffer layer. The next layer is high density isotropic pyrocarbon. A thin layer of SiC, which is highly impervious to metallic fission products, is deposited outside the inner isotropic pyrocarbon layer. The outermost layer is a strong high density isotropic pyrocarbon. Details of the fuel particles are shown on Figure 5 (FSV Reference Design TRISO Fuel Particles). Particle loading characteristics in each block are provided in Table 12.

### Grain Effect

The FSV fuel block has fuel granules loaded in a fuel rod, which are located in graphite fuel block, which causes a "double heterogeneity" of the fuel. The effect of fuel particles within fuel rods (or grain effect) is summarized below.

A series of calculations have been performed using the MICROX two region lattice code in order to assess the effect of the spatial heterogeneity of the fuel particles, bonded with graphite shim material into cylindrical fuel compacts, on the reactivity of a standard Fort St. Vrain (FSV) fuel element. The number densities and fuel characteristics used are provided in Tables 11 and 12. The results show that the "grain effect" on FSV fuel is small and slightly positive, with a maximum increase in  $\Delta\rho=0.003$ . This means that if the fuel grain material is homogenized over the volume of the fuel compacts as part of a reactivity calculation, the resulting  $k_{eff}$  will be about  $0.003\Delta\rho$  less than a more explicit model that properly accounts for grain structure in the fuel. A correction factor of  $+0.003\Delta\rho$  should therefore be applied to all calculational results which neglect grain structure in FSV fuel.

### Number Densities

The fuel was modelled homogeneously throughout the graphite fuel block for the FSV-1 analysis. Fuel rods or grains were not modelled for the analysis (the "double heterogeneity" was previously taken into account through the use of the GGC and MICROX codes). The maximum fuel loading was assumed for the fuel. Number densities were calculated by:

$$\text{Number Density (atoms/b-cm)} = \frac{(\text{Avagadro's No. - atoms/gram atomic weight})(\text{Density - gram/cc})(\text{Weight Fraction})}{(\text{Atomic Weight - gram/gram atomic weight})}$$

where the density is the homogeneous density of the fuel and graphite block. Results are provided in Table 11.

The most reactive single fuel element loadings (Table 11) were used to generate homogenized number densities for the fuel and graphite block in the original analysis. No credit was taken for the six burnable poison rods (assumed to be carbon). Additionally, Table 11 contains the number densities for explicitly modelling fuel rods within a graphite block.

Under normal conditions of transport, the six fuel elements occupy 81.4% of the inner container of the shipping cask (See Figure 6-2 in the SAR). The number densities for the six elements, homogenized over the inner container are shown on Table 13, along with the number densities corresponding to the cask itself.

If, in addition, independent criticality calculations are to be undertaken, the effect of the grains within a rod may be quantified using the information previously presented. The effect of fuel rods within a block may be easily modelled using Monte Carlo techniques. It is PSC's understanding is that Monte Carlo techniques have been applied to FSV fuel at ORNL in informal calculations. ORNL may therefore be of assistance in questions of spatial heterogeneity and the application of a bias to Monte Carlo codes used to model FSV fuel (Mr. Brian Worley is a possible contact at ORNL).

#### Accident Conditions

The material concentrations used for most reactive unflooded (Table 14) and flooded (Table 15) conditions are listed on the following tables. The region number corresponds to SAR Figure 6-2 and SAR text in section 6.4.2.a and 6.4.2.b.

## **CRITICALITY**

### **Question 5**

Provide the Appendix referenced in Section 6.3.b of the application.

### **Response 5**

Section 6.3.b of the SAR states "Cross sections were calculated with a GGC-4 code, a description of which is provided in the Appendix." Appendix 6.7 is included in the revised SAR pages. It contains a description of the GGC-4 code, and several other codes used in criticality calculations.

Table 11

## SINGLE BLOCK HOMOGENIZED NUMBER DENSITIES AND DATA

	Total Loading per Block (Kg)	Number Densities	
		Homogenized Block (atoms/b-cm)	Homogenized Rods in a Block (atoms/b-cm)
Th-232	11.25	3.28E-4	1.624E-3
U-235	1.31	3.76E-5	1.866E-4
U-238	0.078	2.22E-6	1.087E-5
Si	4.63	1.12E-3	5.524E-3
C (in rods)	16.295	--	4.545E-2
C (block only)	95.005	--	8.874E-2
C (homogenized)	111.3	6.72E-2	--

## Data:

Approximate volume of block based on outside dimensions: 8.8767E4 cc  
 Approximate volume of coolant holes (102 @ d=0.625", 6 @ d=0.5"): 1.6613E4 cc  
 Approximate volume of fuel rods (total of 210 rods): 1.7874E4 cc  
 Approximate volume of graphite plugs (above/below rods): 3.1217E3 cc

Table 12

## PARTICLE CHARACTERISTICS

Parameter	Fissile	Fertile
Nominal Th/U Ratio	3.6 or 4.25	All Th
Particle Composition	(Th/U)C <sub>2</sub>	ThC <sub>2</sub>
Average Fuel Particle Diameter, $\mu\text{m}$	200	450
Average Total Coating Thickness, $\mu\text{m}$	130	140
Nominal Density, gm/cm <sup>3</sup>	9.0	8.8

Table 13

## SIX ELEMENT HOMOGENIZED NUMBER DENSITIES

Region Number Corresponding SAR Figure 6-2	Material	Homogenized Number Density atoms/b-cm
1	Th-232	2.67E-4
	U-235	3.06E-5
	U-238	1.81E-5
	Silicon	9.12E-4
	Carbon	5.10E-2
2	Iron	8.50E-2
3	U-238	4.80E-2
	U-235	9.60E-5
4	Iron	8.50E-2
5	Void	--

- Notes:
- 1) Region 1 is the same number densities as in Table 14 but multiplies by 81.4%.
  - 2) Region 3 for the FSV-TN Cask is not depleted Uranium, but is lead, with an approximate number density of 3.30E-2 atoms/b-cm
  - 3) Radii for regions 3 and 4 for TN-FSV Cask are approximately 3" longer than those shown on SAR Figure 6-2 to increased thickness of lead.

Table 14

## CONCENTRATIONS FOR MOST REACTIVE CONDITION (UNFLOODED)

Region	Material	Concentration (atoms/b-cm)		
		10% Particle Loss		20% Particle Loss
1	Th-232	2.4E-4		2.14E-4
	U-235	2.75E-5		2.45E-5
	U-238	1.63E-5		1.45E-5
	Si	8.21E-4		7.30E-4
	C	5.01E-2		4.91E-2
2	Th-232		7.41E-4	
	U-235		8.49E-5	
	U-238		5.02E-5	
	Si		2.53E-3	
	C		6.92E-2	
3	Fe		8.5E-2	
4	U-238		4.78E-2	
	U-235		9.6E-5	
5	H		6.68E-2	
	O		3.34E-2	

- Notes: 1) Height of Particle Accumulation: 10% loss 24 cm  
20% loss 48 cm
- 2) Number densities for 10% and 20% were derived from homogeneous block number densities
- 3) Region 4 is now lead with an approximate number density of 3.30E-2 atoms/b-cm

Table 15

## CONCENTRATIONS FOR MOST REACTIVE FLOODED CONDITIONS

Region	Material	Case 1	Case 2	Case 3	Case 4	Case 5
1	C	4.09E-2	4.09E-2	4.09E-2	4.09E-2	--
	H	3.47E-2	3.47E-2	3.47E-2	3.47E-2	--
	O	1.74E-2	1.74E-2	1.74E-2	1.74E-2	--
2	Th-232	7.41E-4	5.93E-4	4.94E-2	3.71E-4	2.67E-4
	U-235	8.49E-5	6.79E-5	5.66E-5	4.25E-5	3.06E-5
	U-238	5.02E-6	4.02E-6	3.35E-6	2.51E-6	1.81E-6
	Si	2.53E-3	2.03E-3	1.69E-3	1.27E-3	9.12E-4
	C	6.92E-2	6.35E-2	5.98E-2	5.50E-2	5.11E-2
	H	1.21E-2	1.66E-2	1.96E-2	2.34E-2	2.65E-2
	O	6.05E-3	8.30E-3	9.80E-3	1.17E-2	1.33E-2

Figure 3

Standard Fuel Element

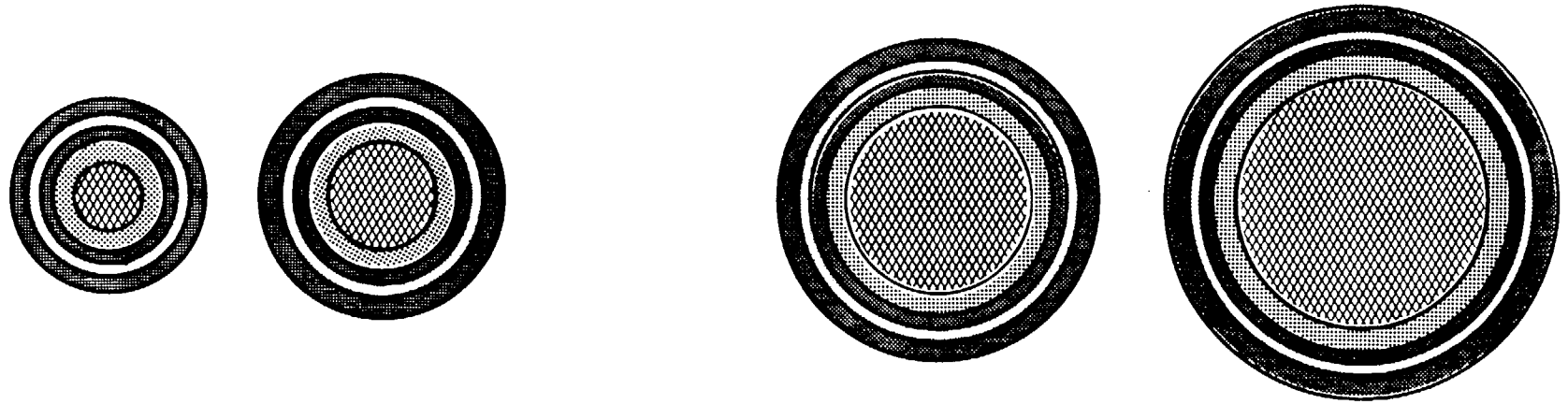
**FIGURE WITHHELD UNDER 10 CFR 2.390**

Figure 4  
Control Rod Fuel Element

**FIGURE WITHHELD UNDER 10 CFR 2.390**

Figure 5

Schematic Drawings of Fort St. Vrain Reference Design TRISO Fuel Particles



<u>FISSILE</u> (Th,U)C <sub>2</sub>		<u>FORM</u>	<u>FERTILE</u> ThC <sub>2</sub>	
<u>A (SMALL)</u>	<u>B (LARGE)</u>		<u>A (SMALL)</u>	<u>B (LARGE)</u>
100.175 μ	175.275 μ	PARTICLE SIZE	300.450 μ	450.600 μ
50 μ	50 μ	BUFFER COATING	50 μ	50 μ
20 μ	20 μ	ISOTROPIC PyC COATING	20 μ	20 μ
20 μ	20 μ	SiC COATING	20 μ	20 μ
30 μ	40 μ	ISOTROPIC PyC COATING	40 μ	50 μ
120 μ	130 μ	TOTAL COATING	130 μ	140 μ

## **OPERATING PROCEDURES**

### **Question 1**

Revise the operating procedures to show that the lifting points on the impact limiters are rendered inoperable for tie-down of the package.

### **Response 1**

The operating procedures (Chapter 7 of the SAR) state that the impact limiters are installed after the cask tie-down operation is completed. No further tie-down activity is required or called out after impact limiter installation. Also, the impact limiters are removed from the cask before the lifting operation of the cask is initiated. Since the impact limiter lifting points are not a structural part of the cask, and all tie-down activity is completed before the impact limiters are installed, the operating procedures do not need to be revised.

### **Question 2**

Revise the operating procedures to show that the drain plug seal is leak tested prior to each shipment, after loading.

### **Response 2**

The cask will be certified and used for dry loading and unloading as stated in Chapter 7 of the SAR. In Section 7.1.2 of the SAR, a statement is made that the drain port is not used for loading or unloading operations under dry conditions. Hence it is not necessary to leak test the drain plug seal prior to each shipment, after loading. However, the drain plug seal shall be leak tested annually as required in Section 8.2.2 of the SAR.

## **ACCEPTANCE TESTS AND MAINTENANCE PROCEDURES**

### **Question 1**

Provide additional details of the leak testing proposed in Section 8.1.3.1, i.e., describe the test method and show that the test will have a sensitivity of at least  $5 \times 10^{-4}$  std cm<sup>3</sup>/s. Note that several optional methods may be described.

### **Response 1**

The test method to be used is the halogen or helium mass spectrometer. The optional method will be the gas pressure rise method. These test methods have a sensitivity of at least  $5 \times 10^{-4}$  std cm<sup>3</sup>/s per ANSI NI4.5. These test methods are identified in Section 8.1.3.1 of the SAR.

### **Question 2**

Revise the maintenance procedures to specify periodic testing to assure that the impact limiters remain adequately sealed and that the wood maintains the proper moisture content.

### **Response 2**

The maintenance procedures will be revised to specify an annual humidity test for the impact limiter periodic testing. This will assure that no water has leaked into the impact limiter and the wood maintains the proper moisture content.

## REFERENCES

1. General Atomics Report 910061, "FSV ISFSI Predicted Spent Fuel Fission Product Inventories", May 4, 1990.
2. FSV Updated Final Safety Analysis Report, Revision 9, submitted to the NRC on July 22, 1991 (P-91230).
3. Bardes, R.G., et al., "Results of HTGR Critical Experiments Designed to Make Integral Checks on Cross Sections in Use at GA," USAEC Report GA-8468, Gulf General Atomic February 12, 1968.
4. HTGR Base Program Quarterly Progress Reports:
  - GA-9227, for the period ending February 28, 1969, issued March 28, 1969.
  - GA-9090, for the period ending November 30, 1968, issued December 30, 1968.
  - GA-8860, for the period ending August 31, 1968, issued September 27, 1968.
  - GA-8662, for the period ending May 31, 1968, issued June 28, 1968.
  - GA-8530, for the period ending February 28, 1968, issued March 29, 1968.
  - GA-8356, for the period ending November 30, 1967, issued December 29, 1967.
5. General Atomics Report A9354, "Experimental and Analytical Results for HTGR Type Control Rods of Hafnium and Boron in the HTGR Critical Facility".

Attachment 2  
P-94018  
February 24, 1994

**REVISED PAGES FOR THE SAFETY ANALYSIS REPORT  
FOR THE TN-FSV PACKAGING**

Instructions for Inserting Revision 1 Pages in the  
TN-FSV Safety Analysis Report

List of Effective Pages

Insert the new List of Effective Pages

Cover Page

Replace the Rev. 0 cover page with the Rev. 1 cover page.

Table of Contents

Replace the Rev. 0 Table of Contents with the Rev. 1 Table of Contents.

Chapter 1

Remove Rev. 0 page 1-17, -18 and replace with the new page 1-17, -18. Replace Rev. 0 drawings 1090-SAR-1 through 1090-SAR-10 with Rev. 1 drawings 1090-SAR-1 through 1090-SAR-10.

Chapter 2

Appendix 2.10.1: Remove Rev. 0 page 2.10.1-i, -ii and replace with the new page 2.10.1-i, -ii. Remove Rev. 0 pages 2.10.1-33 through 2.10.1-38 and replace with new pages 2.10.1-33, -34, -35, -35a, -36, -36a, -37, -37a, -37b and -38.

Appendix 2.10.3: Remove Rev. 0 page 2.10.3-1 and insert new Rev. 1 page 2.10.3-i, -ii and Rev. 1 pages 2.10.3-1 through 2.10.3-40.

Chapter 5

Remove Rev. 0 page 5-i, -ii and replace with the new page 5-i, -ii. Remove Rev. 0 pages 5-1 through 5-6 and replace with new pages 5-1, -2, -3, -3a, -4, -5 and -6.

Chapter 6

Remove Rev. 0 page 6-i, -ii and replace with the new page 6-i, -ii. Remove Rev. 0 pages 6-1 through 6-12 and replace with new pages 6-1 through 6-15.

Appendix 6.7: Insert Rev. 1 pages 6.7-1 through 6.7-6.

Chapter 8

Remove Rev. 0 page 8-i and replace with the new page 8-i. Remove Rev. 0 pages 8-3 through 8-7 and replace with the new pages 8-3 through 8-7.

<u>SECTION</u>	<u>EFFECTIVE PAGES</u>	<u>REVISION NO.</u>
Cover Page	Original	1
List of Effective Pages	1 through 3	1
Table of Contents	i through ii	1
Table of Contents Chapter One	1-i through 1-ii	0
Chapter One, General Information	1-1 through 1-17	0
	1-18	1
	Figures 1-1 through 1-4	0
	Table 1-1	0
	Drawings 1090-SAR-1 through -10	1
Chapter Two Table of Contents	2-i through 2-viii	0
Chapter Two, Structural Evaluation	2-1 through 2-79	0
	2-79a	0
	2-80 through 2-124	0
	Figures 2.5-1 through 2.7-3	0
	Tables 2.1-1 through 2.7-28	0
Appendix 2.10.1	2.10.1-i	0
	2.10.1-ii	1
	2.10.1-iii through 2.10.1-v	0
	2.10.1-1 through 2.10.1-33	0
	2.10.1-34	1
	2.10.1-35	0
	2.10.1-35a	1
	2.10.1-36	0
	2.10.1-36a	1
	2.10.1-37	0
	2.10.1-37a through 2.10.1-37b	1
	2.10.1-38 through 2.10.1-40	0
	2.10.1-40a	0
	2.10.1-41 through 2.10.1-42	0
	2.10.1-42a	0
	2.10.1-43 through 2.10.1-53	0
	2.10.1-53a	0
	2.10.1-54	0
	2.10.1-54a	0
	2.10.1-55 through 2.10.1-56	0
	2.10.1-56a through 2.10.1-56b	0
	2.10.1-57 through 2.10.1-58	0
	2.10.1-58a through 2.10.1-58b	0
	2.10.1-59 through 2.10.1-64	0
	2.10.1-64a through 2.10.1-64b	0
	2.10.1-65 through 2.10.1-101	0
	Figures 2.10.1-1 through 2.10.1-18	0
	Figure 2.10.1-18a	0
	Figure 2.10.1-19 through 2.10.1-22	0
	Tables 2.10.1-1a through 2.10.1-1b	0
	Tables 2.10.1-1 through 2.10.1-11	0
	Table 2.10.1-11a	0
	Table 2.10.1-12	0
	Table 2.10.1-12a	0
	Tables 2.10.1-13a through 2.10.1-13d	0

<u>SECTION</u>	<u>EFFECTIVE PAGES</u>	<u>REVISION NO.</u>
	Tables 2.10.1-14a through 2.10.1-14d	0
	Tables 2.10.1-15a through 2.10.1-15b	0
	Tables 2.10.1-16a through 2.10.1-16b	0
	Tables 2.10.1-17a through 2.10.1-17d	0
	Table 2.10.1-18	0
	Table 2.10.1-18a	0
	Tables 2.10.1-19a through 2.10.1-19c	0
	Tables 2.10.1-19 through 2.10.1-25	0
Appendix 2.10.2	2.10.2.1 through 2.10.2-iii	0
	2.10.2-1 through 2.10.2-62	0
	Figure 2.10.2-1a through 2.10.1-1b	0
	Figures 2.10.2-1 through 2.10.2-13	0
	Tables 2.10.2-1 through 2.10.2-18	0
Appendix 2.10.3	2.10.3-i through 2.10.3-ii	1
	2.10.3-1 through 2.10.3-40	1
Appendix 2.10.4	2.10.4-1	0
	2.10.4-1 through 2.10.4-15	0
	Figures 2.10.4-1 through 2.10.4-3	0
	Table 2.10.4-1	0
Appendix 2.10.5	2.10.5-1 through 2.10.5-5	0
Table of Contents Chapter Three	3-i through 3-iii	0
Chapter Three, Thermal Evaluation	3-1 through 3-31	0
	Figures 3-1 through 3-9	0
	Tables 3-1 through 3-7	0
Table of Contents Chapter Four	4-i through 4-ii	0
Chapter Four, Containment	4-1 through 4-12	0
	Figure 4-1	0
	Table 4-1	0
Table of Contents Chapter Five	5-1	1
	5-ii	0
Chapter Five, Shielding Evaluation	5-1	1
	5-2	0
	5-3 through 5-3a	1
	5-4	1
	5-5 through 5-12	0
	Figures 5-1 through 5-2	0
	Tables 5-1 through 5-6	0

REV 1

TN-FSV SAR  
LIST OF EFFECTIVE PAGES

<u>SECTION</u>	<u>EFFECTIVE PAGES</u>	<u>REVISION NO.</u>
Table of Contents Chapter Six	6-1 through 6-11	1
Chapter Six, Criticality Evaluation	6-1 through 6-15 Figures 6-1 through 6-3	1 0
Appendix 6.7	6.7-1 through 6.7-6	1
Table of Contents Chapter Seven	7-1	0
Chapter Seven, Operating Procedures	7-1 through 7-9	0
Table of Contents Chapter Eight	8-1	1
Chapter Eight, Acceptance Tests and Maintenance Program	8-1 through 8-2 8-3 through 8-5 8-6 8-7	0 1 0 1

**SAFETY ANALYSIS REPORT  
FOR THE  
TN-FSV PACKAGING**

**E-12564**

**Prepared for  
Public Service Company of Colorado**

**Rev. 0  
March 31, 1993**

**Rev. 1  
February 28, 1994**

**Transnuclear, Inc.  
Two Skyline Drive  
Hawthorne, New York 10532**

**TABLE OF CONTENTS**

	<u>Page</u>
1. GENERAL INFORMATION .....	1-1
1.1 Introduction .....	1-1
1.2 Package Description .....	1-2
1.3 Appendix .....	1-18
2. STRUCTURAL EVALUATION .....	2-1
2.1 Structural Design .....	2-1
2.2 Weights and Centers of Gravity .....	2-11
2.3 Mechanical Properties of Materials .....	2-12
2.4 General Standards for All Packages .....	2-23
2.5 Lifting and Tiedown Standards for All Packages .....	2-24
2.6 Normal Conditions of Transport .....	2-33
2.7 Hypothetical Accident Conditions .....	2-65
2.8 Special Form .....	2-90
2.9 Fuel Rods .....	2-90
2.10 Appendices .....	2.10.1-1
3. THERMAL EVALUATION .....	3-1
3.1 Discussion .....	3-1
3.2 Summary of Thermal Properties of Materials .....	3-3
3.3 Technical Specifications of Components .....	3-6
3.4 Thermal Evaluation for Normal Conditions of Transport .....	3-6
3.5 Hypothetical Accident Thermal Evaluation .....	3-16
3.6 References .....	3-31
4. CONTAINMENT .....	4-1
4.1 Containment Boundary .....	4-1
4.2 Requirements for Normal Conditions of Transport .....	4-6
4.3 Containment Requirements for Hypothetical Accident Conditions .....	4-11
4.4 References .....	4-12
5. SHIELDING EVALUATION .....	5-1
5.1 Discussion and Results .....	5-1
5.2 Source Specification .....	5-4
5.3 Model Specification .....	5-7
5.4 Shielding Evaluation .....	5-11
5.5 References .....	5-12

**TABLE OF CONTENTS (Cont'd)**

	<u>Page</u>
6. CRITICALITY EVALUATION .....	6-1
6.1 Discussion and Results .....	6-1
6.2 Packaging Fuel Loading .....	6-3
6.3 Model Specification .....	6-5
6.4 Criticality Calculations .....	6-8
6.5 Criticality Benchmark .....	6-15
6.6 References .....	6-15
6.7 Appendix .....	6.7-1
7. OPERATING PROCEDURES .....	7-1
7.1 Procedures for Loading Package .....	7-1
7.2 Procedures for Unloading Package .....	7-6
7.3 Preparation of Empty Package for Transport .....	7-9
8. ACCEPTANCE TESTS AND MAINTENANCE PROGRAM .....	8-1
8.1 Acceptance Tests .....	8-1
8.2 Maintenance Program .....	8-6

The total heat load dissipated by the fuel storage container is 360 watts which is the decay heat load design basis for the TN-FSV packaging.

The loaded weight of the FSC including the fuel and the depleted uranium plug is approximately 4,225 lbs.

## 1.3 APPENDIX

## TN-FSV DRAWINGS/DOCUMENTS

<u>DRAWING/DOCUMENT NO.</u>	<u>TITLE</u>	<u>REVISION</u>
1090-SAR-1	TN-FSV Packaging - Assembly	1
1090-SAR-2	Shell Assembly	1
1090-SAR-3	Details and Shell Parts List	1
1090-SAR-4	Shell Details	1
1090-SAR-5	Lid Assembly and Parts List	1
1090-SAR-6	Front Impact Limiter Assembly	1
1090-SAR-7	Front Impact Limiter Details & Parts List	1
1090-SAR-8	Rear Impact Limiter Assembly	1
1090-SAR-9	Rear Impact Limiter Details & Parts List	1
1090-SAR-10	Impact Limiter Attachment Bolt	1



# FIGURE WITHHELD UNDER 10 CFR 2.390

1	9/20/83	476	P.S.	65
RECEIVED BY MAIL 9/20/83 MAIL ROOM 1090 SAFARZ ALL INFORMATION CONTAINED HEREIN IS UNCLASSIFIED DATE 11/19/01 BY 60322/UC/STP				
APPROVALS	DATE	INITIALS	DATE	INITIALS
65	9/20/83	JTG	9/20/83	
TRANSNUCLEAR, INC. INTERNATIONAL, INC.				
TRANSY PACKAGING CELL ASSEMBLY				
476	9/20/83	D	1090 SAFARZ	1

**FIGURE WITHHELD UNDER 10 CFR 2.390**

NO.	DATE	DESCRIPTION	UNIT	QTY.	PRICE
APPROVALS	DATE	 <b>TRANSNUCLEAR, INC.</b> SUFFERN, N.Y.			
AS	7/1/93	TM-PV. PACKAGING SHELL DETAILS & FACTS LIST.			
JM	5/1/93				
JTG	27 Jan 93				
		AS AND R	10905 SAR-3	1	

**FIGURE WITHHELD UNDER 10 CFR 2.390**

1	1973	TRANSNUCLEAR, INC. REQUEST FOR APPROVAL OF A SHIELD PACKAGE FOR THE TRANSPORT OF RADIOACTIVE MATERIALS IN THE FORM OF A SHIELD PACKAGE UNDER 10 CFR 2.390	JTG	P.S.	ll
NO.	DATE	DESCRIPTION	INITIALS	CHK.	DATE
APPROVALS	DATE	 <b>TRANSNUCLEAR, INC.</b> BUFFALO, N.Y.  TN-15X PACKAGING SHELL DETAILS			
ll	9/1/73				
spm	7/1/73				
JTG	27 JAN 73	AT SHAW	D	1090-SAR-4	1

**FIGURE WITHHELD UNDER 10 CFR 2.390**

**FIGURE WITHHELD UNDER 10 CFR 2.390**

**FIGURE WITHHELD UNDER 10 CFR 2.390**

APPROVALS	DATE	TRANSNUCLEAR, INC. <small>HAIGHTON, N.Y.</small>			
<i>CC</i>	<i>7/1/73</i>	<i>TN-FSV PACKAGING FRONT IMPACT LIMITER DETAILS &amp; PARTS LIST</i>			
<i>JPM</i>	<i>7/1/73</i>				
<i>JTG</i>	<i>27 Jan 93</i>	<i>AS NOTED</i>	<i>D</i>	<i>1090-SAR-7</i>	<i>1</i>

**FIGURE WITHHELD UNDER 10 CFR 2.390**

APPROVALS	DATE	TRANSNUCLEAR, INC. BARTHOLOMEW, N.Y.			
<i>[Signature]</i>	7/1/73	TN-FSV PACKAGING REAR IMPACT LIMITER ASSEMBLY			
<i>[Signature]</i>	7/1/73				
JIG.	27 Jan 73	16 6/4	D	1090-SAR-B	1

**FIGURE WITHHELD UNDER 10 CFR 2.390**

SPECIALS	DATE	TRANSNUCLEAR, INC. <small>BRITTON, N.Y.</small>			
RF	2/10/93	TN-FSV PACKAGING REAR IMPACT LITER DETAILS & PARTS LIST			
JIG	27 Jan 93				
		AS NOTED	D	1090-SAR-9	1

# FIGURE WITHHELD UNDER 10 CFR 2.390

NO.	1	REV.	1/28	DATE	3/11/93	REVISIONS	DRAW.	J.T.G.	CR'D.	P.S.	PROJ.	85
APPROVALS	NOTE 2 - SEE 2580 HAS ACR 4414, LOT 2, DIM WAS 1.187" DIA, CYLINDRICAL PLATE THICKNESS WAS .002"											
PROJ.												
CR'D. BY												
DATE	27 JAN 93											
 <b>TRANSNUCLEAR, INC.</b> HAWTHORNE, N.Y.												
TN-FSV PACKAGING IMPACT LIMITER ATTACHMENT BOCT												
SCALE	NONE		SIZE	B		DATE	1090-SAR-10		REV. NO.	1		

CHAPTER TWO  
APPENDIX 2.10.1  
LIST OF FIGURES

		<u>PAGE</u>
Figure 2.10.1-1	TN-FSV Structure ANSYS Model-2D Axisymmetric	2.10.1-4
Figure 2.10.1-2	Boundary Conditions for Impact at Lid End	2.10.1-6
Figure 2.10.1-3	Boundary Conditions for the Following Load Cases: Pressure, 1G Down, Vibration, Shock, Tiedown, Side Drop, Bolt Preload, Thermal, 15° Drop, 45° Drop, 70° Drop, C.G. Over Corner Drop, Bottom End Drop	2.10.1-7
Figure 2.10.1-4	Load Distribution-Internal Pressure	2.10.1-11
Figure 2.10.1-5	Load Distribution-External Pressure	2.10.1-12
Figure 2.10.1-6	Load Distribution-Impact at Bottom End	2.10.1-13
Figure 2.10.1-7	Load Distribution-Impact at Lid End	2.10.1-16
Figure 2.10.1-8	Fourier Coefficients for the Function $\cos \theta$ ( $90^\circ \sim 270^\circ$ )	2.10.1-19
Figure 2.10.1-9	Fourier Coefficients for the Function $\cos \theta$ ( $-90^\circ \sim 90^\circ$ )	2.10.1-20
Figure 2.10.1-10	Locations of C.G., Trunnions and Saddle	2.10.1-22
Figure 2.10.1-11	Load Distribution-1G Longitudinal (Cask Horizontal Supported by 2 Rear Trunnions)	2.10.1-23
Figure 2.10.1-12	Load Distribution-1G Vertical Down (Cask Horizontal Supported by 2 Rear Trunnions and Front Saddle)	2.10.1-27
Figure 2.10.1-13	Load Distribution - Side Drop	2.10.1-29
Figure 2.10.1-14	Load Distribution - C.G. Over Corner Drop	2.10.1-32
Figure 2.10.1-15	Load Distribution - 15° Slap Down (Second Impact at Lid End)	2.10.1-35

CHAPTER TWO  
APPENDIX 2.10.1  
LIST OF FIGURES

		<u>PAGE</u>
Figure 2.10.1-15a	Rotational Quasistatic Equilibrium -15° Slapdown (Second Impact at Lid)	2.10.1-35a
Figure 2.10.1-16	Load Distribution - 45° Oblique Drop Impact at Lid End	2.10.1-36
Figure 2.10.1-16a	Rotational Quasistatic Equilibrium -45° (Oblique Drop Impact at Lid End)	2.10.1-36a
Figure 2.10.1-17	Load Distribution -70° Oblique Drop Impact at Lid End	2.10.1-37
Figure 2.10.1-17a	Rotational Quasistatic Equilibrium -70° (Oblique Drop Impact at Lid End)	2.10.1-37a
Figure 2.10.1-17b	Transverse G Load Combinations	2.10.1-37b
Figure 2.10.1-18	Standard Stress Reporting Locations	2.10.1-40
Figure 2.10.1-18a	Additional Stress Reporting Locations for Lid End Drop, Bottom End Drop, Side Drop, C.G. Over Corner Drop and 70° Drop	2.10.1-40A
Figure 2.10.1-19	TN-FSV Lid Closure	2.10.1-79
Figure 2.10.1-20	TN-FSV Lid Bolt	2.10.1-80
Figure 2.10.1-21	TN-FSV Lid Bolt Arrangement	2.10.1-81
Figure 2.10.1-22	Schematic of Stress Histogram at Bolts (K=4)	2.10.1-94

5. Oblique (15°, 45°, 70°) impact at lid end.

- (a) The crush footprint of the impact limiter was projected to the cask surface. The impact force was determined from the inertial loading reported in Appendix 2.10.2. The crush force was converted into an equivalent element surface pressure (which varies sinusoidally in both the circumferential and axial directions) which was applied normal to the surfaces.
- (b) The axial and lateral inertia loads of the cask, were applied as inertia (body) loads in the finite element model.
- (c) The cask contents inertia load was again resolved into components acting in two mutually perpendicular directions. The component in the axial direction was applied as a pressure acting on the inside surface of the lid. The lateral component was applied as a pressure acting over the lower half of the inside surface of the inner shell. In this case, these pressures are not only varied sinusoidally around the circumference but also varied linearly with distance from the center of the surface to which they are applied since the containment vessel is being subjected to rotational as well as axial and lateral accelerations.

- (d) A rotational acceleration,  $\alpha$ , was also input to the finite element model to satisfy the rotational quasistatic equilibrium condition:

$$\Sigma M_{C.G.} = 0$$

The rotational acceleration,  $\alpha$ , required to place the model in equilibrium was calculated based on:

$$I_{C.G.} \alpha = \Sigma M = F_1 d_1 + F_2 d_2 + F_3 d_3 + \dots$$

$$\alpha = \frac{F_1 d_1 + F_2 d_2 + F_3 d_3 + \dots}{I_{C.G.}}$$

where  $F_1$ ,  $F_2$ , etc. are the various inertial loadings in the systems of forces.

Where

$I_{C.G.}$  = Mass moment of inertia of containment vessel about its C.G.

$\Sigma M_{C.G.}$  = net moment about the center of gravity resulting from loads acting normal and axial on the finite element model.

Figures 2.10.1-15, 2.10.1-15a, 2.10.1-16, 2.10.1-16a, 2.10.1-17 and 2.10.1-17a graphically depict these loadings.

- (e) As described above, except  $0^\circ$  side drop and  $80^\circ$  c.g. over corner drop, all the oblique impacts will include the axial, normal and rotational accelerations. The transverse G loads predicted by ADOC computer program reported in Appendix 2.10.2 are based on combining the normal and rotational accelerations as shown on Figure 2.10.1-17b.

2.10.1-35

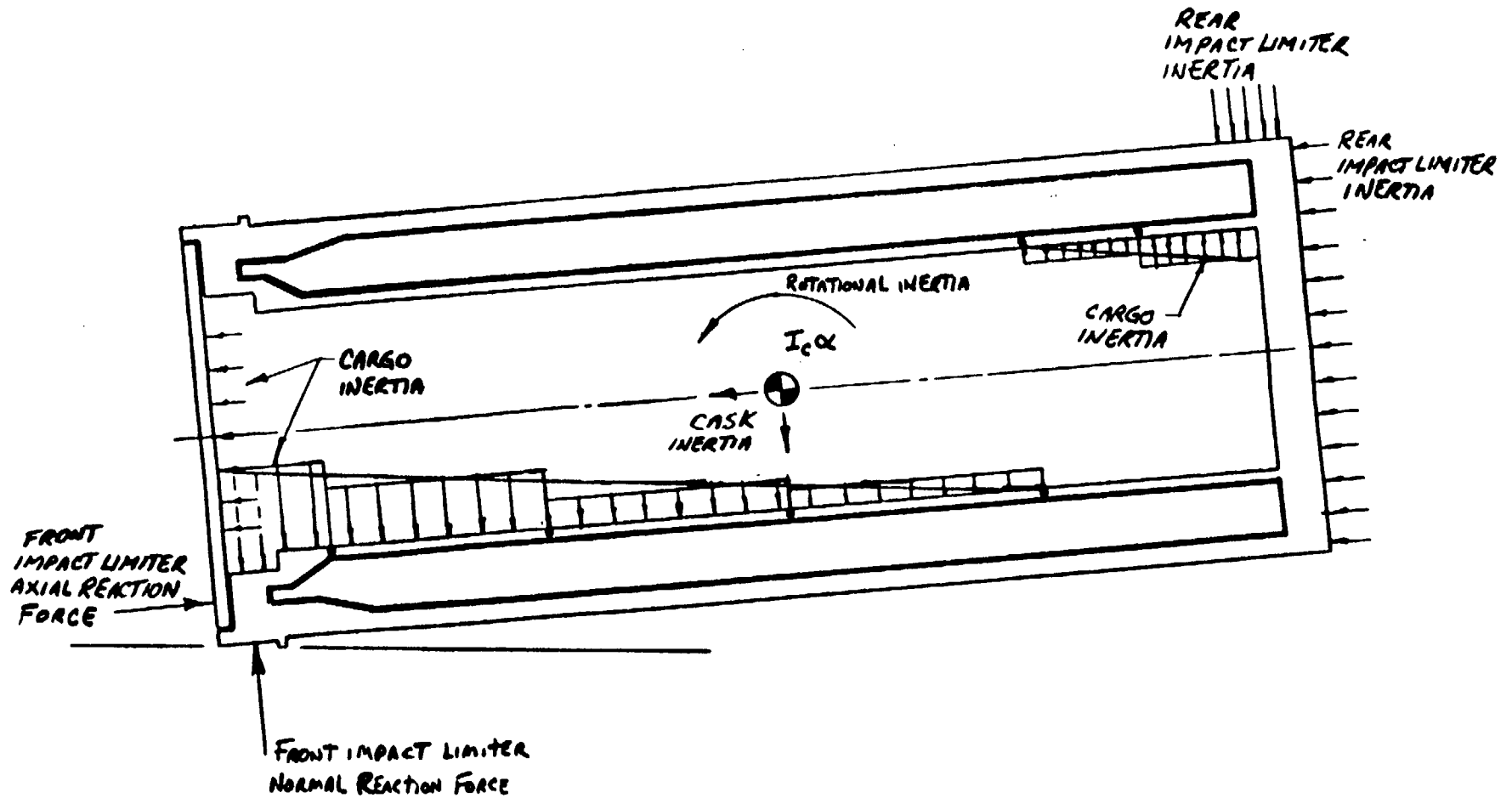
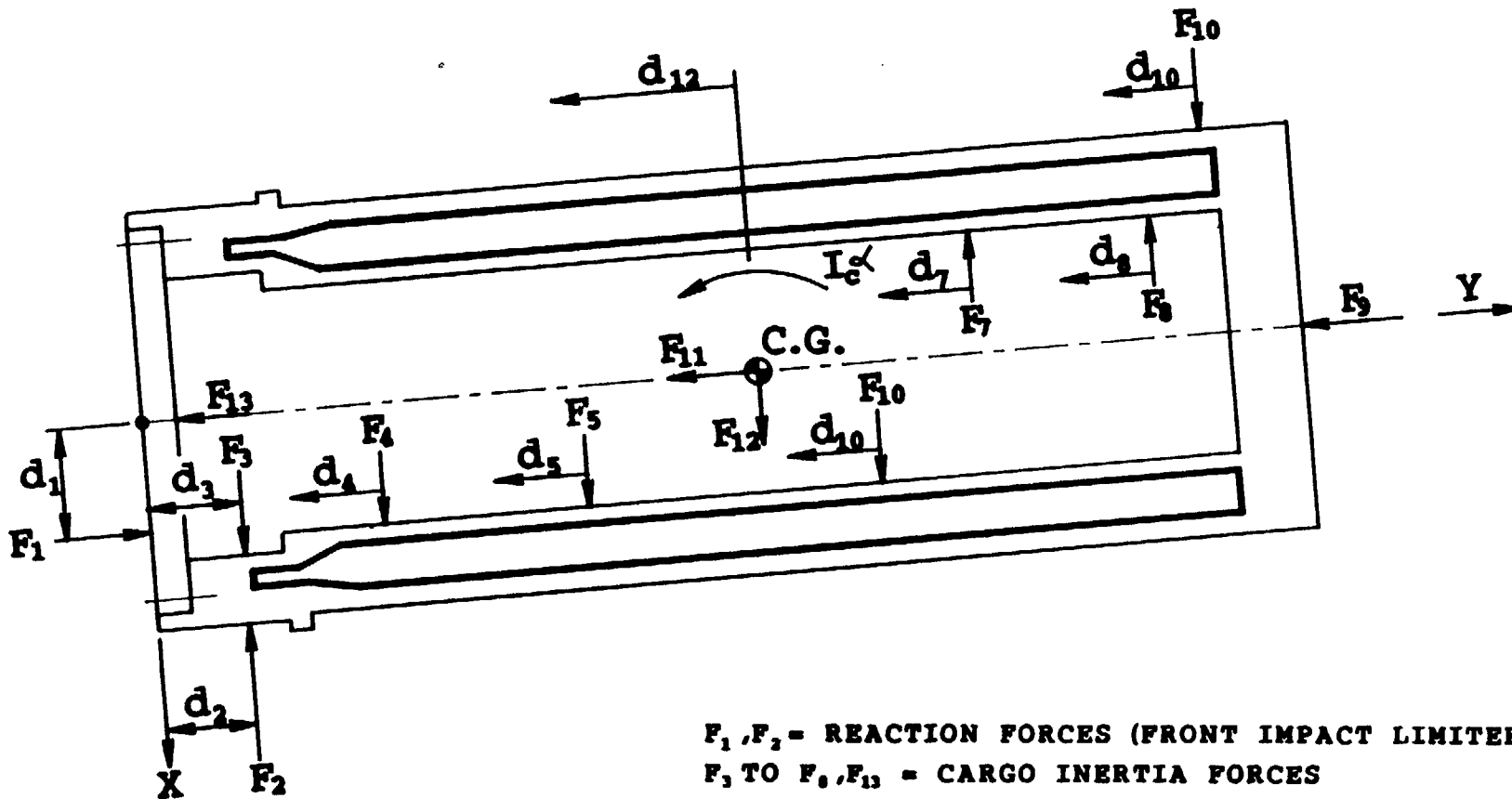


FIGURE 2.10.1-15  
LOAD DISTRIBUTION - 15° SLAP DOWN (SECOND IMPACT AT LID END)

2.10.1-35a



$F_1, F_2$  = REACTION FORCES (FRONT IMPACT LIMITER)  
 $F_3$  TO  $F_8, F_{13}$  = CARGO INERTIA FORCES  
 $F_9, F_{10}$  = REACTION FORCES (REAR IMPACT LIMITER)  
 $F_{11}, F_{12}$  = CASK INERTIA FORCES  
 $I_c$  = MASS MOMENT INERTIA OF CASK  
 $\alpha$  = ROTATIONAL ACCELERATION

**FIGURE 2.10.1-15a**

**ROTATIONAL QUASISTATIC EQUILIBRIUM - 15° SLAP DOWN  
(SECOND IMPACT AT LID)**

REV. 1

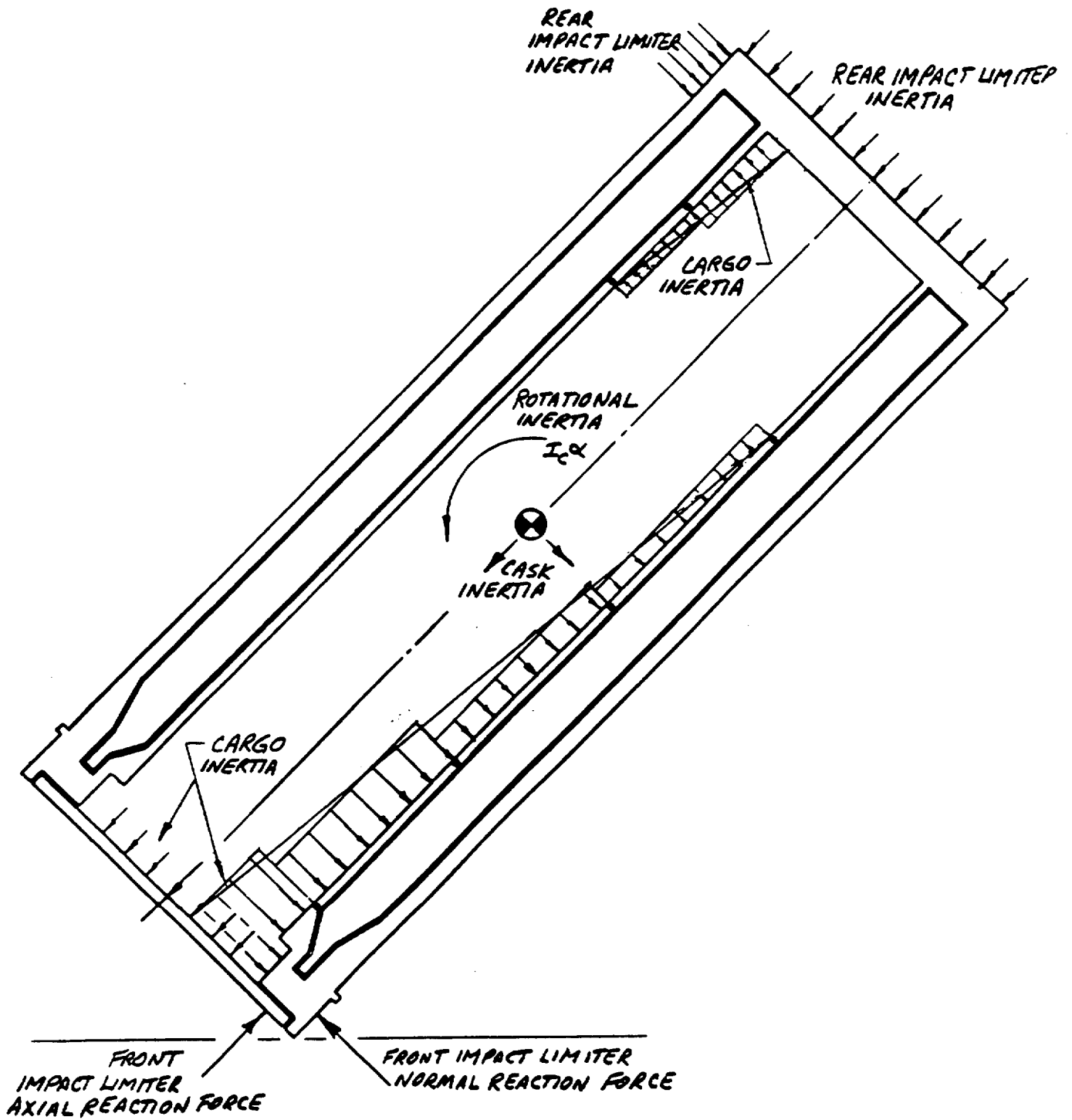
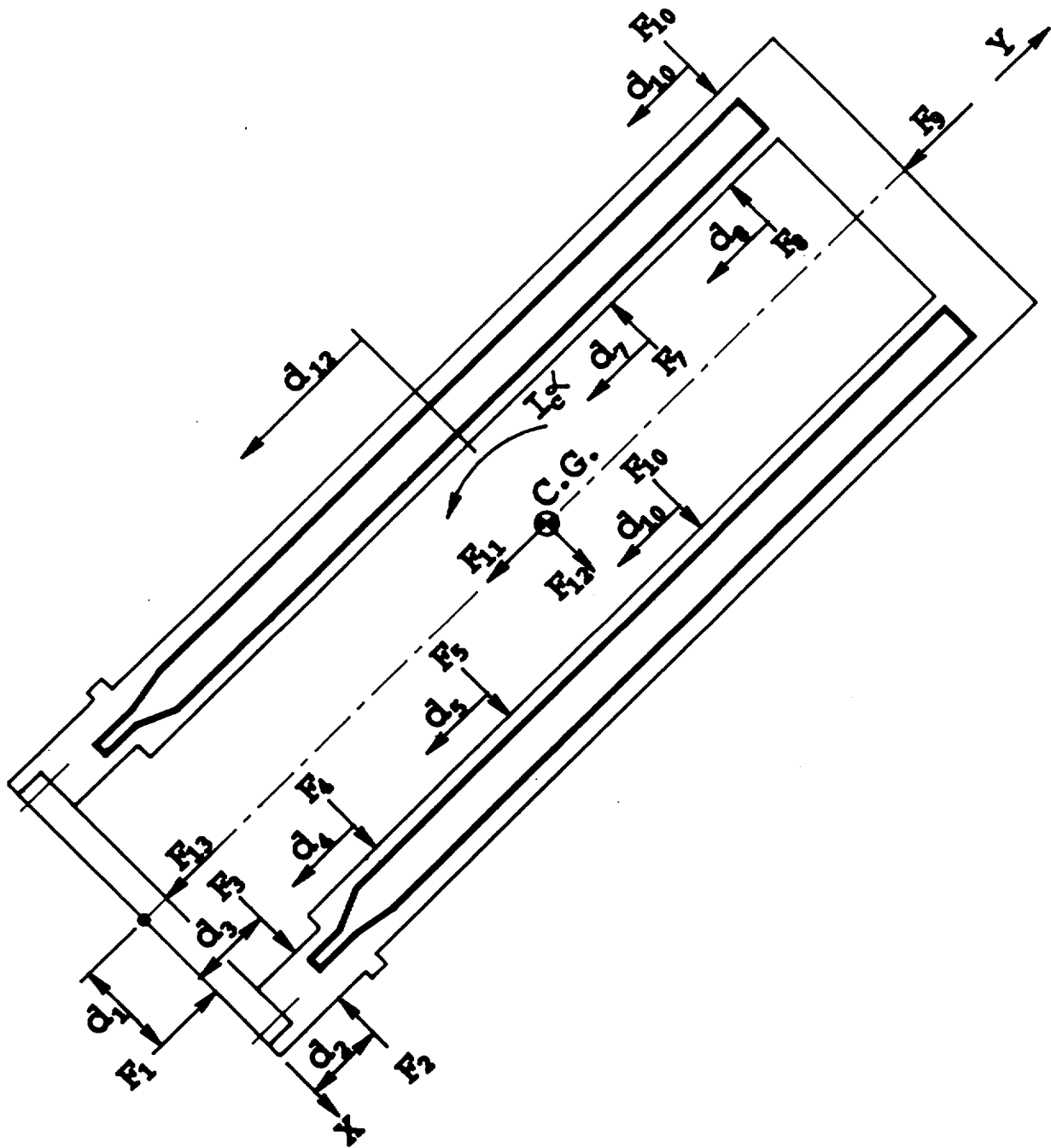


FIGURE 2.10.1-16  
LOAD DISTRIBUTION - 45° OBLIQUE DROP IMPACT AT LID END



$F_1, F_2$  = REACTION FORCES (FRONT IMPACT LIMITER)  
 $F_3$  TO  $F_8, F_{13}$  = CARGO INERTIA FORCES  
 $F_9, F_{10}$  = REACTION FORCES (REAR IMPACT LIMITER)  
 $F_{11}, F_{12}$  = CASK INERTIA FORCES  
 $I_c$  = MASS MOMENT INERTIA OF CASK  
 $\alpha$  = ROTATIONAL ACCELERATION

**FIGURE 2.10.1-16a**  
**ROTATIONAL QUASISTATIC EQUILIBRIUM-45°**  
**(OBLIQUE DROP IMPACT AT LID END)**

2.10.1-36a

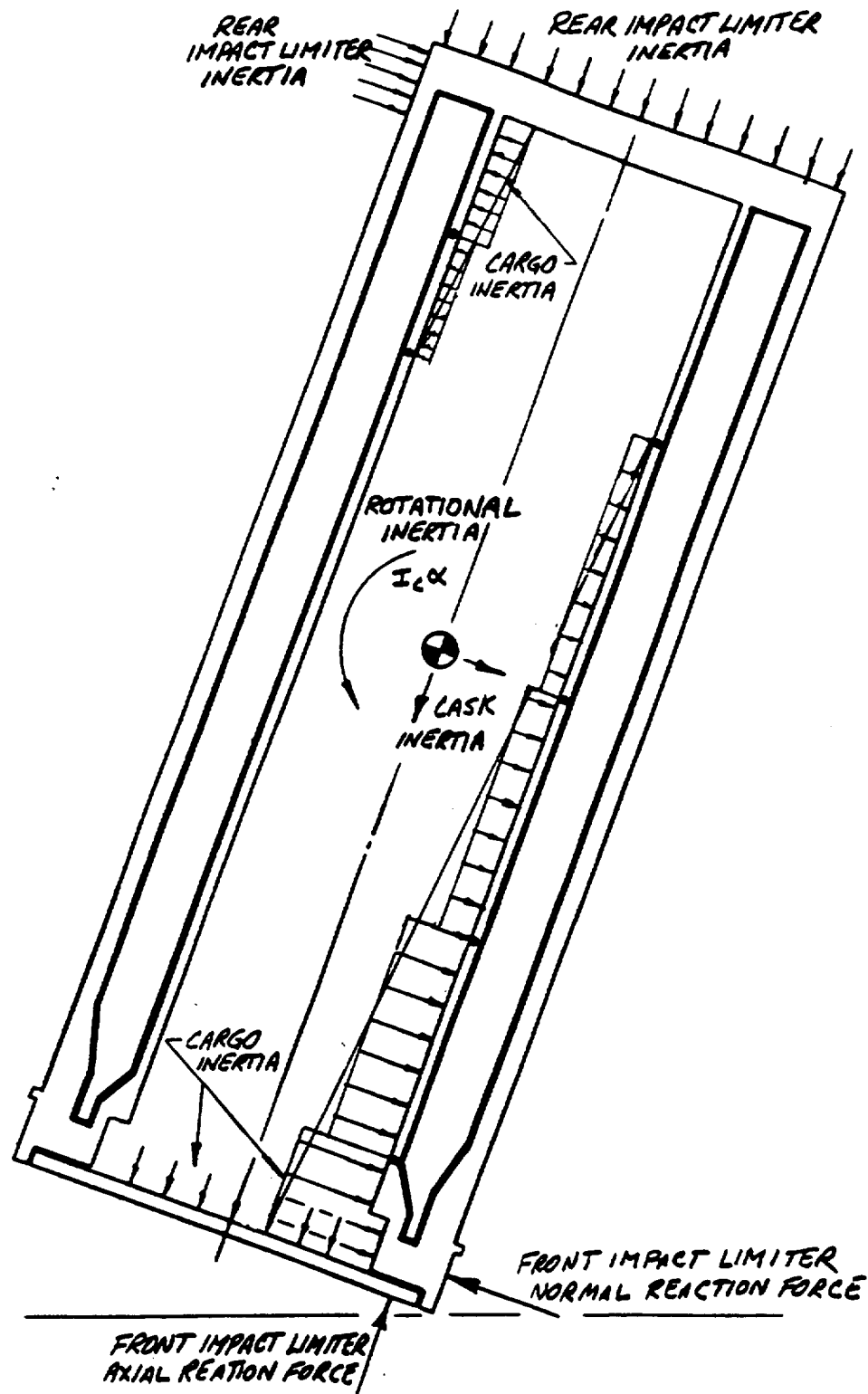
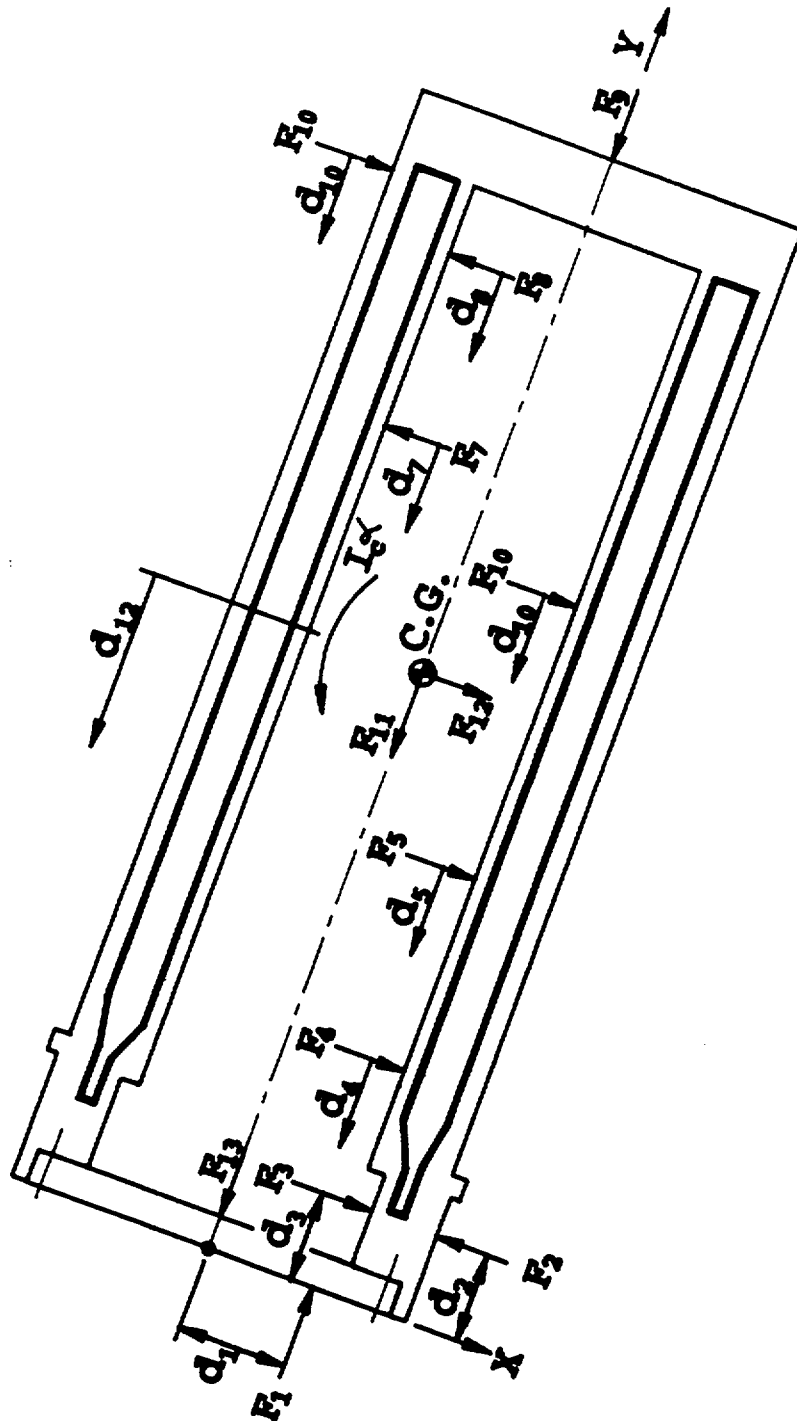


FIGURE 2.10.1-17  
LOAD DISTRIBUTION - 70° OBLIQUE DROP IMPACT AT LID END

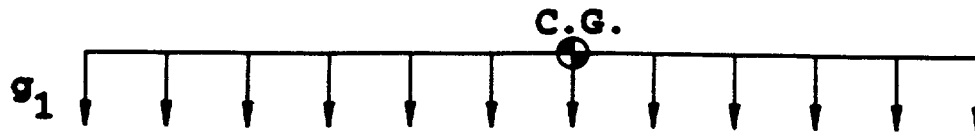


$F_1, F_2$  = REACTION FORCES (FRONT IMPACT LIMITER)  
 $F_3$  TO  $F_8, F_{13}$  = CARGO INERTIA FORCES  
 $F_9, F_{10}$  = REACTION FORCES (REAR IMPACT LIMITER)  
 $F_{11}, F_{12}$  = CASK INERTIA FORCES  
 $I_c$  = MASS MOMENT INERTIA OF CASK  
 $\alpha$  = ROTATIONAL ACCELERATION

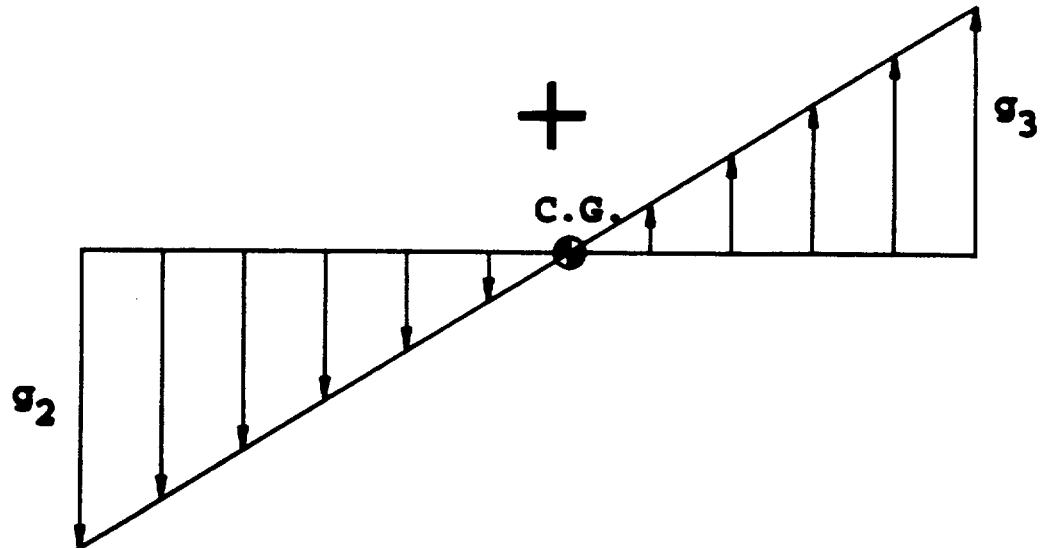
**FIGURE 2.10.1-17a**

**ROTATIONAL QUASISTATIC EQUILIBRIUM-70°**  
**(OBLIQUE DROP IMPACT AT LID END)**

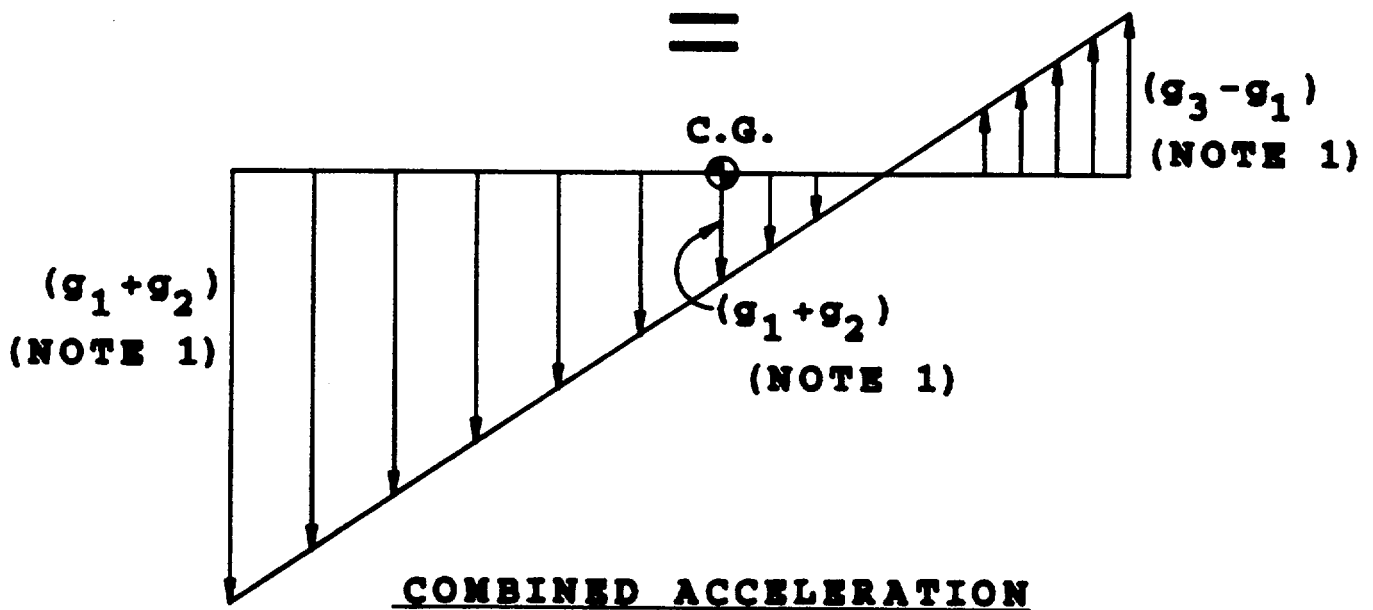
2.10.1-37a



NORMAL ACCELERATION



ROTATIONAL ACCELERATION



COMBINED ACCELERATION

NOTE: 1. TRANSVERSE G LOADS REPORTED  
IN TABLES 2.10.2-3 AND 2.10.2-4

FIGURE 2.10.1-17b

TRANSVERSE G LOAD COMBINATIONS

2.10.1-37b

## Stress Results

Detailed stresses and displacements in the ANSYS model of the cask body are obtained and stored (on magnetic tape) for every node location for each individual load case. These stored results are postprocessed to printout the stresses at the 17 standard locations on the cask body structure shown in Figure 2.10.1-18. The locations selected as shown in Figure 2.10.1-18 are key points that, when carefully studied, indicate the behavior of the entire structure. The maximum stress may occur at a different location for each individual load.

The individual load cases analyzed are listed in Table 2.10.1-1A. Linear elastic analyses were performed for all load cases. The meridional and hoop membrane and bending stress components for each of the eighteen ANSYS finite element model load cases are reported in Tables 2.10.1-1 to 2.10.1-18 as listed in Table 2.10.1-1A. These stress components are combined for the various load combinations as described in Sections 2.6 and 2.7 by factoring and algebraic addition. Then the stress intensities of each category are determined and compared to the specific limits. See Sections 2.6 and 2.7.

The local stresses at the trunnion locations for cases where the cask is supported on the trunnions are not included in these results. The local stresses are obtained as described below in Section 2.10.1.2 and they are reported in that section. The method used is the "Bijlaard" analysis using hand calculations rather than the ANSYS model.

It should be noted that, for the axisymmetric analyses, the stress is constant around the cask at every location. For asymmetric analyses with significant differences in stress magnitudes on the extreme opposite sides of the cask the stresses at locations on both sides of the cask (contacting side and side opposite contact during

CHAPTER TWO  
APPENDIX 2.10.3  
LIST OF FIGURES

	<u>PAGE</u>
Figure 2.10.3-1	2.10.3-5
Figure 2.10.3-2	2.10.3-6
Figure 2.10.3-3	2.10.3-9
Figure 2.10.3-4	2.10.3-11
Figure 2.10.3-5	2.10.3-13
Figure 2.10.3-6	2.10.3-17
Figure 2.10.3-7	2.10.3-18
Figure 2.10.3-8	2.10.3-19
Figure 2.10.3-9	2.10.3-20
Figure 2.10.3-10	2.10.3-21
Figure 2.10.3-11	2.10.3-24
Figure 2.10.3-12	2.10.3-27
Figure 2.10.3-13	2.10.3-28

CHAPTER TWO  
APPENDIX 2.10.3  
LIST OF TABLES

		<u>PAGE</u>
TABLE 2.10.3-1	Comparison of One-Half Scale Model Static Crush Test Results With Predictions	2.10.3-14
Table 2.10.3-2	Comparison of One-Half Scale Model Static and Dynamic Test Results	2.10.3-26

## APPENDIX 2.10.3 IMPACT LIMITER TESTING

2.10.3.1 Introduction

A series of static and dynamic tests was performed on three one-half scale models of the TN-FSV impact limiters. The tests were performed to evaluate the effect of the 30-foot free drop hypothetical accident defined in 10 CFR 71.73(c)(1). The test results were used to verify the analyses performed for the TN-FSV. The objectives of the test program were to:

- ° Demonstrate that the inertia g values and forces calculated in Appendix 2.10.2 and used in the analyses presented in Appendix 2.10.1 are acceptable.
- ° Develop load-displacement curves resulting from the crushing of the impact limiters at various orientations.
- ° Demonstrate that the impact limiters do not "bottom out".
- ° Verify the adequacy of the impact limiter attachment bolts.
- ° Demonstrate the adequacy of the impact limiter enclosure.

The three one-half scale impact limiters were identified as A, B and C and tested by the following sequence:

STATIC TEST		DYNAMIC TEST			
0°	80°	15° SLAPDOWN		80° CORNER DROP	
SIDE TEST	CORNER TEST	FIRST IMPACT	SECOND IMPACT	FIRST IMPACT	SECOND IMPACT
A	A ROTATED 180°	C	B	C ROTATED 180°	B ROTATED 180°

Static Crush tests to establish load versus displacement curves were performed at room temperature for the following orientations:

- 1) 0° side crush
- 2) 80° corner crush

The 0° orientation was selected because it has the highest transverse g loading at the center of gravity. The 80° corner crush test was selected because it has high axial g loadings, and higher expected impact limiter deformations than the end drop.

Two 30-foot drop tests were performed at low temperature to evaluate the adequacy of the impact limiter enclosure and attachments. The orientations were:

- 1) 15° slap down (shallow angle side drop)
- 2) 80° corner drop.

The 15 degree slap down orientation was selected because it puts the highest stresses on the attachment bolts, and it is the orientation for which the highest impact force is expected for a side drop orientation. The 80 degree corner drop was selected to compare with the static test and because it is the orientation for which limiter deformation is expected to be large and for which significant decelerations are expected.

#### 2.10.3.2 Scaling Relationships

The models were constructed with a geometric scale factor of  $1/\lambda = 1/2$ . As a consequence, the following scale factors were applied:

Length:

$$L_p = \lambda L_m$$

Surface area:

$$A_p = \lambda^2 A_m$$

Moment of Inertia:

$$I_p = \lambda^4 I_m$$

Section Modulus:

$$S_p = \lambda^3 S_m$$

Weight:

$$W_p = \lambda^3 W_m$$

Energy absorbed during drop (from same height h):

$$E_p = W_p h = \lambda^3 W_m h = \lambda^3 E_m$$

Velocity at beginning of impact:

$$V_p = \sqrt{2gh} = V_m$$

where  $\lambda$  : scale factor  
 the subscript p: refers to the full size  
 the subscript m: refers to the model

During impact, the impact limiter materials deform or crush. As the model and full size impact limiters are made of the same materials, they deform under the same stress:

$$S_p = S_m$$

Therefore we have:

Force during impact:

$$F_p = S_p A_p = S_m \lambda^2 A_m = \lambda^2 F_m$$

Deformation:

$$D_p = E_p/F_p = \lambda^3 E_m/\lambda^2 F_m = \lambda D_m$$

Impact Duration:

$$T_p = D_p/V_p = \lambda D_m/V_m = \lambda T_m$$

Impact Deceleration:

$$a_p = V_p/T_p = V_m/\lambda T_m = 1/\lambda a_m$$

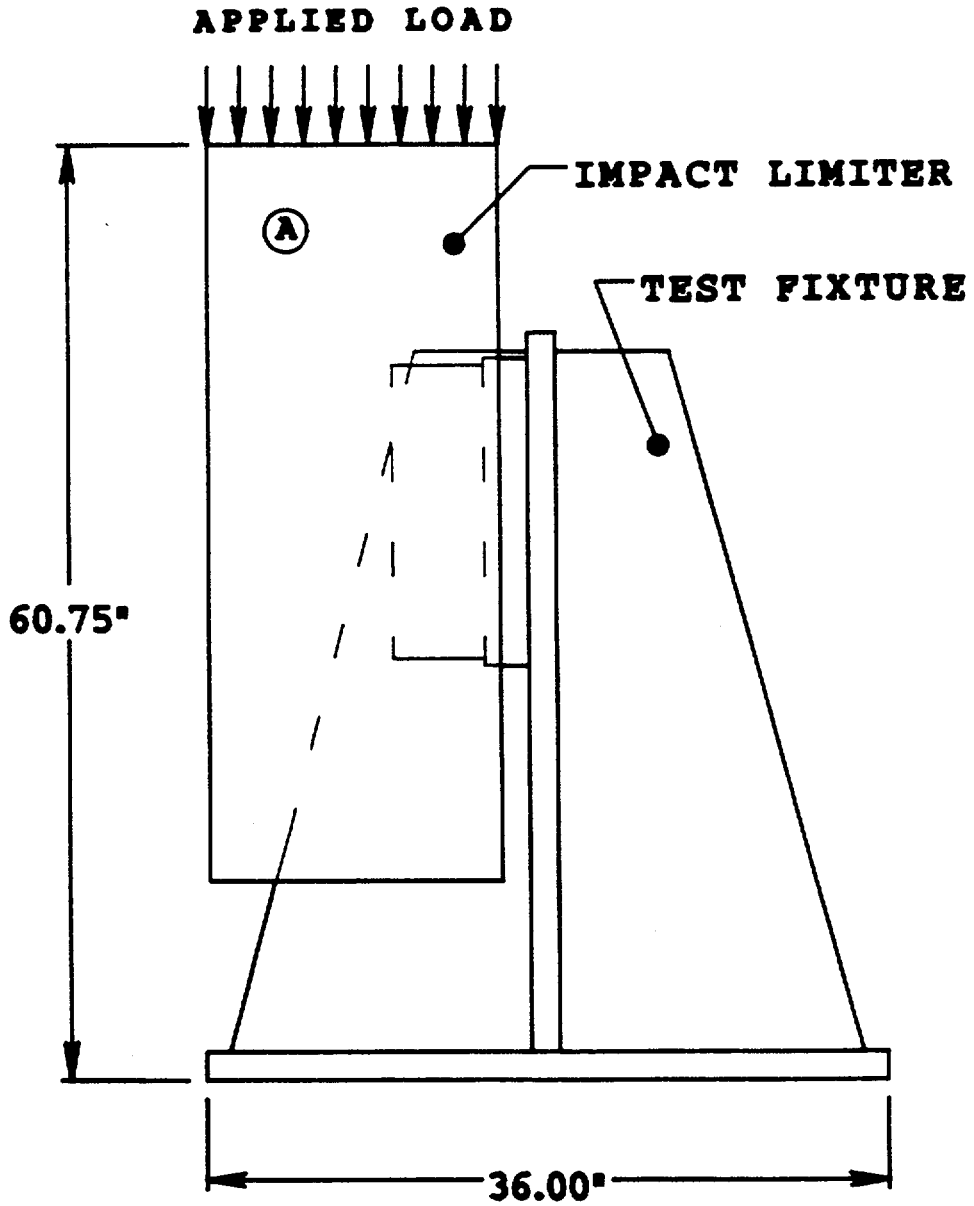
### 2.10.3.3 Static Testing

#### Test Model and Test Description

Two static crush tests of a one-half scale TN-FSV impact limiter were performed at the Pittsburgh Testing Laboratory to generate load versus displacement curves to compare with the force-deflection curves generated by the ADOC computer code described in Appendix 2.10.2 for two orientations. The following tests were performed:

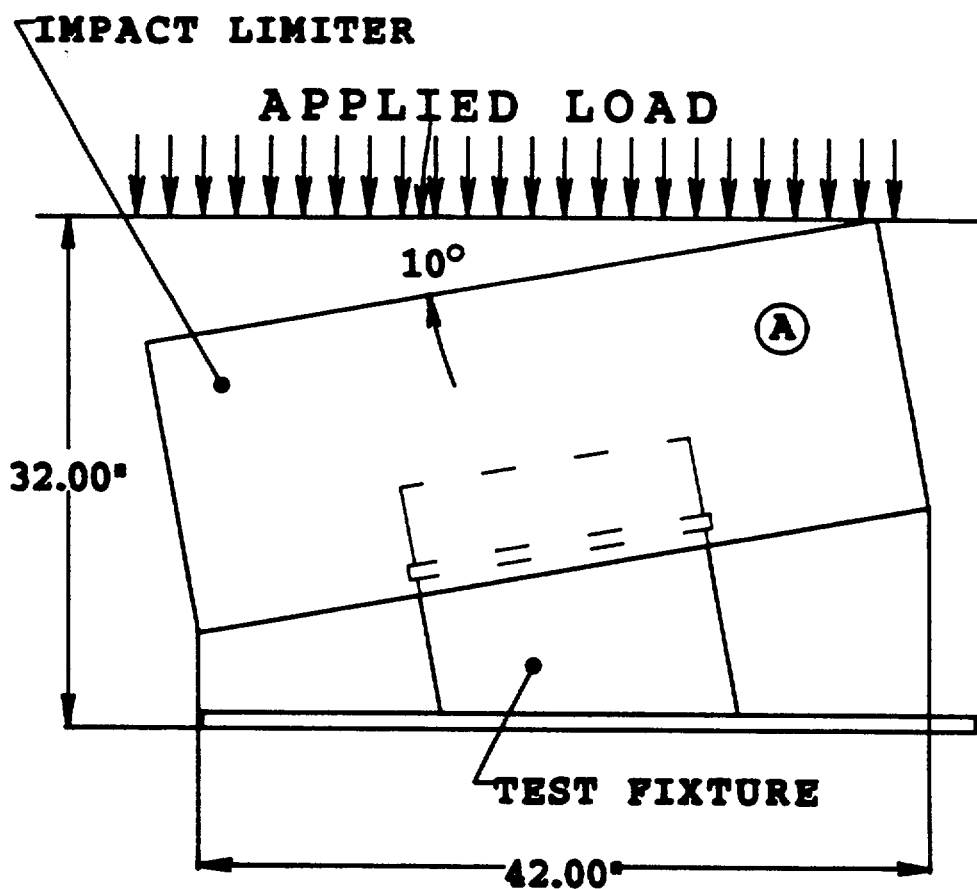
- ° Load applied radially on the side of the impact limiter (Figure 2.10.3-1)
- ° Load applied on the corner at an angle of 10° to simulate the 80° corner drop (Figure 2.10.3-2).

The one-half scale model impact limiter is a scale model of the full size front impact limiter. The stainless steel impact limiter structure is the same as that described in Appendix 2.10.2, i.e., steel shells closed off by flat plates and reinforced by six (6) radial gussets. The model and full scale configurations are identical, but all linear dimensions in the model are one-half scale. The balsa and redwood densities used in the model are consistent with



○ - IMPACT LIMITER REFERENCE NUMBER

**FIGURE 2.10.3-1  
SIDE CRUSH TEST CONFIGURATION**



○ - IMPACT LIMITER REFERENCE NUMBER

**FIGURE 2.10.3-2  
CORNER CRUSH TEST CONFIGURATION**

that specified for fabrication of the full scale impact limiters. The wood used in the models had densities on the high end of the specified range. The model contains the same number of wood blocks as the full size impact limiters. The wood blocks are made up of a number of smaller pieces of wood glued together with phenol resorcinol adhesive, using the same procedure to be used on the full-size impact limiters.

The attachment bolts are made from the material specified for the full size limiters. Bolts (5/8-11-2A) with an undercut shank diameter of 0.511 in. were used on the models.

The fusible plugs, alignment pins with reinforcement pads, supports and support pads, handles and handle pads were not included in the models. They do not affect the compression properties of the impact limiter. The lifting lugs were made larger than half-scale to facilitate handling. These lifting lugs were positioned so that they would not interfere with the tests.

The fixtures were made of carbon steel, and modeled the following dimensions of the cask:

- ° outside diameter
- ° impact limiter attachments holes (6)
- ° The 1.62" (full scale) shelf ring located 11.38 inches below the top of the cask.

The fixtures were heavy weldments which could not deflect during the crush test.

The impact limiters were mounted to the test fixtures as shown in Figures 2.10.3-1 and -2. The testing was performed using a  $1.2 \times 10^6$  lb. compression testing machine capable of generating much more than the required load. The loading surface was maintained perpendicular to the direction of crushing and the massive impact limiter support fixture was restrained from shifting during loading.

### Required Energy Absorption Versus Test Orientation

100% of the kinetic energy of the model cask must be absorbed by a single limiter for the 80° corner test which is very nearly a CG over corner test. In a 0° side impact, 50% of the total energy must be absorbed by each of the two limiters. During a shallow angle (slapdown) side drop, the energy is not equally shared by the two limiters. Based on ADOC analyses for a 15° side drop, roughly 68% of the energy is absorbed by the impact limiter hitting second. The hit on the second impact limiter is nearly the same as a 0° side drop. Therefore, the 0° static crush test was continued to an energy level beyond 50% to approximate the second hit of the 15° side drop.

### Side Crush Test Sequence

The deflection of the impact limiter was measured continuously during the test using a linear potentiometer mounted to the testing machine crosshead. The crush force versus vertical movement of the test plate was recorded continuously on an x-y plotter. The side crush test was terminated when the deflection reached approximately 5 inches and a total of 81% of the required energy was absorbed (5 of the 6 attachment bolts were simultaneously broken at this point). The load versus displacement plot is shown in Figure 2.10.3-3.

Significant deformation of the impact limiter was evident after the test. The bolt tunnels above the heads of the attachment bolts collapsed so that the heads of the bolts were inaccessible. The weld seams between the outer cylindrical shell and the flat plates on the front edge of the impact limiter tore approximately 3-4 inches in length in two places directly below the impact surface. Similarly a 3 inch tear on the back edge of the impact limiter was evident. After the impact limiter was removed from the fixture, evidence of inside crushing of the impact limiter was noticed. The seam between the inner cylindrical shell and circular plate had split in the region closest to the impact.

Deformation of the impact limiters was measured and recorded. Due to deformation of the bolt hole tunnels, the impact limiter could not be

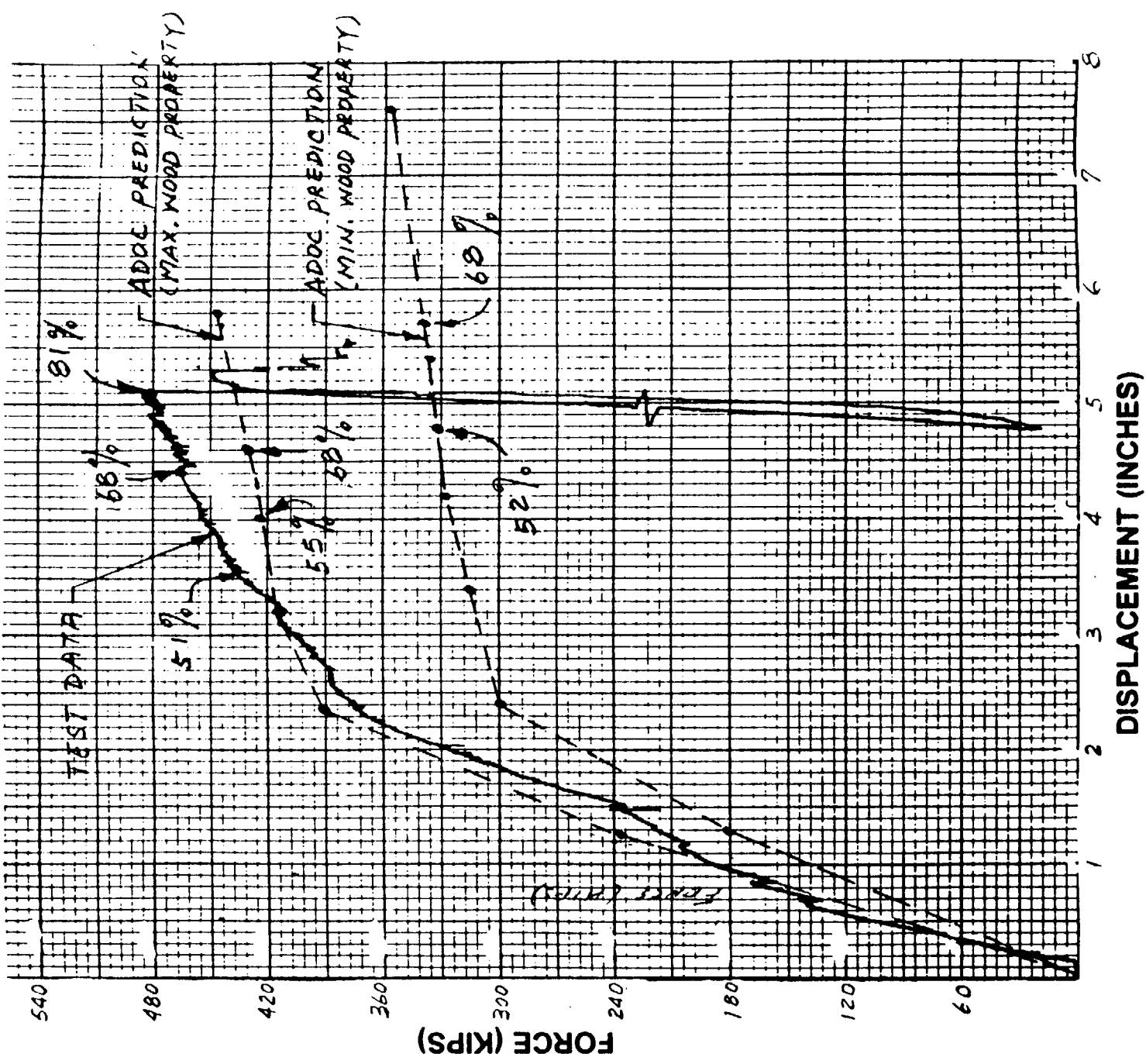


**FIGURE 2.10.3-3**  
**ONE-HALF SCALE MODEL IMPACT LIMITER**  
**LOAD VS DISPLACEMENT- 0' SIDE TEST**

removed from the test fixture without machining off the head of the remaining attachment bolt.

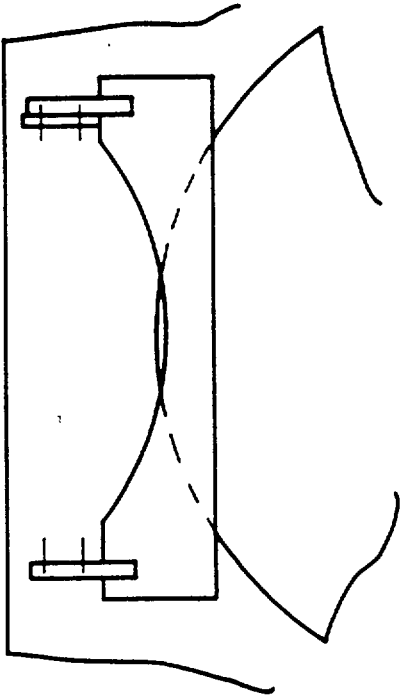
#### Corner Crush Test Sequence

After the limiter was removed from the side crush fixture, the same limiter was placed onto the corner crush fixture (Figure 2.10.3-2). Because of distortion from the side crush test, only one (1) bolt hole lined up with the corner crush fixture and was installed. A hold down plate on the lower edge of the limiter was used to keep the impact limiter from rotating on the fixture (Figure 2.10.3-4). The load was applied until the loading plate touched the limiter. The LVDT and recorder were zeroed.

During the initial loading sequence, the recorder pen began to oscillate and a smooth force displacement curve was not possible. At 100,000 lbs., the recorder was shut off to stop the motion. When it was turned back on, the pen went back to the original displacement and load at a force of 120,000 lbs. The test was put on hold while the oscillation problem was investigated. It turned out that welding was being performed in the area and the sensitive recorder was picking up electrical signals from the welding torch. The welding was stopped and the crush test continued. The deflection at this time was 1 1/2 inch. The load was increased, and the hold down plate was removed just before the loading plate contacted it. At this point, the load was 190,000 lbs. and the deflection was 1.9 inches.

The test was terminated after the deflection reached 7 inches and a total of 113% of the required energy was absorbed. (See Figure 2.10.3-5)

The bolt tunnels above where the bolts are installed had buckled and folded closing the bolt holes. The outer cylinder bulged near the top seam. No exterior seams opened as a result of the corner crush test.



TOP VIEW

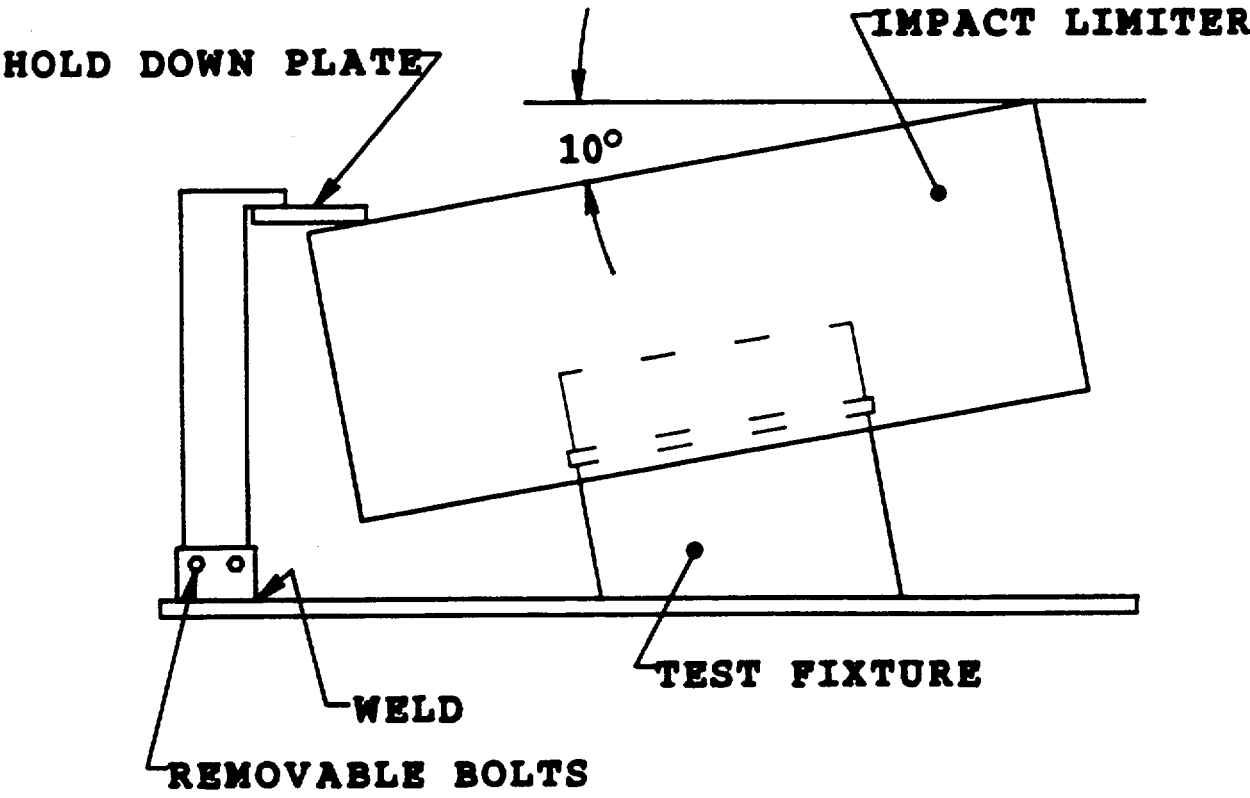


FIGURE 2.10.3-4  
CORNER CRUSH TEST  
SET UP

After the 80° corner crush test, one segment of the impact limiter was cut open and the wood removed and examined. It was noted that glue joints between the individual pieces of wood in the blocks did not fail as the wood crushed.

#### Test Data and Test Results

The measured load versus displacement (force versus deflection) curves for the model impact limiter are shown on Figures 2.10.3-3 and 2.10.3-5 for the 0° side and 80° corner static crush tests, respectively. The results of these tests are summarized in Table 2.10.3-1 and compared to predictions made using the ADOC computer program.

Table 2.10.3-1 identifies the angular orientation of the impact limiter axis relative to the test machine loading plate (target) and the energy to be absorbed. The correlation between measured data and predictions is good. As shown in Figures 2.10.3-3 and 2.10.3-5, the measured force deflection curves are slightly higher than the curves predicted by ADOC. Since the density of the wood in the test impact limiter was on the high end of the acceptable range, it was expected that the measured force deflection curves would follow the maximum wood properties curve. The wood blocks in the limiter are well positioned by the metal structure at these crush orientations. The forces used in the stress calculations in Appendix 2.10.1 are higher than the predicted and measured crush forces. Based on these tests, it can be concluded that:

- ° The static tests demonstrated that the impact limiters can absorb the required energy without failing or "bottoming out".
- ° The impact limiter attachment bolts can withstand the loading for the side drop and second hit of the 15° slapdown.

2:10.3-13

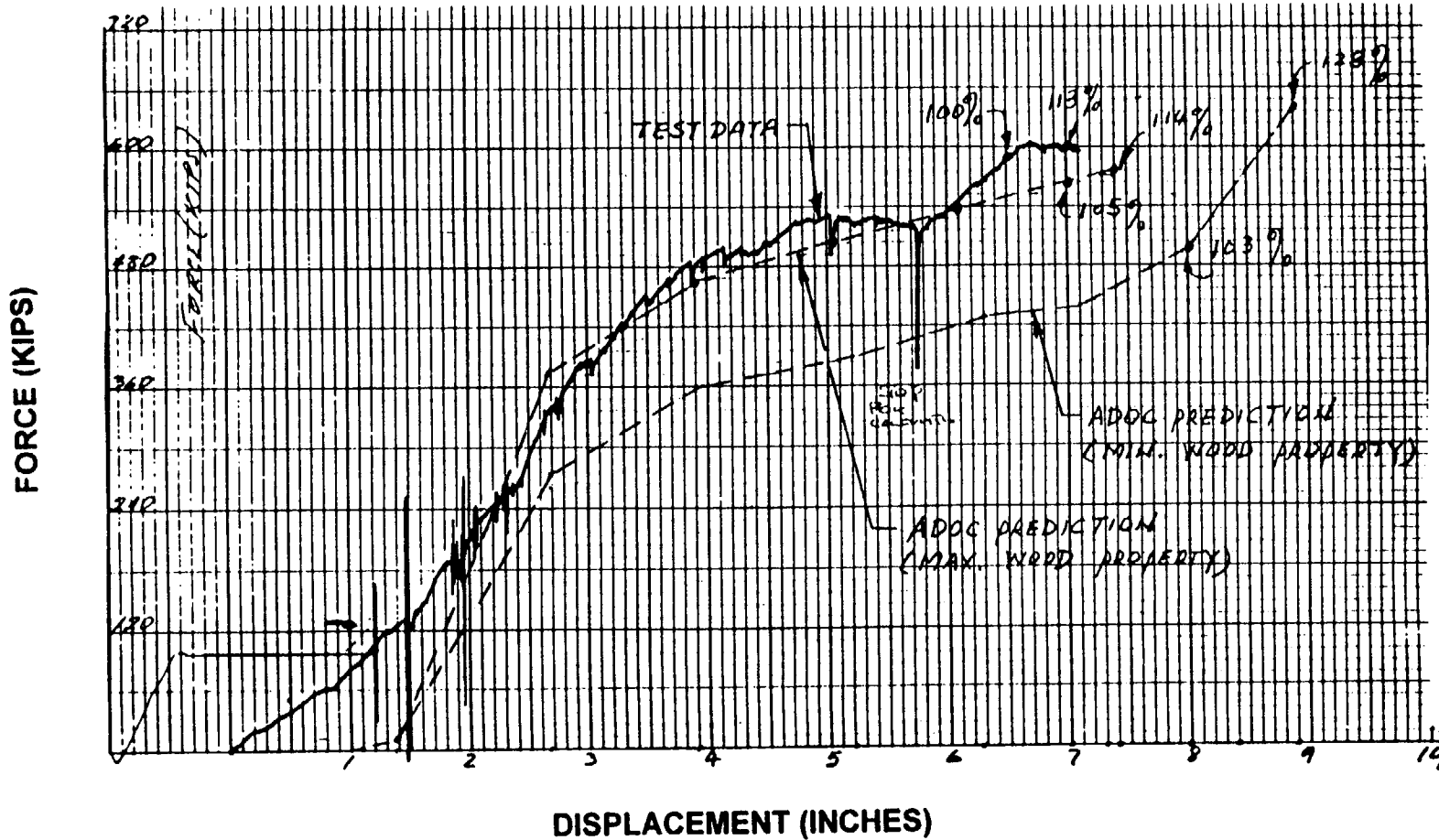


**FIGURE 2.10.3-5**  
**ONE-HALF SCALE MODEL IMPACT LIMITER**  
**LOAD VS DISPLACEMENT- 80° CORNER TEST**

REV. 1

TABLE 2.10.3-1  
 COMPARISON OF ONE-HALF SCALE MODEL  
 STATIC CRUSH TEST RESULTS WITH PREDICTIONS

TEST ANGLE	0° (SIDE CRUSH)	80° (CORNER CRUSH)
REQUIRED ENERGY ABSORPTION (IN-LB)	2.15 X 10 <sup>6</sup>	2.15 X 10 <sup>6</sup>
MEASURED DEFLECTION (INCHES)	3.6 (NOTE 1)	6.5 (NOTE 2)
PREDICTED DEFLECTION RANGE (INCHES)	4.0 - 4.8	7.0 - 8.9
MEASURED FORCE (KIPS)	435 (NOTE 1)	590 (NOTE 2)
PREDICTED FORCE RANGE (KIPS)	330 - 423	575 - 643
FORCE USED FOR STRESS CALCULATION (KIPS)	437 (NOTE 3)	643

NOTES 1: UP TO 50% OF REQUIRED ENERGY ABSORPTION.

2. UP TO 100% OF REQUIRED ENERGY ABSORPTION.

3. REFERENCE TO APPENDIX 2.10.1, PAGE 2.10.1-30, THE TOTAL FORCE APPLIED AT CASK OUTER SURFACE IS  $R_r + R_r = 3,072,000$  LBS. THIS FORCE IS 71 G'S TIMES THE WEIGHT OF THE CASK AND CONTENTS ONLY. THE TOTAL REACTION FORCE AT THE BOTTOM SURFACE OF THE LIMITERS IS 3,500,840 LBS. (3,072,000 LBS. 71 X WEIGHT OF LIMITERS). THEREFORE, THE REACTION FORCE FOR EACH OF THE 1/2 SCALE IMPACT LIMITER IS  $3500840 / (2X4) = 437,605$  LBS.

### Full Scale Load Versus Displacement

The static impact limiter load versus displacement curves have been scaled to full size for the TN-FSV and are provided in this Section. The bases of the curves presented are the two, one-half scale model curves shown in Figures 2.10.3-3 and 2.10.3-5 for the 0° side and 80° corner tests.

The one-half scale model load is multiplied by a factor of four (4) since the TN-FSV impact limiter area is 4 times that of the model at any corresponding section. The model displacement is multiplied by a factor of two (2). The final deflection at which the required TN-FSV energy is absorbed is also shown on each curve. The full scale TN-FSV load versus displacement curves are shown in Figures 2.10.3-6 and 2.10.3-7 for the 0° side and 80° corner orientations.

The final displacements are those where the required energy is absorbed. The entire TN-FSV kinetic energy is absorbed in a single impact limiter for the 80° corner orientation. The 0° side orientation also approximates the secondary impact after a 15° oblique drop where 68% of the energy is absorbed by this impact limiter.

#### 2.10.3.4 Dynamic Testing

##### Test Model Description

The test model for the dynamic tests is a solid carbon steel test body with a front impact limiter on each end. The test model, as shown in Figure 2.10.3-8, was constructed to be as close as possible to one-half of the full size packaging.

The test body is 103.5 inches long with an outside diameter of 15.5 inches. The test body model and full size packaging dimensions are shown below.

	TEST BODY	FULL SIZE PACKAGING
BODY LENGTH	103.5 IN.	207 IN.
BODY DIAMETER	15.5 IN.	31 IN.
LENGTH INCLUDING IMPACT LIMITER	123.5 IN.	247 IN.

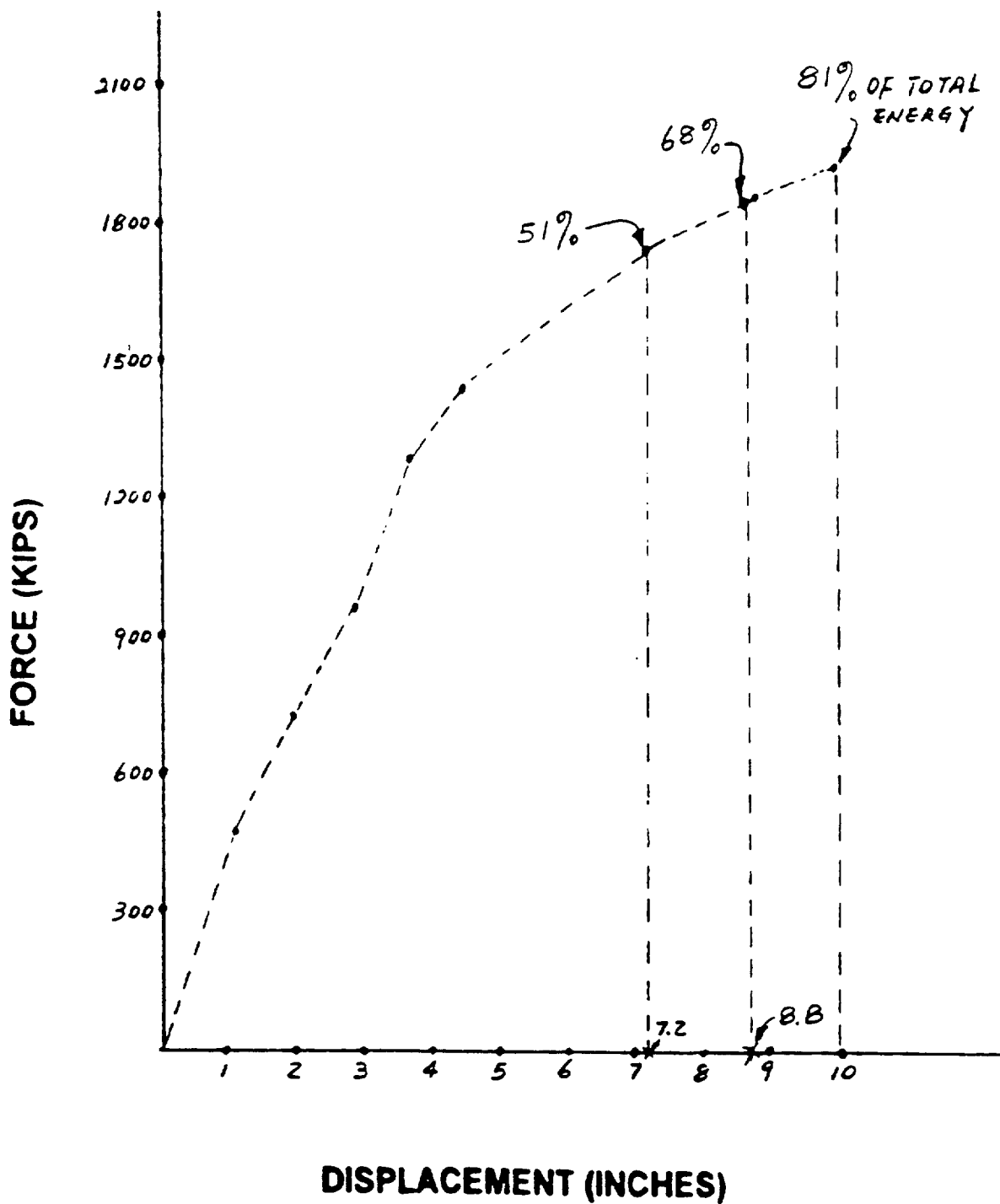
The scale model impact limiters were described earlier in Section 2.10.3.3.

#### Test Description

The test setup for the slapdown test is shown in the Figure 2.10.3-9 and the test setup for the 80° corner drop is shown in Figure 2.10.3-10.

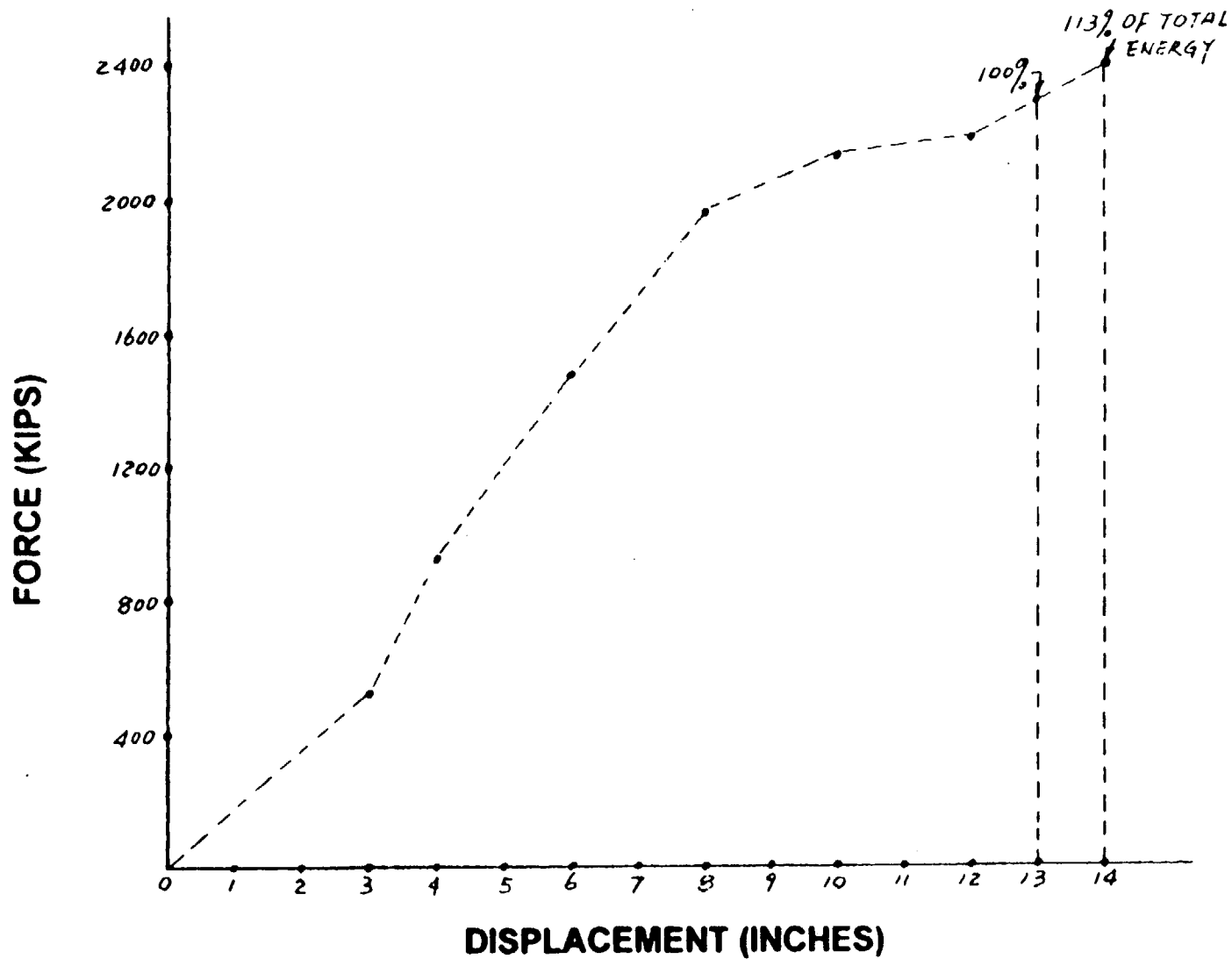
These tests were performed at National Technical Systems in Acton, MA. in accordance with approved written procedures. A protractor was placed on the test body to measure the initial angle ( $\pm 2$  degrees) of its longitudinal axis with respect to the target (i.e., impact surface). The impact surface consists of an unyielding concrete pad weighing more than 250,000 lbs. resting on bedrock. An A-36 hot rolled mild steel plate, two (2) inches thick, was secured to the surface of the concrete pad. A steel tape was used to measure the initial height of the lowest surface of the test model above the target. The height was 30 feet + 1.0 in./-0.0 in. Each drop was photographed and videotaped. After each drop, the following data was measured and recorded:

- ° Observation of crush on the impact limiters and attachment bolts.
- ° Dimensional measurements of the impact limiters and their contour lines, establishing the deformed shape.
- ° Torque values of the attachment bolts.



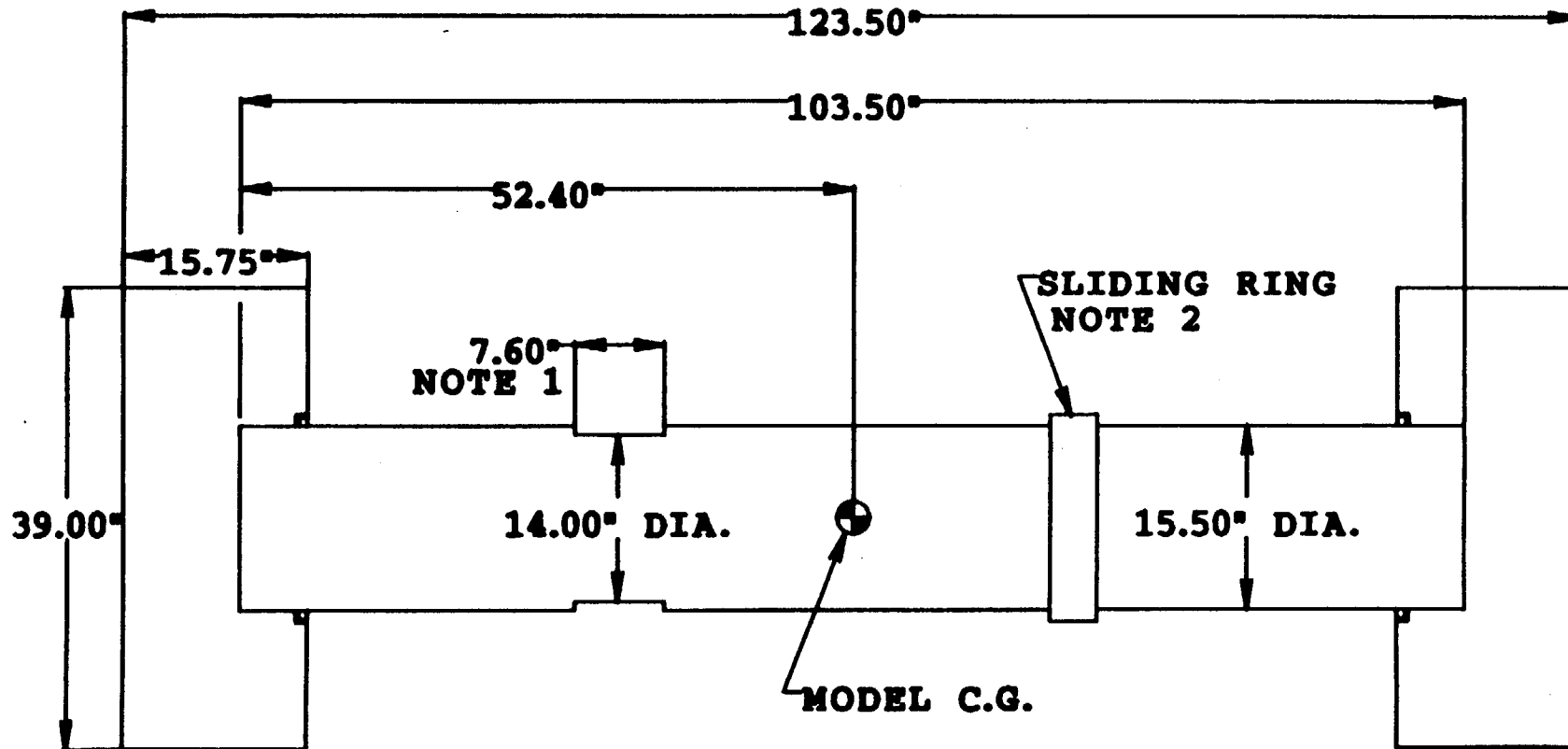
**FIGURE 2.10.3-6**  
**FULL SCALE MODEL IMPACT LIMITER**  
**LOAD VS DISPLACEMENT- 0° SIDE TEST**

2.10.3-18



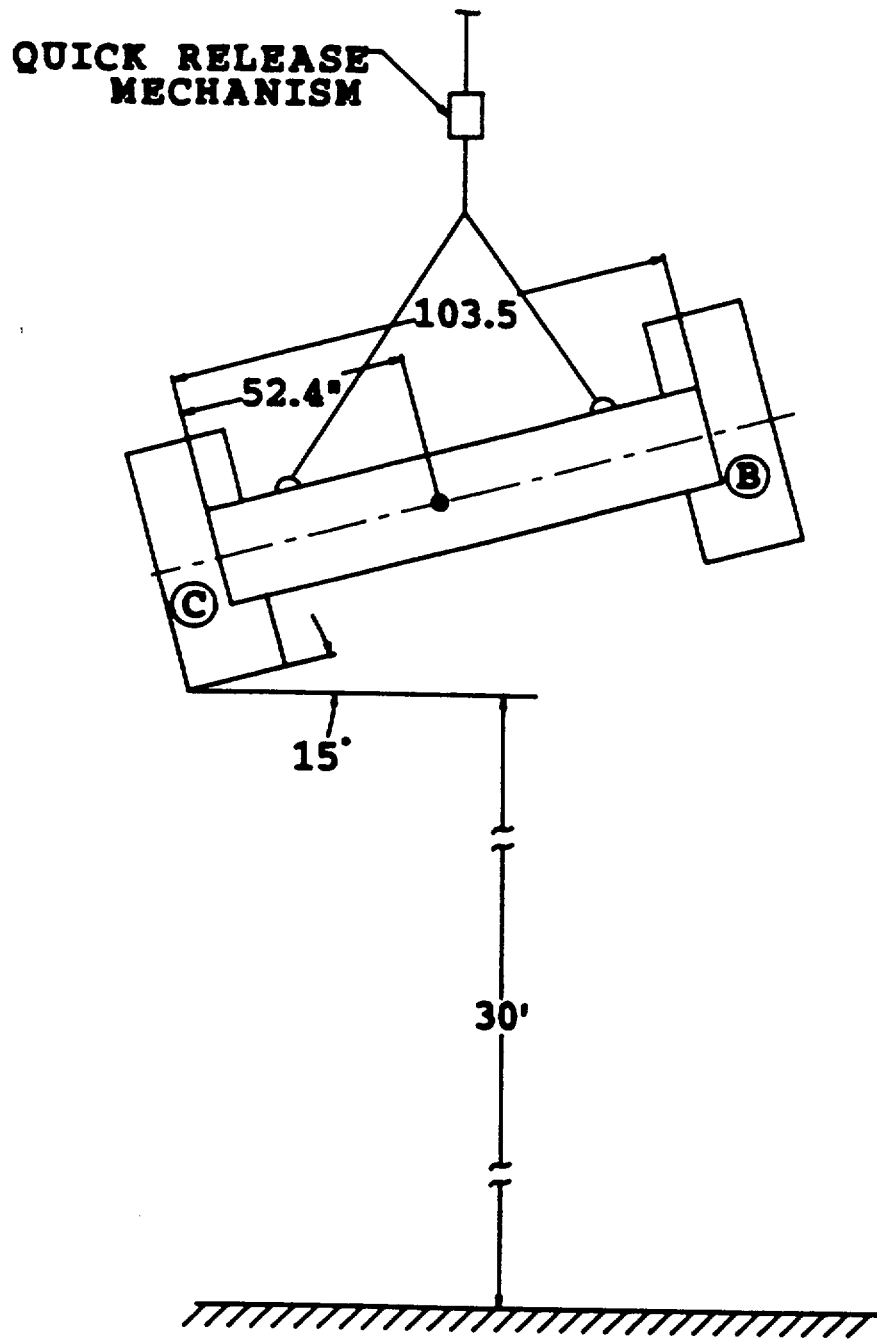
**FIGURE 2.10.3-7**  
**FULL SCALE MODEL IMPACT LIMITER**  
**LOAD VS DISPLACEMENT- 80° CORNER TEST**

REV. 1

**NOTES:**

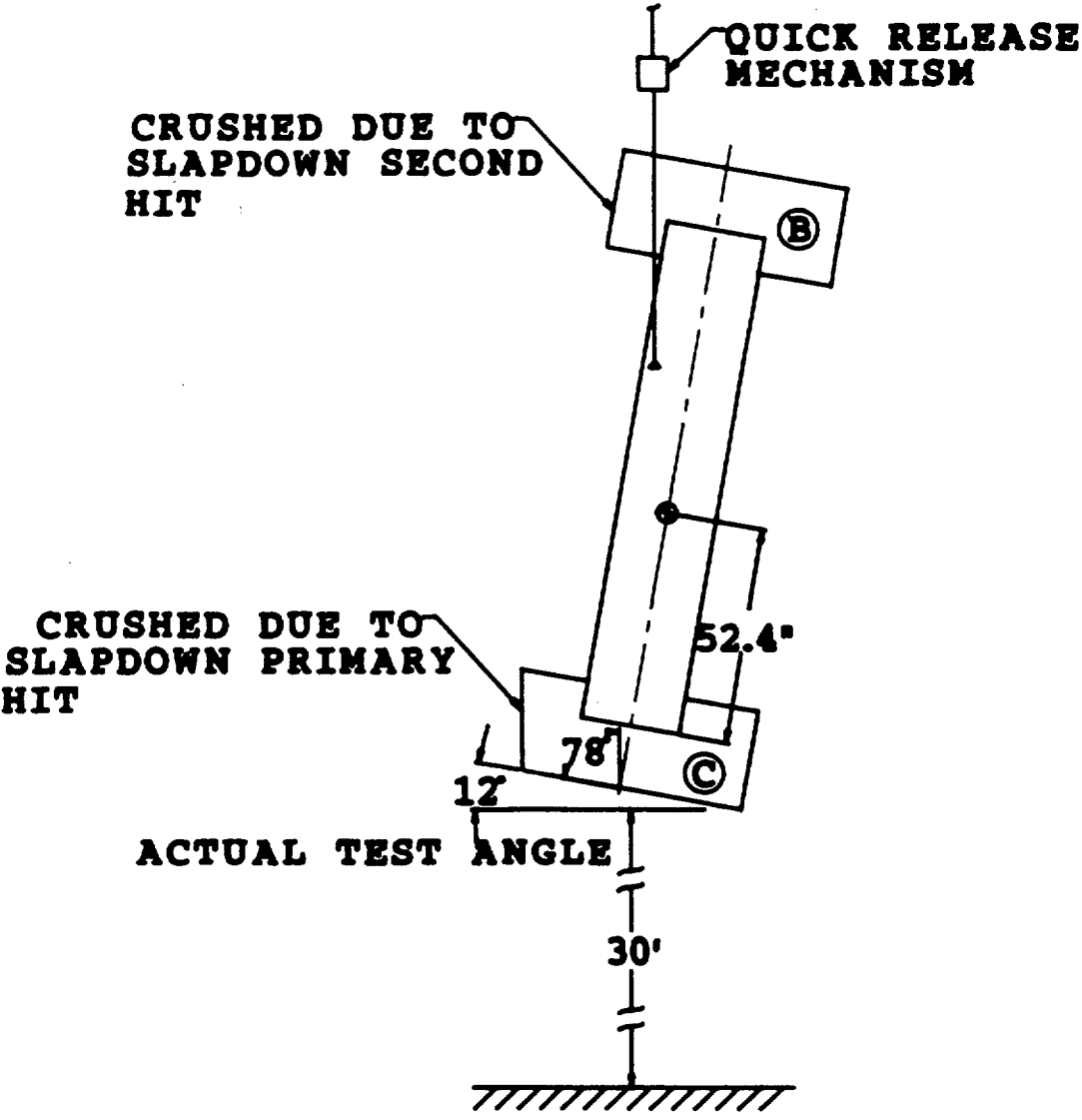
1. ADJUST SLOT SIZE TO ACHIEVE TOTAL WEIGHT REQUIRED.
2. ADJUST SLIDING RING LOCATION TO ACHIEVE C.G. LOCATION

**FIGURE 2.10.3-8  
DYNAMIC TEST MODEL**



○ - IMPACT LIMITER REFERENCE NUMBER

FIGURE 2.10.3-9  
TN-FSV SCALE MODEL  
SLAPDOWN TEST SET UP



○ - IMPACT LIMITER REFERENCE NUMBER

FIGURE 2.10.3-10  
TN-FSV SCALE MODEL  
CORNER DROP TEST SETUP

At the completion of the slapdown test and the subsequent 80° corner drop test, the impact limiters were removed and the following data was measured and recorded:

- ° Inside crush of the impact limiter.
- ° Torque values of the attachment bolts.

#### 15° Slapdown Drop Test

The slapdown test was performed first. The impact limiter which impacts second was cooled for over 18 hours to a temperature of -20°F prior to attachment to the test body. This limiter was covered during transportation and idle time with at least 8 inches of insulating foam to maintain the -20°F. The ambient temperature was 9°F during the drop test. The test model was dropped from a height of 30 feet (impact surface to lowest point on the impact limiter) at an impact angle of 15° as shown in Figure 2.10.3-9. At the completion of the slapdown drop test, the test body and impact limiters were examined and the impact limiter deformations were measured.

#### 80° Corner Drop Test

Following the slapdown test, the test model was rotated 180° so that the impact for the 80° corner drop was on the uncrushed side of the impact limiter which was used for the primary hit in the slapdown case as shown in Figure 2.10.3-10. The drop height was 30 feet and the measured drop angle was 78°. As before, the ambient temperature was around 9°F.

#### Test Results

After the slapdown test, all the attachment bolts on the impact limiter which hit first lost their torque. Upon examination, the reason for the torque relaxation was determined to be deformation of the washers beneath the bolt heads, and tightening of the impact limiter against the test body due to the drop. None of the bolts were broken. Two weld seams between the gussets and flat segments

opened slightly. The primary impact limiter pushed inward toward the test body indicating inside crushing, and also crushed on the outside at a 15° angle. The crushing on the secondary impact limiter (B) was similar to a side drop crush.

After the corner crush test, the attachment bolts also lost their torque. There was evidence of both inside and outside crushing. The side of the impact limiter closest to the edge hitting first pushed around the test body, so that the impact limiter appeared slightly cocked on the test body due to inside crushing of the limiter on one side.

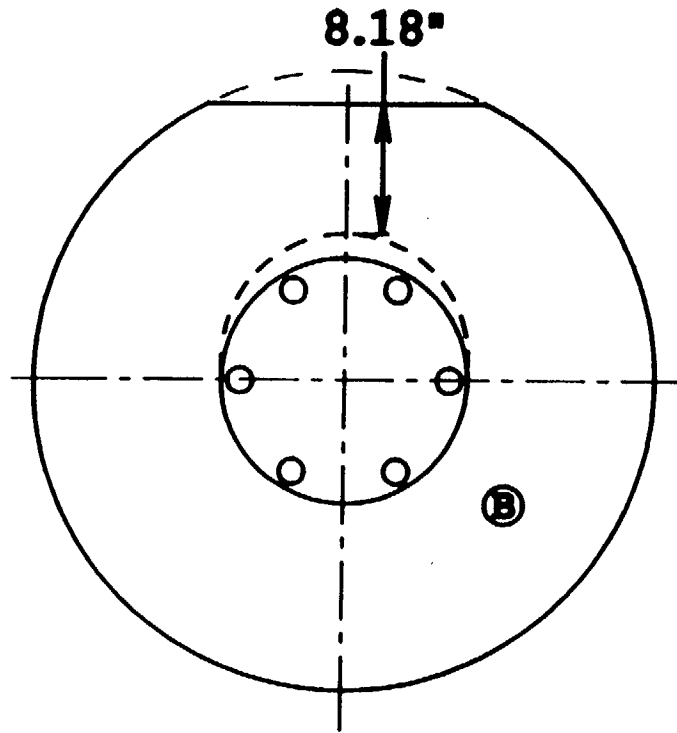
The results of these tests are shown in Figure 2.10.3-11. From measurements on these deformed limiters, total deflections were calculated to be 3.57" on the limiter impacting second during the 15° drop and 6.3" for the 80° corner drop without accounting for springback. In summary, the results of the dynamic tests demonstrate that:

- ° The crush depths do not result in lockup of the wood in the limiters.
- ° The impact limiter attachment bolts can withstand the dynamic loads without failure.
- ° The design of the impact limiter enclosure is acceptable.
- ° The impact limiters remain intact during the 30 foot drop.

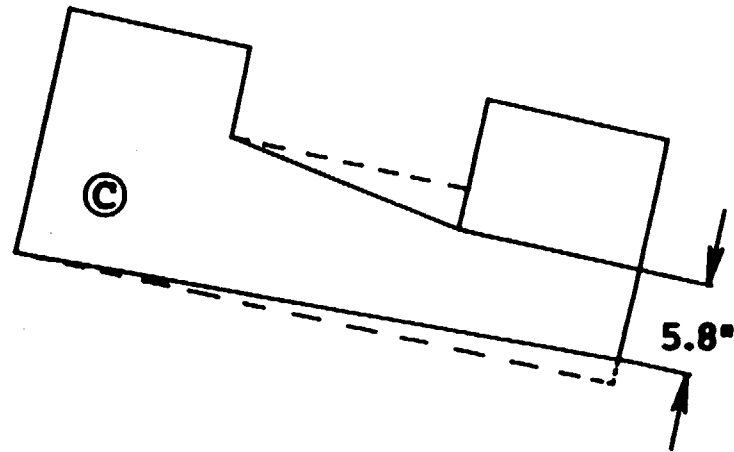
#### 2.10.3.5 Comparison Between Static and Dynamic Test Results

The one-half scale model impact limiter test program provided both static and dynamic data for two orientations. The static results from the 80° corner crush test can be compared directly to the dynamic results from the 80° corner drop test since the motion is unidirectional (no horizontal or rotation motion during impact) and all the kinetic energy is absorbed by one impact limiter. The static results from the 0° side crush test can also be compared with the dynamic results from the 15° slapdown test, but the complex motion during the dynamic test (primary impact followed by rotation followed by secondary impact) makes the comparison imprecise.

2.10.3-24



0° SIDE DROP (SECOND IMPACT)



80° CORNER DROP

○ - IMPACT LIMITER REFERENCE NUMBER

**FIGURE 2.10.3-11  
THE DEFORMED IMPACT LIMITERS  
AFTER DYNAMIC DROP TESTS**

REV. 1

0° Side Test

The static and dynamic test results are compared in Table 2.10.3-2. The dynamic results listed were obtained from the data recorded from the secondary impact after the 15 degree slapdown test. The crushing of the second limiter during that test was at approximately a 0 degree angle (perpendicular to the cask axis). The data from that secondary impact is compared with the static test data for an absorbed energy to 68% of the total kinetic energy (rather than 50% that would be absorbed in a true side drop). The dynamic test data shows that the secondary impact was more severe than the primary impact. However, the difference in absorbed energy cannot be determined from the data. The 68% energy figure was determined from the previously described ADOC dynamic analysis.

The permanent crush depth after the dynamic test (second impact) was about 3.57 inches not including the elastic springback. The total would be about 3.82 inches assuming 0.25 inch of springback (estimated from static crush test). The corresponding measured deflection from Figure 2.10.3-3 load-versus-displacement curve is 4.4 inches. The crush deformations therefore agree within about 14%.

80° Corner Test

The last two numerical columns in Table 2.10.3-2 compare the results for the 80° corner drop orientation. The impact limiter was permanently crushed about 6.3 inches after the dynamic test. The total would be about 6.5 inches assuming 0.2 inches spring back (estimated from static crush test). The impact limiter deformation during the static test when the required energy was absorbed was about 6.5 inches. The correlation between the dynamic and static tests is excellent for this test orientation.

It can be concluded from these studies that static and dynamic test results compare reasonably well.

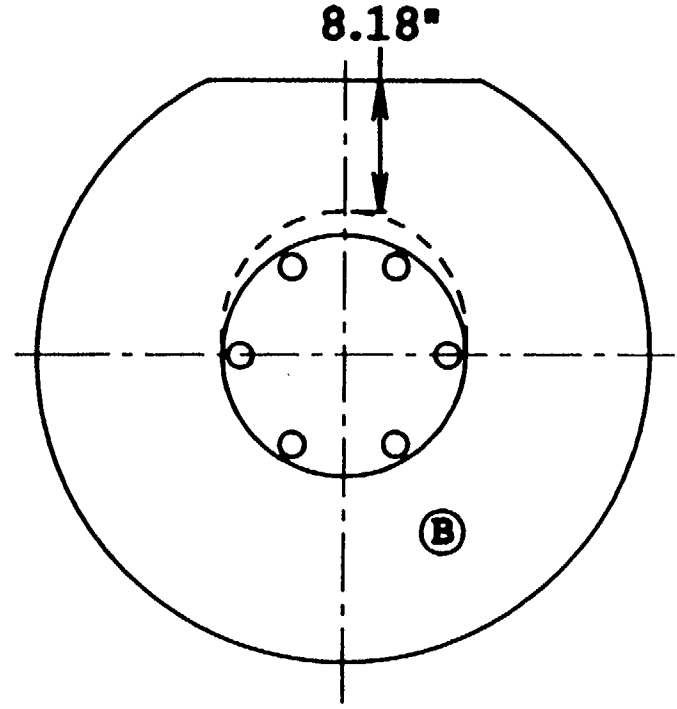
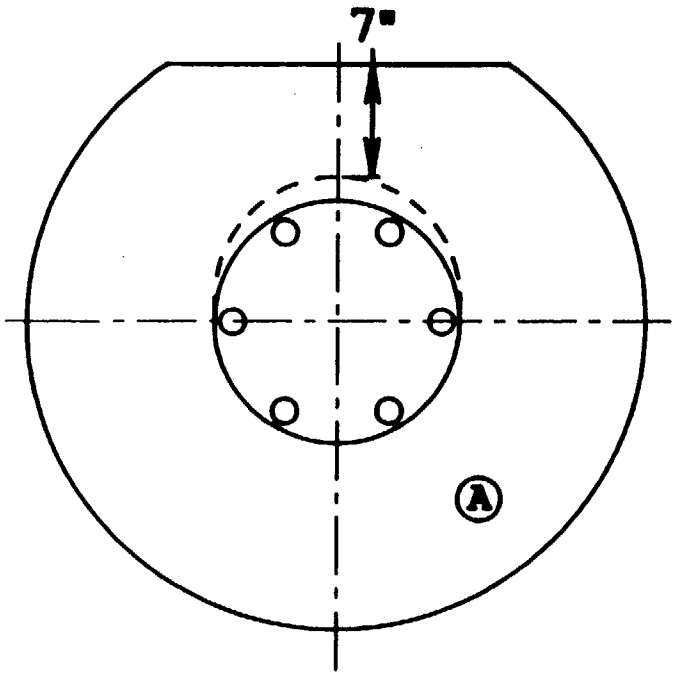
TABLE 2.10.3-2

COMPARISON OF ONE-HALF SCALE MODEL  
STATIC AND DYNAMIC TEST RESULTS

	0° SIDE TEST			80° CORNER TEST	
	STATIC	DYNAMIC		STATIC	DYNAMIC
		FIRST IMPACT	SECOND IMPACT		
UNCRUSHED DEPTH OF LIMITERS	7" (FIGURE 2.10.3-12)	---	8.18" (5) (FIGURE 2.10.3-12)	5" (5) (FIGURE 2.10.3-13)	5.8" (5) (FIGURE 2.10.3-13)
DEFLECTION (NOTE 5)	4.75"	---	3.57"	6.8"	6.3"
DEFLECTION (FROM STATIC TEST CURVE)	5.0"	---	---	7.0"	---
ESTIMATED SPRINGBACK	0.25"	---	0.25"	0.2"	0.2"
DEFLECTION INCLUDING SPRINGBACK	5.0" (NOTE 1)	---	3.82" (NOTE 2)	7.0" (NOTE 3)	6.5" (NOTE 4)

- NOTES:
- 1) UP TO 81% OF REQUIRED ENERGY.
  - 2) UP TO 68% OF REQUIRED ENERGY.
  - 3) UP TO 113% OF REQUIRED ENERGY.
  - 4) UP TO 100% OF REQUIRED ENERGY.
  - 5) CALCULATED FROM MEASURED DATA.

2.10.3-27



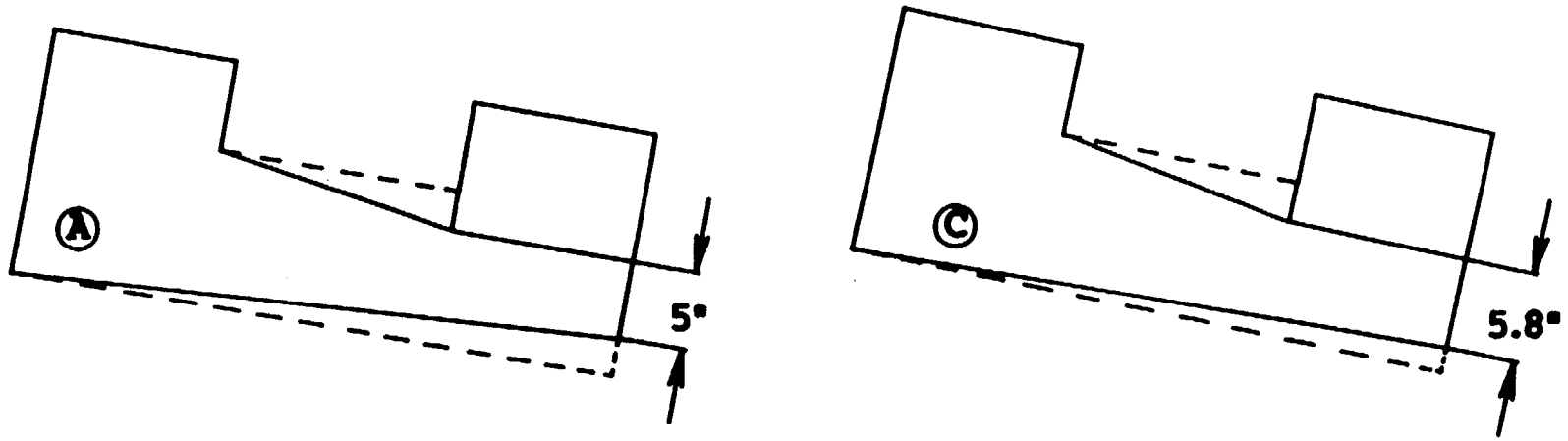
STATIC TEST  
(UP TO 81% OF REQ'D. ENERGY)

DYNAMIC TEST (SECOND IMPACT)  
(UP TO 68% OF REQ'D. ENERGY)

○ - IMPACT LIMITER REFERENCE NUMBER

**FIGURE 2.10.3-12**  
**COMPARISON OF DEFORMED LIMITERS BETWEEN**  
**STATIC AND DYNAMIC TESTS (0° SIDE TEST)**

REV. 1



STATIC TEST

(UP TO 113% OF REQ'D. ENERGY)

DYNAMIC TEST

(UP TO 100% OF REQ'D. ENERGY)

○ - IMPACT LIMITER REFERENCE NUMBER

**FIGURE 2.10.3-13**  
**COMPARISON OF DEFORMED LIMITERS BETWEEN**  
**STATIC AND DYNAMIC TESTS (80° SIDE TEST)**

#### 2.10.3.6 Conclusions

Based on the results of the 1/2 scale static and dynamic test program, it has been concluded that the full scale impact limiters will absorb the required energy and remain on the packaging after undergoing the hypothetical accident event defined in 10CFR71.73(c)(1).

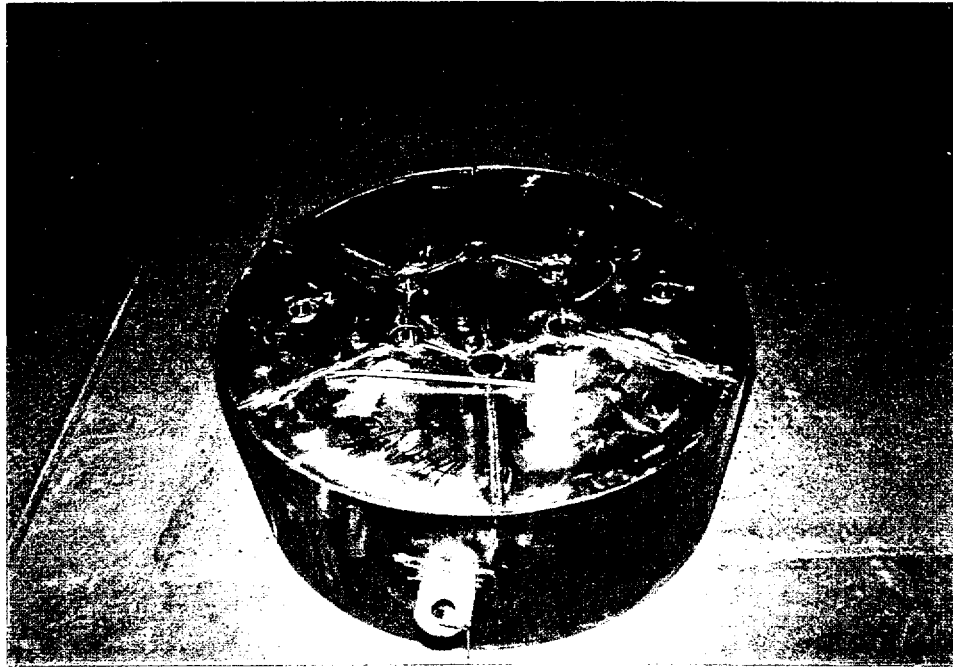
The test results are conservative. Both of the dynamic tests were performed on the same test model (same impact limiters) so even cumulative damage from two drops did not cause failure of the attachment bolts or impact limiter enclosures.

The loads (forces) used in Appendix 2.10.1 for stress calculations are conservative and acceptable since:

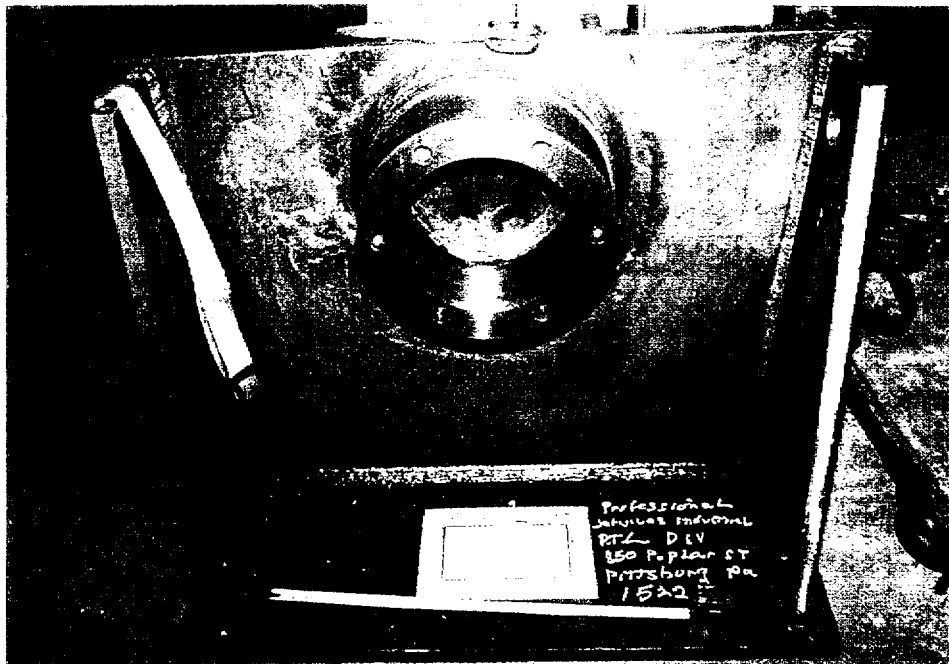
- ° Forces used for the stress calculations are higher than those measured from the static crush tests (see table 2.10.3-1).
- ° The deformations observed, following the dynamic tests are qualitatively consistent with those observed from the static tests and correlate reasonably well given the impression inherent in measuring post test deformations.
- ° All stresses due to 30 foot drops in other orientations analyzed in Appendix 2.10.1 have very large margins of safety with respect to the allowables.

#### 2.10.3.7 Photographs

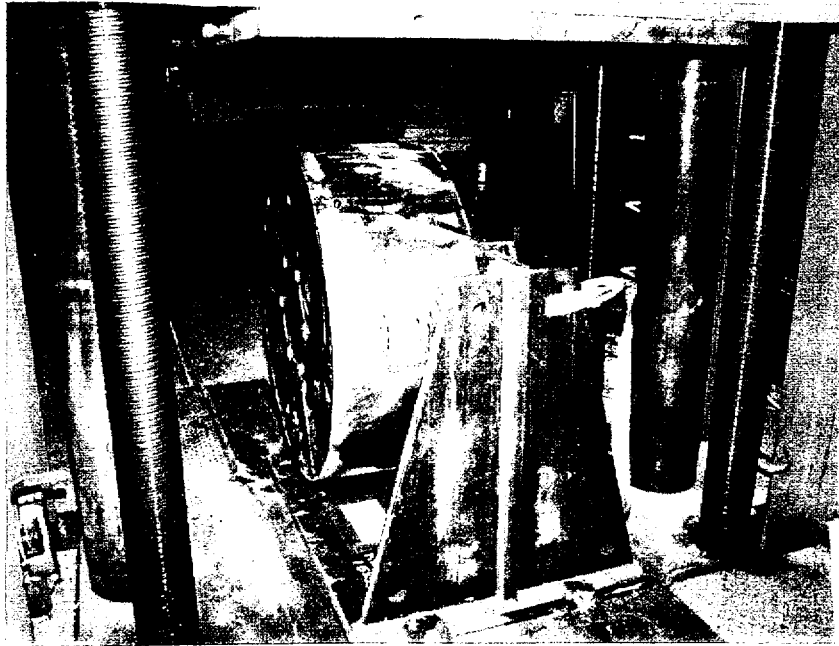
Photographs depicting the static and dynamic tests are included in this section.



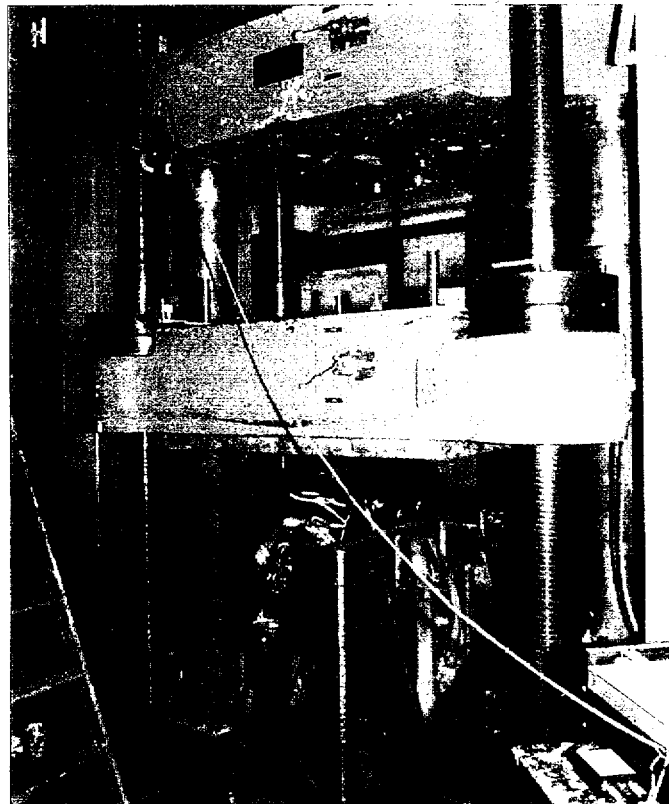
1/2 SCALE IMPACT LIMITER



SIDE CRUSH TEST FIXTURE



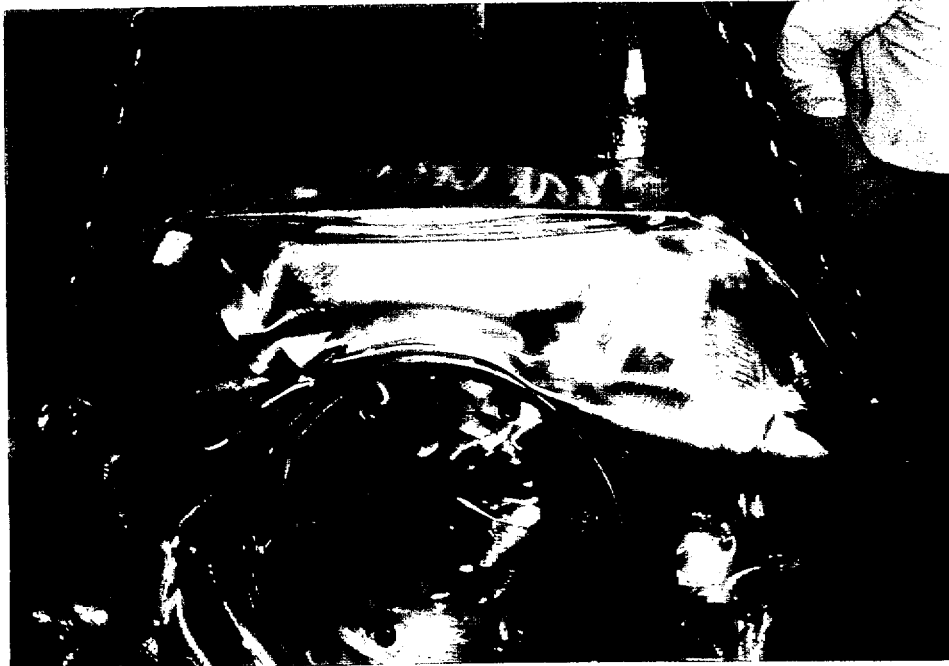
TEST SET-UP SIDE CRUSH



SIDE CRUSH TEST DURING LOADING



LIMITER AFTER SIDE CRUSH (FRONT VIEW)



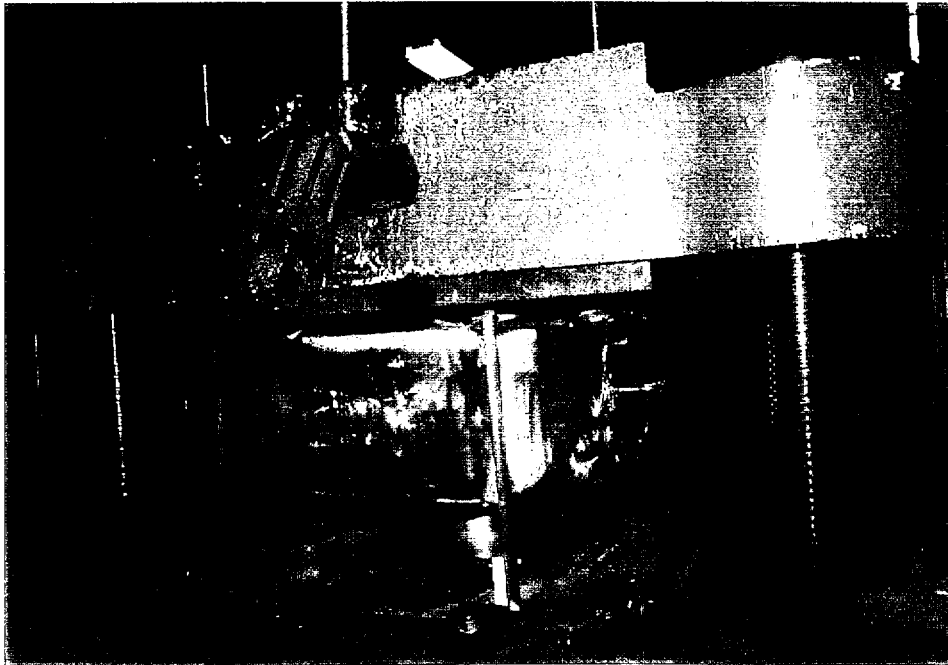
LIMITER AFTER SIDE CRUSH (REAR VIEW)



CORNER CRUSH TEST FIXTURE



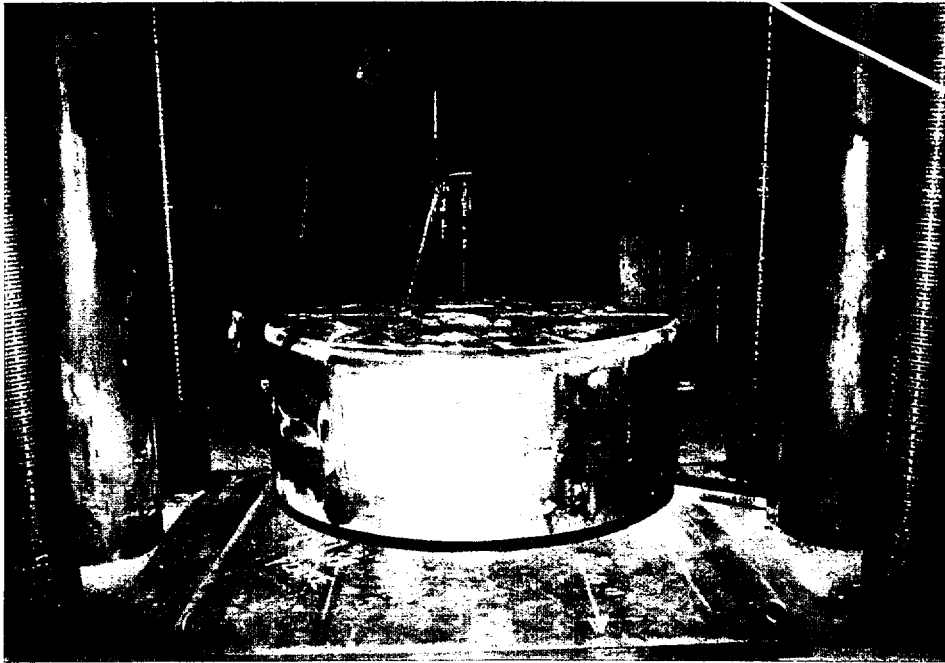
TEST SET-UP CORNER CRUSH



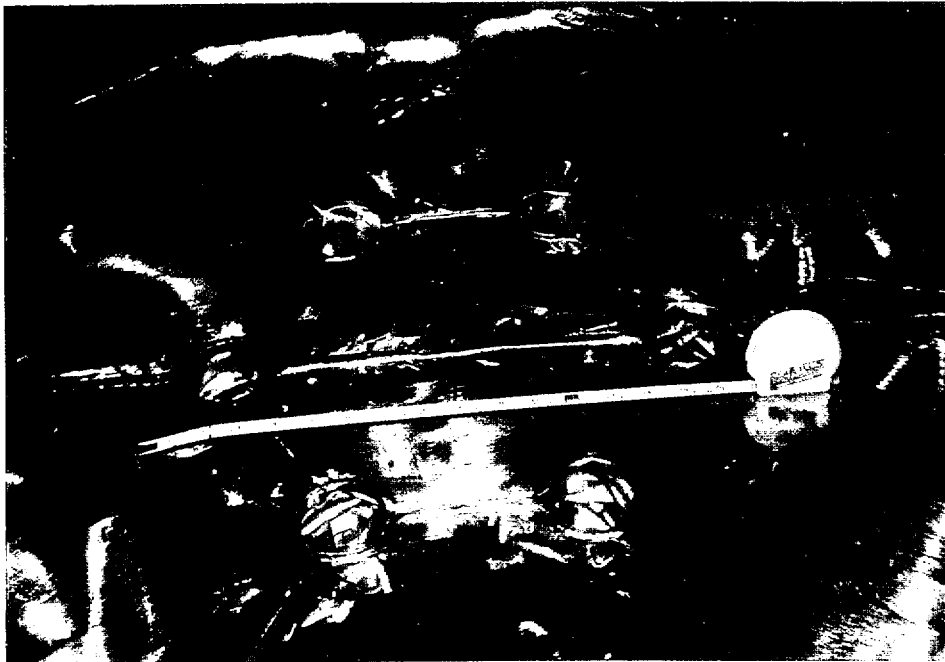
LOADING PRIOR TO REMOVAL OF BACK HOLD DOWN



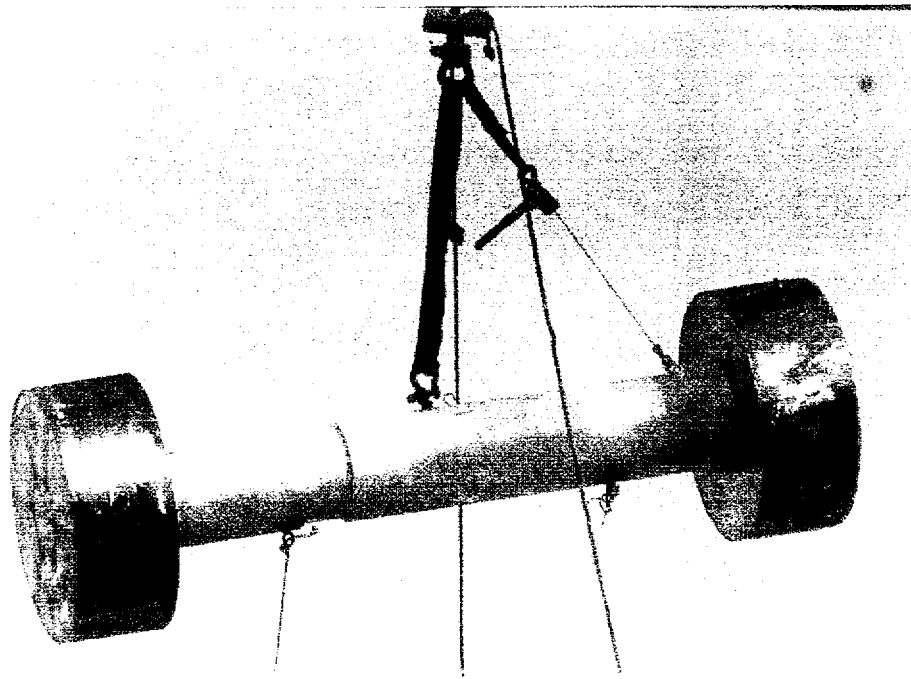
TOP OF LIMITER AFTER CORNER CRUSH



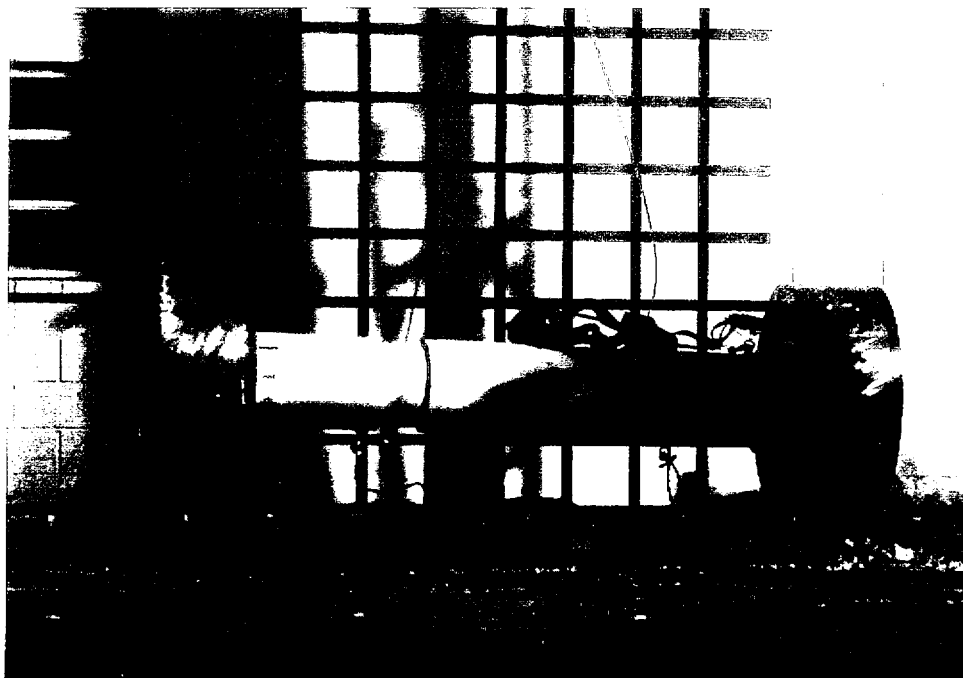
LIMITER AFTER CORNER CRUSH (SIDE VIEW)



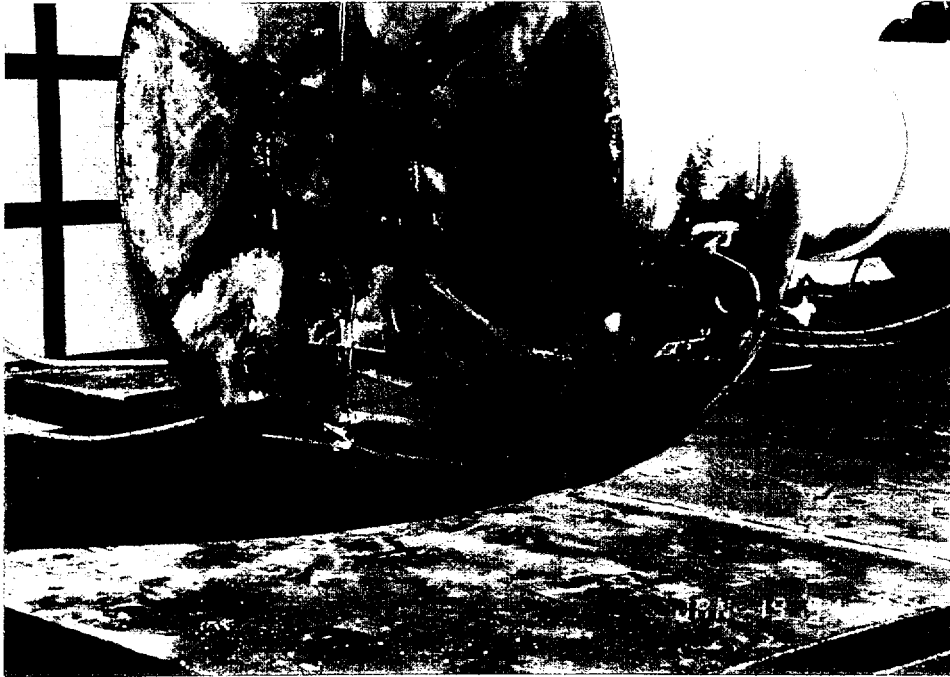
LIMITER AFTER CORNER CRUSH (TOP VIEW)



TEST SET-UP 15° SLAPDOWN



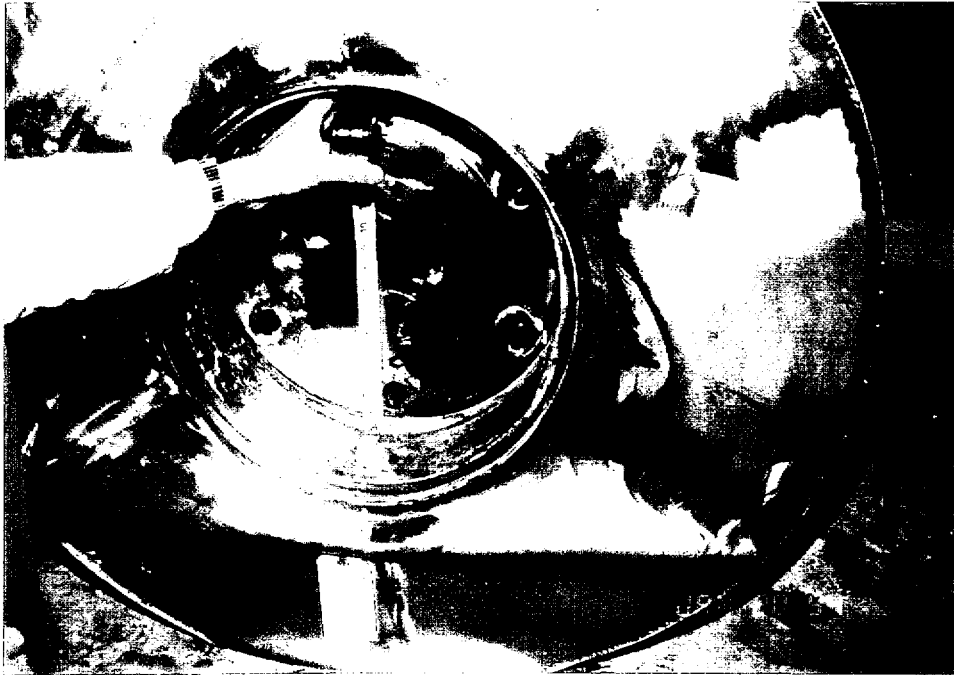
15° SLAPDOWN SECOND IMPACT



15° SLAPDOWN POST FIRST IMPACT



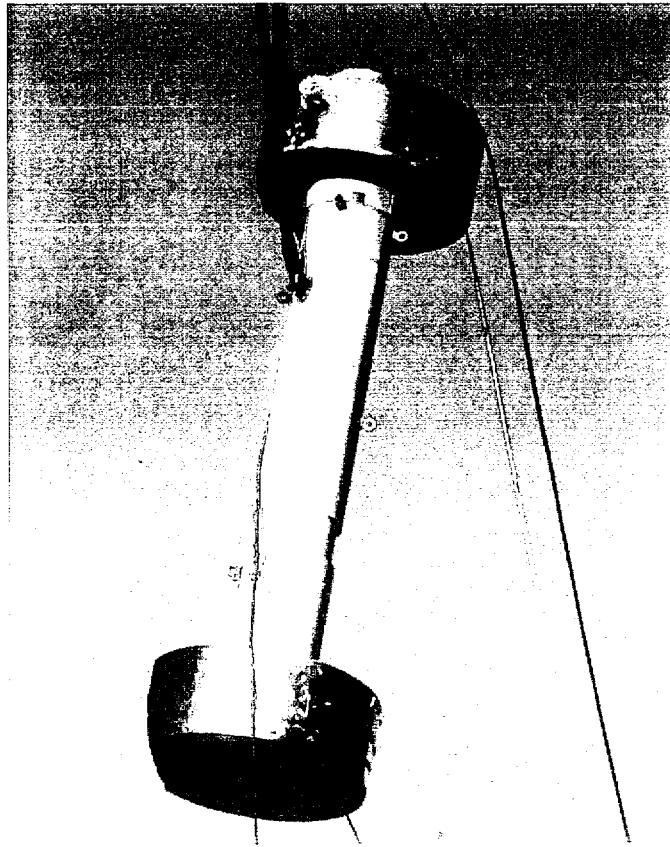
15° SLAPDOWN POST SECOND IMPACT



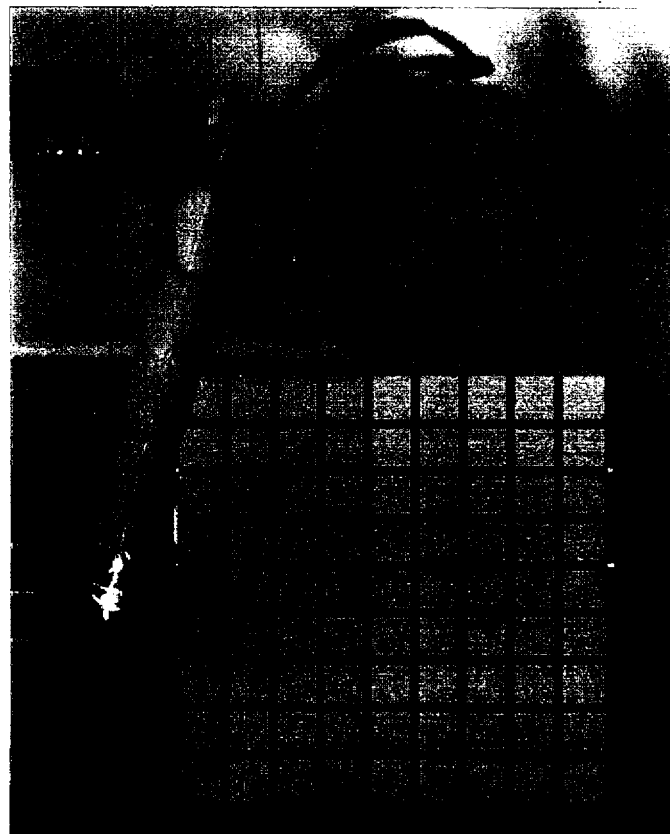
15° SLAPDOWN SECOND IMPACT REMOVED FROM TEST BODY



15° SLAPDOWN SECOND IMPACT (ROTATED 180°)



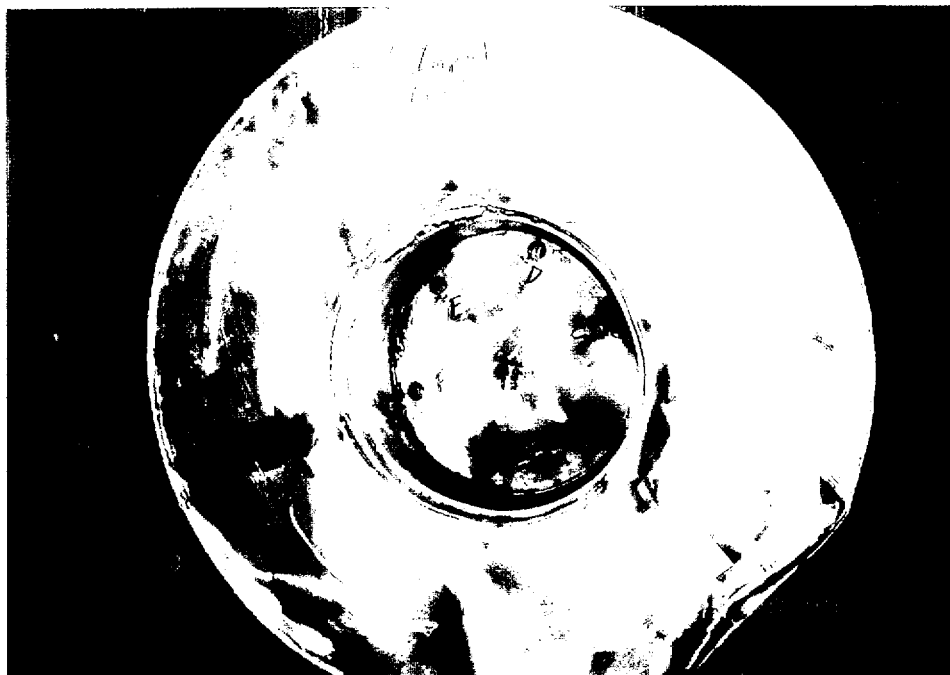
TEST SET-UP 80° CORNER DROP



80° CORNER DROP PRIOR TO IMPACT ON TARGET



IMPACT LIMITER POST 80° CORNER DROP (REAR VIEW)



IMPACT LIMITER POST 80° CORNER DROP REMOVED FROM TEST BODY

CHAPTER FIVE  
SHIELDING EVALUATION  
TABLE OF CONTENTS

	<u>Page</u>
5.1 DISCUSSION AND RESULTS.....	5-1
5.2 SOURCE SPECIFICATION .....	5-3a
5.2.1 Fuel Parameters	
5.2.2 Gamma Source	
5.2.3 Neutron Source	
5.3 MODEL SPECIFICATION .....	5-7
5.3.1 Description of Radial and Axial Shielding Configurations	
5.3.2 Source and Shielding Regional Densities	
5.4 SHIELDING EVALUATION .....	5-11
5.4.1 Radial Analysis	
5.4.2 Axial Analysis	
5.5 REFERENCES .....	5-12

CHAPTER FIVE  
SHIELDING EVALUATION  
LIST OF FIGURES

	<u>Page</u>
Figure 5-1 Radial Analysis Model	5-8
Figure 5-2 Axial Analysis Model	5-9

LIST OF TABLES

Table 5-1 TN-FSV Shield Configuration	5-2
Table 5-2 Calculated Dose Rates	5-3
Table 5-3 ORIGEN-S Gamma Spectra	5-5
Table 5-4 SCALE 18 Group Gamma Spectra	5-5
Table 5-5 Neutron Spectra	5-6
Table 5-6 Source and Shield Material Densities	5-10

## CHAPTER FIVE SHIELDING EVALUATION

### 5.1 DISCUSSION AND RESULTS

An evaluation of the shielding performance of the TN-FSV is performed to demonstrate compliance with the dose rate limits of 10CFR71.47. This also demonstrates compliance with the accident dose rate limit of 10CFR71.51 (2) because the components of the package shielding which are not an integral part of the body (the impact limiters, the lid, and the thermal shield) will remain in position under all accident conditions, as demonstrated in Appendices 2.10.1 and 2.10.2. The contents of the TN-FSV consist of six irradiated FSV fuel elements enclosed within a fuel storage container (FSC). The fuel elements have a maximum burnup of 70,000 MWD/MTU (Megawatt-Days/Initial Metric Tons of Thorium and Uranium) and have been decayed for at least 1600 days since discharge from the reactor.

The most significant shielding design feature of the TN-FSV is the cask body, which consists of an inner layer of stainless steel, followed by lead and an outer layer of stainless steel. The impact limiters, which consist of wood in stainless steel cases, provide additional axial shielding, and the thermal shield, a stainless steel shell, provides additional radial shielding. Additional shielding at the top of the packaging is provided by a depleted uranium plug which is inserted into the closure lid of the FSC. The shield layers and thickness are listed in Table 5-1.

The shielding analysis of the TN-FSV is performed with regulatory acceptable codes from the SCALE system (Ref. 5-1). Conservative modeling of the source provides an upper bound on the dose rates. Table 5-2 summarizes the calculated dose rates and shows that all applicable limits are satisfied.

TABLE 5-1  
TN-FSV SHIELD CONFIGURATION

<u>Axial, Bottom</u>	<u>Axial, top</u>	<u>Radial</u>
2.0 inch steel (1)	1.19 inch steel (1)	0.5 inch steel (1)
2.69 inch Al	4.38 inch dep U (1)	1.12 inch steel
5.5 inch steel	0.56 inch Al	3.38 inch lead (2)
0.25 inch steel (3)	2.5 inch steel	1.50 inch steel
19.37 inch balsa (3)	0.25 inch steel (3)	0.25 inch steel (4)
0.19 inch steel (3)	19.37 inch balsa (3)	
	0.19 inch steel (3)	

(1) Fuel storage canister (See Figure 1-2).

(2) 3.44 nominal, 3.38 minimum

(3) Impact limiter

(4) Thermal shield

TABLE 5-2  
CALCULATED DOSE RATES

		<u>Dose Rates, mrem/hr</u>		
		<u>Calculated(1)</u>		
<u>Normal</u>		<u>Gamma</u>	<u>Neutron</u>	<u>Limit</u>
Package Surface	Side	99	3.2	200
	Top	<0.01	nil	200
	Bottom	76.8	nil	200
Two Meters from	Side	9.5	0.22	10
	Top	<0.01	nil	10
	Bottom	6.1	nil	10
Occupied Position(2)		<0.01	nil	2
 <u>Accident</u>				
One Meter from	Side	<99	<1.0	1000
Package Surface	Ends	<77	nil	1000

- (1) All dose rates are calculated using the minimum lead thickness.
- (2) The occupied position is assumed to be in a cab five meters from the package top. No credit is taken for shielding by cab materials.
- (3) Because there is no loss of shielding under hypothetical accident conditions, the normal condition surface dose rate results are adequate to demonstrate that the one meter accident dose rates are less than 1000 mrem/hr.

## 5.2 SOURCE SPECIFICATION

5.2.1 Fuel Parameters

The FSV core was divided into six fuel segments, identified as Segments 4 - 9 (segments 1 - 3 were previously shipped to INEL). Each segment consisted of approximately 1/6 of the 1482 fuel elements in the core. Each segment had slightly different initial fuel loadings. Segments 4 - 6 were part of the original core and had the highest burnup. Segment 7 was added at the first fuel reload (replacing Segment 1) and Segments 8 and 9 on the subsequent two reloads.

Each fuel segment was analyzed with an individual ORIGEN-S computer run. The average fresh fuel densities, and burnup in Effective Full Power Days (EFPD) are listed below.

FRESH FUEL NUMBER DENSITIES PER FUEL BLOCK (GRAM-ATOMS)

	Segment 4	Segment 5	Segment 6	Segment 7	Segment 8	Segment 9
Th -232	4.351E+1	4.447E+1	4.347E+1	4.110E+1	4.110E+1	4.113E+1
U-234	1.940E-2	1.832E-2	1.940E-2	2.373E-2	2.492E-2	2.668E-2
U-235	2.465E+0	2.328E+0	2.465E+0	3.015E+0	3.166E+0	3.390E+0
U-236	7.377E-3	6.967E-3	7.379E-3	9.023E-3	9.477E-3	1.015E-2
U-238	1.526E-1	1.441E-1	1.525E-1	1.866E-1	1.960E-1	2.099E-1
Silicon	1.127E+2	1.109E+2	1.127E+2	1.002E+2	1.002E+2	1.013E+2
Carbon	9.043E+3	9.044E+3	9.258E+3	9.258E+3	9.285E+3	9.179E+3
Actual EFPD	889.3	889.3	889.3	715.3	526.5	232.0

Each fuel segment was conservatively modelled using a single pulse burn based on a normalized core average thermal flux of 5.815E13 n/cm<sup>2</sup>-s. The fuel segment with the highest burnup (highest resulting gamma and neutron source) was used in the shielding analyses.

### 5.2.2 Gamma Source

An ORIGEN-S calculation was performed for the highest burnup FSV fuel element (70,000 MWD/MTU). Table 5-3 shows the ORIGEN-S gamma spectra for a FSV irradiated element decayed for 1600 days. The SCALE 18 group gamma library structure is not the same as the gamma structure output by ORIGEN-S. Therefore, the ORIGEN-S source terms were converted, conserving energy, into the SCALE 18 group gamma structure as shown in Table 5-4. The gamma source terms are increased by a factor of 1.8 to conservatively account for burnup peaking. The homogenized source volume is assumed to be a cylinder 187.3 inches long and 16.6 inches in diameter. The source volume is 6.67E5cc and the resulting volumetric source strength is:

$$\frac{1.20E14 \gamma/s/ele \times 6 \text{ ele} \times 1.8}{6.67 \text{ E5 cc}} = 1.94 \text{ E9 } \gamma/s/cc$$

### 5.2.3 Neutron Source

The ORIGEN-S analyses mentioned above also evaluated the neutron source from the irradiated FSV fuel. The neutron spectra output by ORIGEN-S conforms to the 27 neutron group spectra utilized in the SCALE x-section library. The neutron spectra for a single FSV fuel element, decayed 1600 days is shown in Table 5-5. As mention above, a time weighted peaking factor was calculated for the maximum element resulting in the 1.8 value. An additional ORIGEN-S run was performed using the average flux times the 1.8 peaking factor as input. The result of this analysis showed the neutron source increased by a factor of 5.8. This factor was conservatively applied to all the elements in the packaging. the volumetric neutron source term is:

$$\frac{2.03 \text{ E5 n/s/ele} \times 6 \text{ ele} \times 5.8}{6.675 \text{ E5 cc}} = 10.6 \text{ n/s/cc}$$

TABLE 5-3  
ORIGEN-S GAMMA SPECTRA  
gamma/sec/element

Group	Ave Energy (Mev)	Fission Products	Actinides	Total
1	0.3	4.21E12	2.07E10	4.23E12
2	0.65	1.12E14	2.45E10	1.12E14
3	1.13	3.21E12	7.80E8	3.21E12
4	1.57	8.44E11	1.55E9	8.46E11
5	2.00	1.19E11	4.06E7	1.19E11
6	2.40	3.19E9	3.05E4	3.19E9
7	2.80	4.44E8	1.42E10	1.46E10
8	3.25	6.14E7	1.07E4	6.14E7
9	3.75	2.71E4	6.18E3	<u>3.33E4</u>
				1.20E14

TABLE 5-4  
SCALE 18 Group Gamma Spectra

Group	Upper Energy (Mev)	$\gamma/s/element$
5	4.0	5.70E7
6	3.0	1.55E10
7	2.5	5.54E10
8	2.0	2.91E11
9	1.66	7.21E11
10	1.33	2.27E12
11	1.0	1.70E13
12	0.8	4.16E13
13	0.6	5.82E13
14	0.4	1.81E12
15	0.3	2.54E12
16	0.2	-----

TABLE 5-5

## NEUTRON SPECTRA

<u>Energy (Mev)</u>	<u>n/s/element</u>
6.43 - 20.0	2.96E3
3.0 - 6.43	4.18E4
1.85 - 3.0	6.05E4
1.40 - 1.85	2.72E4
0.9 - 1.40	3.19E4
0.4 - 0.9	3.20E4
0.1 - 0.4	<u>6.22E3</u>
	2.03E5

INTENTIONALLY BLANK

CHAPTER SIX  
CRITICALITY EVALUATION

TABLE OF CONTENTS

	<u>Page</u>
6.1 DISCUSSION AND RESULTS.....	6-1
6.1.1 Discussion	
6.1.2 Fuel Description	
6.1.3 Results	
6.2 PACKAGING FUEL LOADING.....	6-3
6.2.1 Assumptions	
6.3 MODEL SPECIFICATION.....	6-5
6.4 CRITICALITY CALCULATIONS.....	6-6
6.4.1 Normal Conditions of Transport	
6.4.2 Hypothetical Accident Conditions	
6.5 CRITICALITY BENCHMARK.....	6-15
6.6 REFERENCES.....	6-15
6.7 APPENDIX	

CHAPTER SIX  
CRITICALITY EVALUATION  
LIST OF FIGURES

	<u>Page</u>
Figure 6-1 Model FSV-1 Configuration - One Dimensional Model	6-6
Figure 6-2 Model FSV-1 Configuration - Two Dimensional Model	6-7
Figure 6-3 Model FSV-1 with Internal Flooding	6-14

## CHAPTER SIX

### CRITICALITY EVALUATION

#### 6.1 DISCUSSION AND RESULTS

##### 6.1.1 Discussion

The TN-FSV is designed for the transport of six (6) spent fuel elements from the Fort St. Vrain, High Temperature Gas-Cooled Reactor. The Fort St. Vrain fuel elements to be transported in the TN-FSV packaging are identical to the fuel elements which are described in the SAR for the licensed Model FSV-1 packaging. It is therefore the intent of the ensuing discussion in this Chapter to utilize the criticality evaluation presented in the Model FSV-1 packaging SAR (GADR-55) as a basis for the criticality evaluation for the TN-FSV packaging. No new analyses have been performed because the previous analyses are applicable and bounding for the TN-FSV packaging. Although this SAR relies on previous calculations, sufficient detail has been provided in the following sections to allow independence from the previous calculations. Additionally, References 6-2 and 6-3 provide details of the HTGR criticality program, which serves as a basis for the validation of cross section data and analytical methods used in the FSV physics program. The Model FSV-1 is a Fissile Class III package and therefore the TN-FSV shall also be classified as Fissile Class III.

##### 6.1.2 Fuel Description

The fissile material is contained in fuel elements which are hexagonal in cross section with dimensions 14.2 in. across flats by 31.2 in. high as shown in Fig. 1-4. Each fuel element contains coolant and fuel channels which are drilled from the top face of the element. Fuel holes are drilled to within about 0.3 in. of the bottom face and are closed at the top by a 0.5 in. cemented graphite plug. The fuel

channels occupy alternating positions in a triangular array within the element structure, are 0.5 in. in diameter and contain the active fuel.

The element structure consists of needle coke and/or isotropic graphite. The fuel itself is in the form of carbide particles coated with layers of pyrolytic carbon and silicon carbide. The fuel bed contains a homogeneous mixture of two types of particles, called fissile and fertile. Fresh fissile particles contain both thorium and 93.5% enriched uranium, while fresh fertile particles contain only thorium. The important parameters of fresh particles are:

<u>Parameter</u>	<u>Fissile</u>	<u>Fertile</u>
Nominal Th-U Ratio	3.6 or 4.25	All Th
Particle Composition	(Th/U)C <sub>2</sub>	Th C <sub>2</sub>
Average Fuel Particle Diam, mm	200	450
Average Total Coating Thickness, mm	130	140

Irradiated fuel elements contain, besides fission products, thorium, U-233, U-235, other uranium isotopes and a small quantity of plutonium. In the fertile particles, the fissile material is essentially U-233, while the fissile particles contain the residual U-235 and bred U-233.

The effective fissile material enrichment (U-235/U+Th) in fresh fuel for the initial core and reload segments varies between 2% and 12% due to radial and axial fuel zoning requirements. The most reactive fresh fuel element contains a maximum of 1.4 Kg of 93.5% enriched uranium and about 11.3 Kg of thorium. Any irradiated elements will contain a smaller amount of fissile material, since the conversion ratio of the reactor is on the order of 0.7. This conversion ratio yields a negative reactivity change during burnup. Therefore, the use of fresh fuel for criticality analyses is conservative.

### 6.1.3 Results

The TN-FSV and Model FSV-1 packaging are very similar in size and materials of construction. The major difference is that the TN-FSV packaging has a lead shield and the FSV-1 has a depleted Uranium shield. However, both materials act as neutron reflectors/absorbers as concerns reactivity. In fact, experiments (Ref. 6-4) have shown that both lead and depleted Uranium reflected system have approximately the same reactivity. Therefore, the FSV-1 results given below are also applicable to the TN-FSV packaging.

During the normal conditions of transport, the multiplication constant or Keff is 0.41.

During the hypothetical accident conditions with non-flooded spent fuel elements, the Keff is 0.41 and for the flooded spent fuel particle case the Keff is 0.89.

## 6.2 PACKAGE FUEL LOADING

### 6.2.1 Assumptions

The following assumptions were used in the criticality evaluation:

- a) The fuel elements contain the most reactive fresh fuel composition anticipated for fuel shipment, i.e., a maximum of 1.4 Kg of 93.5% enriched uranium and about 11.3 Kg of thorium per element resulting in a maximum of 8.4 Kg of uranium and about 68 Kg of thorium per package. Atom densities for a homogenous fuel element and an element containing homogenous fuel rods are provided in Table 6-1.
- b) The presence of burnable poison or other neutron absorbing material, other than U-235, U-238, thorium, silicon and graphite, is neglected.

Table 6-1

## SINGLE BLOCK HOMOGENIZED NUMBER DENSITIES

	Total Loading per Block (Kg)	Number Densities	
		Homogenized Block (atoms/b-cm)	Homogenized Rods in a Block (atoms/b-cm)
Th-232	11.25	3.28E-4	1.624E-3
U-235	1.31	3.76E-5	1.866E-4
U-238	0.078	2.22E-6	1.087E-5
Si	4.63	1.12E-3	5.524E-3
C (in rods)	16.295	--	4.545E-2
C (block only)	95.005	--	8.874E-2
C (homogenized)	111.3	6.72E-2	--

## DATA:

Volume of Block based on outside dimensions: 8.8767E4 cc  
 Volume of coolant holes (102 @ d=0.625", 6 @ d=0.5"): 1.6613E4 cc  
 Volume of Fuel Rods (total of 210 rods): 1.7874E4 cc  
 Volume of Graphite plugs (above/below rods): 3.1217E3 cc

NOTE: The spatial heterogeneity of fuel particles within a fuel rod affects the reactivity of a FSV fuel element. This "grain effect" is small and slightly positive, with a maximum increase of  $\Delta p = 0.003$ . This effect should be applied to calculational results which neglect grain structure in FSV fuel. Additionally, the effect of fuel rods within a fuel element (easily modelled with current Monte Carlo methods) should be included in criticality analyses. These two effects were previously taken into account through the use of the MICROX and GGC-4 codes.

- c) The fuel is at room temperature.
- d) All fission products are neglected.

These assumptions are all conservative. In general, spent fuel elements will contain considerably less fissile material. Also, all other fresh fuel element types are less reactive due to their lower uranium contents and/or higher thorium content. Hence, elements with a maximum of 1.4 Kg of uranium and a thorium/uranium ratio of at least 8.1/1 are acceptable.

### 6.3 MODEL SPECIFICATION

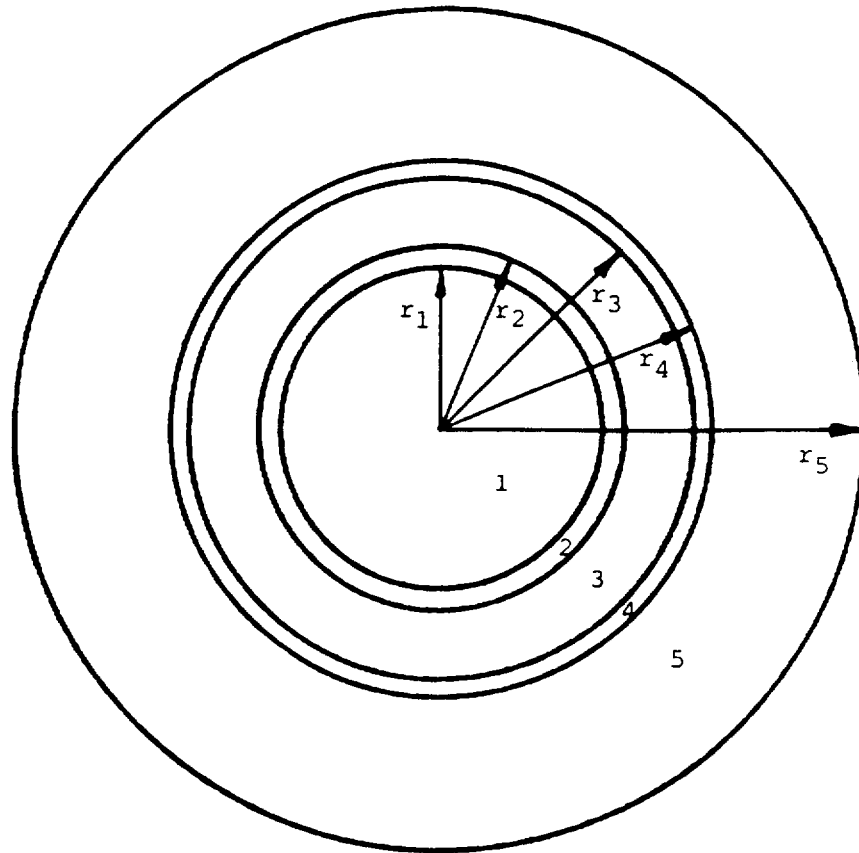
#### a. Geometry

Two geometric models were used to evaluate the criticality situation for the FSV-1 shipping cask. The one-dimensional model is shown in Fig. 6-1, and assumes an infinitely long cylinder. This model is adequate as long as it can be assumed that the fuel is well contained within the fuel elements.

The two-dimensional geometric model, shown in Fig. 6-2, was used for the maximum criticality situation which includes fuel element breakage, internal flooding and an accumulation of fuel particles at the bottom of the cask.

#### b. Cross Sections

Cross sections were calculated with a GGC-4 code, a description of which is provided in the Appendix. The calculational methods and the basic nuclear cross section data are well established and in use for the high temperature gas-cooled reactor (HTGR) nuclear design.



<u>REGION</u>	<u>REGION OUTER RADIUS</u>	<u>REGION CONTENTS</u>
1	$r_1 = 21.11$ cm.	FUEL ELEMENT (+ WATER)
2	$r_2 = 23.97$ cm.	IRON
3	$r_3 = 32.86$ cm.	URANIUM-235 & URANIUM-238
4	$r_4 = 35.40$ cm.	IRON
5	$r_5 = 55.40$ cm.	VOID or WATER

**FIGURE 6.1**  
**MODEL FSV-1 CONFIGURATION - ONE DIMENSIONAL MODEL**

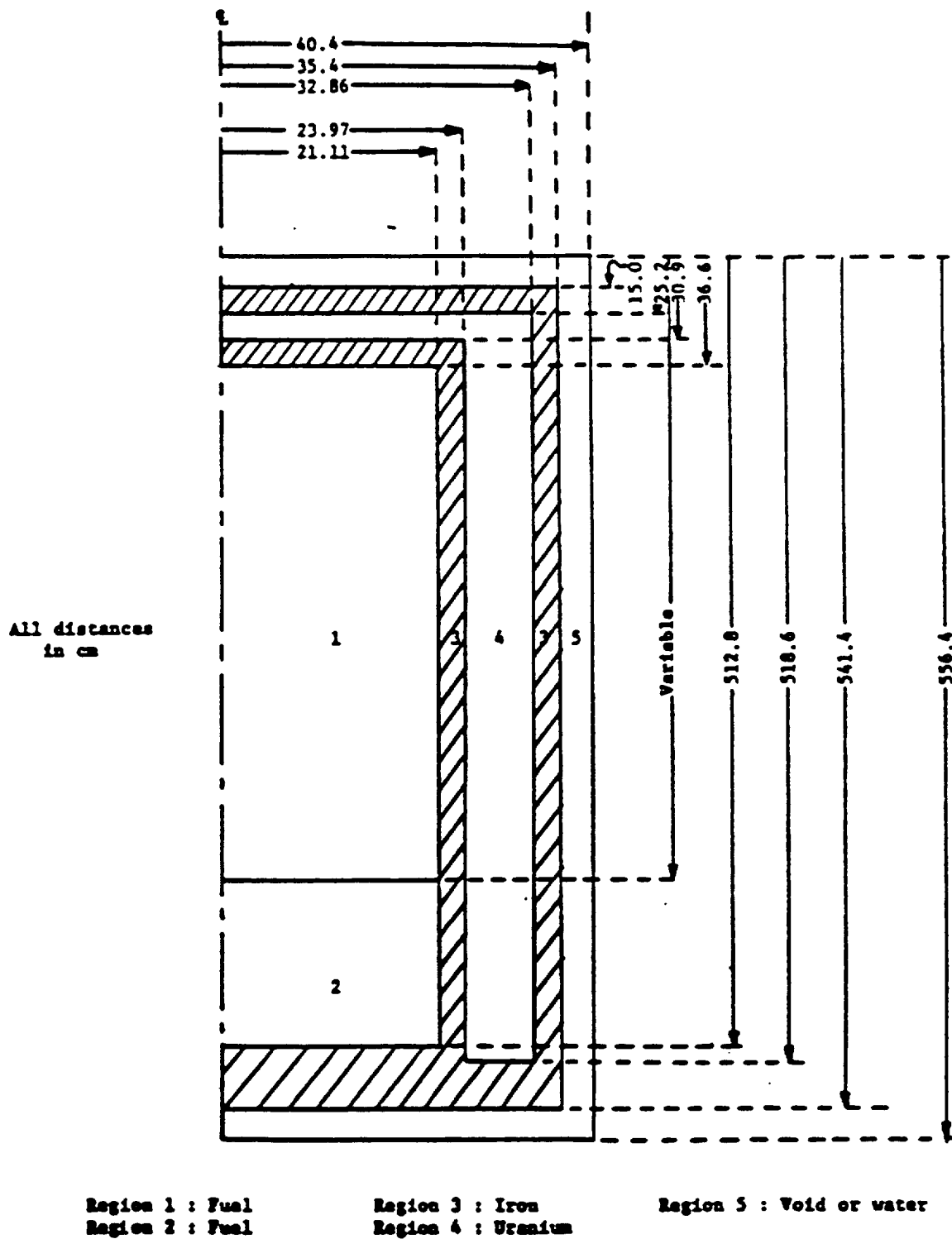


FIGURE 6-2

MODEL FSV-1 CONFIGURATION - TWO DIMENSIONAL MODEL

c. Computer Codes

The DTF-IV transport code was used for one-dimensional and the GAMBLE-5 code was used for the two-dimensional calculations. Descriptions of these codes are provided in the Appendix.

d. TN-FSV

The TN-FSV Packaging is very similar to the Model FSV-1 Cask. The TN-FSV is fabricated from stainless steel and lead while the FSV-1 is composed of stainless steel and depleted Uranium. Both casks consist of the heavy shielding (Pb or dpU) surrounded inside and out by shells of stainless steel. Dimensionally, the TN-FSV has a slightly larger diameter (~ 3 inches) than the FSV-1 due to the thicker lead shielding.

## 6.4 CRITICALITY CALCULATIONS

### 6.4.1 Normal Conditions of Transport

During normal transport not more than 6 fuel elements will be stacked end to end within the inner container. No hydrogenous or other moderating material besides the structural and coating graphite will be present.

The fuel elements occupy 81.4% of the inner container of the shipping cask. The contents of the elements were homogenized over the inner container of the cask and used in one-dimensional transport calculations. Table 6-2 provides atom densities for six homogenized fuel elements.

The calculated multiplication constant (Keff) for the FSV-1 in this condition, assuming an infinitely long container, is 0.40 and no

criticality hazard is to be expected under any circumstances.

#### 6.4.2 Hypothetical Accident Conditions

##### a. Unflooded Fuel

For the hypothetical accident conditions some breakage of the fuel elements has to be expected with possible accumulation of fuel particles in a corner of the cask. Detailed drop test data for irradiated fuel elements, however, are not available and some assumptions have to be made concerning the amount of particles released from the fuel elements. Assuming an upper limit of 20% particle loss and accumulation of these particles in coolant holes and the space between container wall and fuel element at the bottom of the container, the multiplication constant is calculated to be less than 0.41, with the cask completely immersed in water.

In the analysis it was assumed that the fuel particles fall out of the fuel channels into the coolant channels and spaces between element and container wall and form a homogeneous mixture with the remaining fuel element graphite. At 10% particle loss the lowest 24 cm of the cask would be filled with fuel particles and fuel elements. The remaining elements would have a correspondingly reduced fuel loading. At 20% particles loss, the lowest 48 cm would be filled with particles.

The following multiplication constants were calculated with the FSV-1 two-dimensional model:

No particle loss	$K_{eff} = 0.37$
10% particle loss	$K_{eff} = 0.37$
20% particle loss	$K_{eff} = 0.41$

Table 6-2

## SIX ELEMENT HOMOGENIZED NUMBER DENSITIES

Region Number Corresponding SAR Figure 6-2	Material	Homogenized Number Density atoms/b-cm
1	Th-232	2.67E-4
	U-235	3.06E-5
	U-238	1.81E-5
	Silicon	9.12E-4
	Carbon	5.10E-2
2	Iron	8.50E-2
3	U-238	4.80E-2
	U-235	9.60E-5
4	Iron	8.50E-2
5	Void	--

- Notes:
- 1) Region 1 is the same number densities as in Table 14 but multiplies by 81.4%.
  - 2) Region 3 for the TN-FSV Cask is not depleted Uranium, but is lead, with an approximate number density of 3.30E-2 atoms/b-cm.
  - 3) Radii for regions 3 and 4 for TN-FSV Cask are approximately 3" longer than those shown on SAR Figure 6-2 due to increased thickness of lead.

The first result agrees well with the data from the one-dimensional transport calculation. The other results show that partial particle loss from the fuel elements and subsequent particle accumulation at the bottom of the cask do not significantly increase the multiplication constant. Even if the whole cask were filled with particles only, the overall multiplication constant of the immersed cask would be less than 0.55. The presence of water at the outside of the cask has no significant effect on the criticality of the system. The iron and uranium (lead for TN-FSV) shield acts as a sink for thermal neutrons. Fast neutrons escaping from the fuel region are moderated in the water and absorbed before they can return to the fuel. Atom densities for the unflooded case are shown in Table 6-3.

#### b. Flooded Fuel

In order to obtain an upper limit for the multiplication constant of the FSV-1 shipping cask under flooded conditions the following assumptions were made in addition to those stated in Section 6.2.1:

- (1) All fuel particles leave the fuel elements (100% particle loss).
- (2) The fuel particles accumulate in the fuel holes, coolant holes and void spaces between fuel elements and container wall.
- (3) The graphite structure of the fuel elements stays intact allowing the highest concentration of fissile material in the available void space.
- (4) All void space between the fuel particles and in the unfueled section of the cask is filled with water.

In particular, the following cases (atom densities provided in Table 6-4) were considered for the FSV-1:

Case 1: All fuel particles accumulate at the bottom of the cask, filling the available void space. The particle packing fraction is 0.65. The overall height of the fueled section is 171 cm.

Case 2, 3, 4: The fuel particles float in water. A homogeneous mixture of water and particles occupies the available void space up to a height of 214 cm, 257 cm and 343 cm, respectively.

Case 5: The fuel particles float in water. A homogeneous mixture of water and particles fills all available void space in the shipping cask.

Case	Fuel Containing Section		
	Height (cm)	H/U-235	K <sub>eff</sub>
1	171	143	0.84
2	214	244	0.89
3	257	346	0.89
4	343	551	0.85
5	476	866	0.77

Figure 6-3 shows these results graphically. The most reactive situation, a multiplication constant of about 0.9, is obtained if the total fuel contents, in a mixture of water and particles, occupies the available void spaces of about half the cask (235 cm). From these results it is concluded that no critical arrangement can occur even if all the fuel leaves the fuel elements and the cask is completely flooded and that K<sub>eff</sub> is less than 0.95.

**Table 6-3**  
**CONCENTRATIONS FOR MOST REACTIVE CONDITION (UNFLOODED)**

Region	Material	Concentration (atoms/b-cm)		
		10% Particle Loss		20% Particle Loss
1	Th-232	2.4E-4		2.14E-4
	U-235	2.75E-5		2.45E-5
	U-238	1.63E-5		1.45E-5
	Si	8.21E-4		7.30E-4
	C	5.01E-2		4.91E-2
2	Th-232		7.41E-4	
	U-235		8.49E-5	
	U-238		5.02E-5	
	Si		2.53E-3	
	C		6.92E-2	
3	Fe		8.5E-2	
4	U-238		4.78E-2	
	U-235		9.6E-5	
5	H		6.68E-2	
	O		3.34E-2	

- Notes: 1) Height of Particle Accumulation: 10% loss 24 cm  
20% loss 48 cm
- 2) Number densities for 10% and 20% were derived from homogeneous block number densities
- 3) Region 4 is now lead with an approximate number density of 3.30E-2 atoms/b-cm

**Table 6-4**  
**CONCENTRATIONS FOR MOST REACTIVE FLOODED CONDITIONS**

Region	Material	Case 1	Case 2	Case 3	Case 4	Case 5
1	C	4.09E-2	4.09E-2	4.09E-2	4.09E-2	--
	H	3.47E-2	3.47E-2	3.47E-2	3.47E-2	--
	O	1.74E-2	1.74E-2	1.74E-2	1.74E-2	--
2	Th-232	7.41E-4	5.93E-4	4.94E-2	3.71E-4	2.67E-4
	U-235	8.49E-5	6.79E-5	5.66E-5	4.25E-5	3.06E-5
	U-238	5.02E-6	4.02E-6	3.35E-6	2.51E-6	1.81E-6
	Si	2.53E-3	2.03E-3	1.69E-3	1.27E-3	9.12E-4
	C	6.92E-2	6.35E-2	5.98E-2	5.50E-2	5.11E-2
	H	1.21E-2	1.66E-2	1.96E-2	2.34E-2	2.65E-2
	O	6.05E-3	8.30E-3	9.80E-3	1.17E-2	1.33E-2

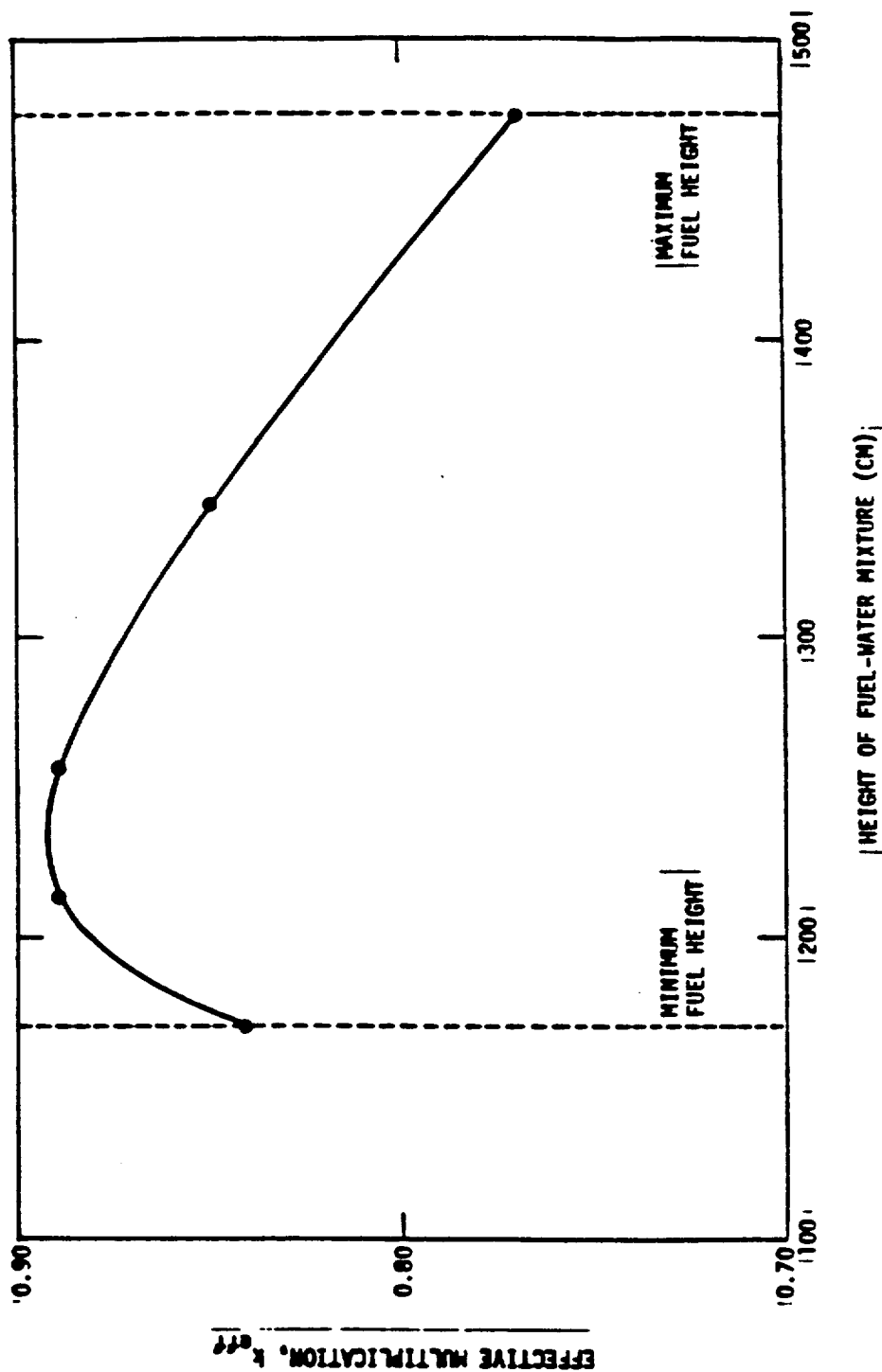


FIGURE 6-3  
MODEL FSV-1 WITH INTERNAL FLOODING  
CONTENTS: 8.4 Kg 93.5% ENRICHED URANIUM  
68.0 Kg THORIUM-232

## 6.5 CRITICALITY BENCHMARK

The calculational methods used for the FSV-1 criticality analysis are essentially the same as those used for HTGR design and the analysis of the HTGR critical facility. Comparisons of experimental and calculational results are documented in References 6-2 to 6-4. These results indicate that the accuracy of the methods used is in the order  $\pm 0.02 \Delta k$ .

## 6.6 REFERENCES

- 6-1 Consolidated Design Report for the Model FSV-1 Shipping Cask, Volumes I and II. GADR-55.
- 6-2 R.G. Bardes, et al., 'Results of HTGR Critical Experiments Designed to Make Integral Checks on the Cross Sections in Use at Gulf General Atomic,' GA-8468, Gulf General Atomic (1968).
- 6-3 R.J. Nirschl, et al., 'Experimental and Analytical Results for HTGR Type Control Rods of Hafnium and Boron in the HTGR Critical Facility,' GA-A9354, Gulf General Atomic (1973).
- 6-4 HTGR Base Program Quarterly Progress Reports:
  - GA-9227, for the period ending February 28, 1969, issued March 28, 1969.
  - GA-9090, for the period ending November 30, 1968, issued December 30, 1968.
  - GA-8860, for the period ending August 31, 1968, issued September 27, 1968.
  - GA-8662, for the period ending May 31, 1968, issued June 28, 1968.
  - GA-8530, for the period ending February 28, 1968, issued March 29, 1968.
  - GA-8356, for the period ending November 30, 1967, issued December 29, 1967.
- 6-5 S.R. Bierman, et al., 'Criticality Experiments with Subcritical Clusters of 2.35 Wt% and 4.29 Wt% <sup>235</sup>U Enriched UO<sub>2</sub> Rods in Water with Uranium or Lead Reflecting Walls' NUREG/CR-0796, Pacific Northwest Laboratories. (1979)

Appendix 6.7 Description of Criticality Codes6.7.1 Designation of Program - GGC4

- a. Nature of physical problem solved - the GGC4 program solves the multigroup spectrum equations with spatial dependence represented by a single positive input buckling. Broad group cross sections (shielded or unshielded) are prepared for diffusion and transport codes by averaging with the calculated spectra over input-designated energy limits. The code is divided into three main parts. A fast (GAM) section which covers the energy range from 14.9 MeV to 0.414 eV, a thermal (gather) section which covers the energy range from 0.001 to 2.38 eV, and a combining (combo) section which combines fast and thermal cross sections into single sets. Basic nuclear data for the fast section which consists of fine group-averaged cross sections and resonance parameters is read from a data tape. The fine group absorption and fission cross sections may be adjusted by performing a resonance integral calculation. Utilizing a fission source and an input buckling, the code solves the P1, B1, B2, or B3 approximation to obtain the energy-dependent fast spectrum. Two or six spatial moments of spectrum (due to a plane source) may also be evaluated. Instead of performing a spectrum calculation, the user may enter the legendre components of the angular flux directly. For as many input-designated broad group structures as desired, the code calculates and saves (for the combining section) spectrum weighted averages of microscopic and macroscopic cross sections and transfer arrays. Slowing down sources are calculated and saved for use in the lower energy range. Given basic nuclear data, the thermal section of GGC4 determines a thermal spectrum by either reading it as input, by calculating a Maxwellian spectrum for a given temperature, or by an iterative solution of the P0, B0, P1, or B1 equations for an input buckling. Time moments of the time and energy-dependent diffusion equations are calculated (as an option) using the input buckling to represent leakage. Broad group cross sections are prepared by averaging fine group cross sections over the calculated spectra. Broad group structures

are read as input. The combining section of GGC4 takes the broad group-averaged cross sections of GGC4 from the fast and thermal portions of GGC4 and forms multigroup cross section tables. These tables are prepared in standard formats for transport or diffusion theory calculations. In addition, it is possible to use the combining section to produce mixtures not used in the spectrum calculation or to combine the results of different fast and thermal section calculations and so on. These options are described in Reference 2.

- b. Method of Solution - In the fast section either the P1 or the B1, B2, or B3 approximation is made to the transport equation using the positive, energy-independent buckling. In each approximation legendre moments of the angular flux are computed by direct numerical integration of the slowing down equations. In the resonance calculations, doppler broadened (at an input temperature) absorption and scattering cross sections are used. The resonance treatment allows up to two admixed moderators in an absorber lump imbedded in a surrounding moderator. The absorber in the lump is treated by using either the narrow resonance approximation, the narrow resonance infinite mass approximation, or a solution of the slowing down integral equations to determine the collision density using either an asymptotic form of, or an integral equation solution for, the collision density. In the resonance calculation either standard geometry collision probabilities are used or tables of collision probabilities are entered. Dancoff corrections can also be made. In the region of unresolved resonances, resonance absorption is calculated by using Porter-Thomas distributions, but only S-wave neutrons are considered. In the thermal section either the B0, B1, P0, or P1 approximation to the transport equation is made, and in all options legendre moments of the angular flux are computed. A trapezoidal energy integration mesh is used, and the resulting equations are solved iteratively by using a source-normalized, over-relaxed, Gaussian technique. Averages over broad groups are performed by simple numerical integration. The results obtained in the fast and thermal sections are stored on special tapes. These tapes may contain results for a number of problems, each problem including fine

group cross section data for a number of nuclides. If the problem number is specified on these tapes, and a desired list of nuclides is given, the combining code will punch microscopic cross sections for the requested list of nuclides. The program also treats mixtures. Given the atomic densities of the nuclides in a mixture, the code will punch macroscopic cross sections.

c. Restrictions on the Complexity of the Problem - Maximum of -

99 fast groups  
 101 thermal fine groups  
 99 fast broad groups  
 50 thermal broad groups  
 50 broad groups in the combining section  
 250 resonances per nuclide  
 2 moderators admixed with a resonance absorber  
 305 entries in the escape probability table for cylindrical geometries  
 505 entries in the escape probability table for slab geometries a single and positive value for the buckling (B2) must be supplied.

- d. Typical Running Time - A 81 calculation in the fast section for 3 nuclides and 6 broad groups takes approximately 4 minutes on the Univac-1108 if a resonance calculation (1/2 minute) is performed for one nuclide. The thermal calculation for 3 broad groups requires approximately 2 minutes, which includes about 7 seconds for the iterative procedure. To punch standard diffusion and standard transport cross sections for this problem requires 2 sec.
- e. Unusual features of the program - there is an option of GGC4 which makes it possible to shorten the punching process for large two-dimensional transfer arrays. This can be done by specifying a maximum number of desired upscattering and downscattering terms.
- f. Related and auxiliary programs - GGC4 is a revision of the earlier program, GGC3. To prepare, handle, and update the

basic cross section tapes which are used as input for GGC4, the following codes are utilized--HAKE, MST, PRINT, MIXER, WTFG, MGT3, SPRINT, COMBIN, and DOP.

## 6.7.2

Designation of Program - 1DF

(DTF - IV is essentially the same.)

- a. Nature of physical problem solved - the linear time-independent Boltzmann equation for particle transport is solved for the energy, space and angular dependence of the particle distribution in 1-D slabs, cylinders, and spheres. Independent source or eigenvalue (multiplication, time absorption, element concentration, zone thickness, or system dimension) problems are solved subject to vacuum, reflective, periodic, or white boundary conditions. A complete energy transfer scattering matrix is allowed for each legendre component of scattering. Solutions to the adjoint transport equation are also obtained.
- b. Method of Solution - Energy dependence is treated by the multi-group approximation and angular dependence by a general discrete ordinates approximation. Anisotropic scattering is approximated by a truncated spherical harmonics expansion of the scattering kernel. Within-group scattering and upsattering iteration processes are accelerated by system-wide renormalization procedures. Chebyshev acceleration is automatically applied to accelerate inner iteration convergence. At the option of the user, Chebyshev acceleration factors can be entered as input. Approximations and iterative cycles have been described in detail by Lathrop (Ref. 1 below). 1DF and DTF-IV are essentially the same.
- c. Restrictions of the complexity of the problem - the variable dimensioning capability of Fortran IX has been utilized so that any combination of number of groups, number of spatial intervals, size of angular quadrature, etc., can be used that will fit within the total core storage available to a user.
- d. Typical running time - a few minutes.

- e. Unusual features of the program - anisotropic distributed sources may be used and the incoming angular flux at the right boundary may be specified.
- f. Related and auxiliary program - GTF, 2DF, and TWOTRAN.

6.7.3                    Designation of Program - GAMBLE-5

- a. GAMBLE-5, is a program for the solution of the multigroup neutron diffusion equations in two dimensions with arbitrary group scattering.
- b. Nature of physical problem solved - the homogenous two-dimensional multigroup diffusion theory equations with arbitrary group-to-group scattering and arbitrary fission transfer are solved for heterogenous assemblies in X-Y and R-Z geometry. Homogenous logarithmic boundary conditions are used at the outer surface of the assembly and at the surface of nondiffusion regions. The results include the group- and point-dependent neutron fluxes, the power distribution, the neutron multiplication factor (k-eff), and a detailed neutron balance.
- c. Method of solution - The multigroup diffusion theory equations are approximated by five-point difference equations for an arbitrary nonuniform mesh grid. The system of difference equations is solved by an extension of the power method to find the eigenvector (neutron flux) and the eigenvalue (k-eff). Successive line overrelaxation is applied in a special form (exponential overrelaxation) that guarantees the nonnegativity of the neutron flux. Coarse mesh rebalancing is used to improve the preasymptotic convergence behavior. A variation of Aitkens' method is used to improve the asymptotic convergence behavior, assuming only one error mode.
- d. Restrictions on the complexity of the problem -
  - Maximum number of energy group - 10
  - Maximum number of space meshpoints - 20,000
  - Maximum number of different material regions - 255

- e. Typical running time - A seven-group problem (three fast groups and four thermal groups) in (R,Z) geometry with 2842 space mesh points took 82 iterations assuming a tight convergence criteria (maximum relative flux change less than 0.000007). The total running time (including extensive output) on the Univac 1108 was 12 min.
  
- f. Unusual features of the program -
  - (1) The coarse mesh rebalancing scheme makes possible the successful solution of difficult problems for which certain group-mesh points are both strongly and weakly coupled to some of their neighbors (e.g., highly nonuniform mesh spacings or material properties, air gaps, cell problems with weak group coupling, etc.).
  - (2) Simultaneous performance of computation and data transfer with virtually no delay caused by the use of drum storage.
  - (3) Ability to do efficient restarts for longer running problems and the ability to accept a flux guess on tape from a similar problem.
  
- g. Related and auxiliary programs - GAMBLE-5 is a major revision of the GAMBLE-4 code. Some of the essentials of the iterative technique used have been adopted from exterminator.

CHAPTER EIGHT ACCEPTANCE TESTS AND MAINTENANCE PROGRAM  
TABLE OF CONTENTS

	<u>PAGE</u>
8.1 ACCEPTANCE TESTS.....	8-1
8.1.1 Visual Inspection	
8.1.2 Structural and Pressure Tests	
8.1.2.1 Lid Lifting Attachment Load Test	
8.1.2.2 Lifting Socket Load Test	
8.1.2.3 Hydrostatic Test	
8.1.2.4 Cask Weight Measurements	
8.1.3 Leak Tests	
8.1.3.1 Containment System Fabrication Verification	
8.1.3.2 Impact Limiter Leakage Rate Test	
8.1.3.3 Humidity Test	
8.1.4 Component Tests	
8.1.5 Tests for Shielding Integrity	
8.1.6 Thermal Acceptance Tests	
8.2 MAINTENANCE PROGRAM.....	8-6
8.2.1 Structural and Pressure Tests	
8.2.2 Leak Tests	
8.2.3 Subsystems Maintenance	
8.2.4 Valves, Rupture Discs and Gaskets on Containment Vessel	
8.2.5 Shielding	
8.2.6 Thermal	
8.2.7 Impact Limiter Humidity	
8.2.8 Miscellaneous	

#### 8.1.2.3 Hydrostatic Test

After the shielding integrity test, the TN-FSV cask body will be hydrostatically tested using demineralized water in accordance with the requirements of the ASME B&PV Code, Section III, Article NB-6200.

The test pressure of 45 psig will be maintained for a minimum time of ten (10) minutes. The cask body and closures will then be examined for any deformations or leakage.

#### 8.1.2.4 Cask Weight Measurements

The assembled cask, as well as major individual components shall be weighed with a precision of  $\pm 0.5$  percent.

#### 8.1.3 Leak Tests

##### 8.1.3.1 Containment System Fabrication Verification

A Containment System Fabrication Verification leakage rate test of the TN-FSV shall be performed at the Fabricator's facility in accordance with the requirements of ANSI N14.5 and Section V of the ASME B&PV Code.

The following tests will be performed in accordance with approved, written procedures on the containment boundary. The test cavities will be evacuated to a pressure of less than  $10^{-2}$  mbar. The total leakage rate for the containment boundary shall be no greater than  $1 \times 10^{-3}$  std cc/sec with a test procedure sensitivity of no greater than  $5 \times 10^{-4}$  std cc/sec. The test method utilized shall be either a helium leak test (mass spectrometer) or a gas pressure rise test. Both of these test methods are described in ANSI N14.5 and meet the sensitivity requirement defined above.

- a) A preliminary test shall be performed on the interspace between the inner and outer o-rings of the lid through a test port using an o-ring sealed test connector. This will show that the lid is seated properly.
- b) The next test shall be performed on the containment boundary formed by the cask cavity and the Drain Port Cover and seal (Hansen coupling removed), and the inner O-ring of the lid. Evacuation shall be through the Vent port using an O-ring sealed test connector.
- c) The next test shall be performed after the Vent port cover is installed. The O-ring seal of the cover shall be leak tested using a test bell. The test bell fits over the vent cover and has an O-ring which seals against a machined surface on the cover surface.

An acceptable alternative test method is to perform the test in paragraph b) through the drain port and then test the drain port cover and seal by the method described in paragraph c). The Hansen coupling must be removed for the test described in paragraph b).

#### 8.1.3.2 Impact Limiter Leakage Rate Test

Following final closure welding, each impact limiter will be tested for leakage in accordance with the methods of ANSI N14.5 and the requirements of Section V of the B&PV Code, using the helium sniffer method or bubble leak test methods. The differential pressure shall be limited to less than 3 psi.

#### 8.1.3.3 Humidity Test

After performing the impact limiter leakage rate test, a humidity test will be performed to determine that there is no in-leakage of water into the impact limiter container during fabrication. The dew point

of a gas sample from the impact limiter container will be determined. The dew point measured shall be less than the equilibrium temperature of the impact limiter. The difference between the measured dew point and the impact limiter wall temperature shall be greater than twice the accuracy of the humidity test system.

#### 8.1.4 Component Tests

Installation and removal tests will be performed for the lid, impact limiters, drain and vent port covers, and other fittings and inserts.

Each component will be observed for difficulties in installation and removal. After removal, each component will be visually examined for indications of deformation, galling, ease of use and proper functioning. Any such defects will be corrected prior to acceptance of the cask.

#### 8.1.5 Tests for Shielding Integrity

A gamma scan or equivalent test shall be performed on the cask after lead installation to detect any shielding deficiencies from lead voids equal to or greater than  $\pm 5\%$  of shielding thickness. The test shall be performed on a maximum grid spacing of three (3) inches.

Following initial loading of the TN-FSV cask, a shield effectiveness test shall be performed prior to delivery to a carrier for transport. Measurements shall be made of the neutron and gamma dose rates of the loaded package to verify that the loaded cask meets the transport dose rate limitations of 10CFR71 and the applicable USDOT regulations.

#### 8.1.6 Thermal Acceptance Tests

There are no thermal tests required for the TN-FSV.

## 8.2 MAINTENANCE PROGRAM

### 8.2.1 Structural and Pressure Tests

There are no periodic structural tests required on the TN-FSV.

### 8.2.2 Leak Tests

After the TN-FSV is loaded and before it is released for transport, a series of pressure rise tests shall be performed on the cask openings to verify proper assembly. See Chapter 7.0 for details of these tests.

No leak tests will be done on the empty cask before it is shipped.

After the third use and every twelve months thereafter, the Containment System Fabrication Verification Test, Section 8.1.3.1, shall be repeated, unless the cask is not in service. Prior to use the cask shall have been tested within the preceding 12-month period.

### 8.2.3 Subsystems Maintenance

This section does not apply.

### 8.2.4 Valves, Rupture Discs and Gaskets on Containment Vessel

All gaskets and the Drain port Hansen quick connect plug will be replaced prior to the third use test and annually thereafter unless the cask is not in service. Prior to use, the maintenance shall have been completed within the preceding 12-month period.

No other maintenance is required prior to transport.

#### 8.2.5 Shielding

A shielding integrity test using gamma scan or equivalent shall be performed after fabrication, and a shield effectiveness test shall be performed following initial loading. See paragraph 8.1.5. Dose rate measurements are required to be taken prior to each shipment. There are no periodic shield effectiveness tests required.

#### 8.2.6 Thermal

There are no thermal tests required for the TN-FSV.

#### 8.2.7 Impact Limiter Humidity

An annual humidity test shall be performed on the impact limiters to assure that no water has leaked into the impact limiter and that the wood has maintained the proper moisture content. The humidity test is described in Section 8.1.3.3.

#### 8.2.8 Miscellaneous

The lid bolts, vent cover bolts and drain cover bolts (if removed) shall be replaced after every 250 round trip shipments to preclude fatigue failure.

Enclosures  
P-94018  
February 24, 1994

**ENCLOSURES TO PSC LETTER P-94018**